

University of Strathclyde

Department of Mechanical and Aerospace Engineering

**Investigation of corrosion protection systems and  
development of design rules for enhanced corrosion  
fatigue life in positive displacement pumps**

Evripidis Tsergas

A thesis submitted for the degree of Doctor of Philosophy

2019

Dedicated to my parents; Apostolos and Aikaterini for their  
continuous help and support.

This thesis is the result of the author's original research. It has been composed by the author and has not been previously submitted for examination which has led to the award of a degree.

The copyright of this thesis belongs to the author under the terms of the United Kingdom Copyright Acts as qualified by University of Strathclyde Regulation 3.50. Due acknowledgement must always be made of the use of any material contained in, or derived from, this thesis.

# Table of Contents

Acknowledgements.....	i
Abstract.....	ii
List of Abbreviations .....	iii
List of Symbols .....	iv
<b>CHAPTER 1: Introduction</b> .....	<b>1</b>
1.1 Thesis Introduction .....	1
1.2 Thesis Layout.....	5
1.3 References .....	6
<b>CHAPTER 2: Literature Review</b> .....	<b>9</b>
2.1 Theoretical Background .....	9
2.1.1 Corrosion Basics .....	9
2.1.1.1 Corrosion of Metals.....	9
2.1.1.2 The Corrosion Potential.....	10
2.1.1.3 The Pourbaix Diagram .....	11
2.1.1.4 The Electromotive Force Series .....	11
2.1.1.5 Faraday's Law .....	12
2.1.1.6 Corrosion Types .....	12
2.1.1.7 Stress–Corrosion Deterioration Modes .....	14
2.1.2 Corrosion Control.....	16
2.1.2.1 Corrosion Prevention and Protection Methods.....	16
2.1.2.2 Principles of Cathodic Protection .....	18
2.1.2.3 Cathodic Protection Criteria.....	21
2.1.2.4 Sacrificial Anodes .....	21
2.1.3 Fatigue.....	22
2.1.3.1 Basic Principles of Fatigue.....	22
2.1.3.2 Fatigue Cycle .....	23
2.1.3.3 Fatigue Analysis Methods .....	25
2.1.3.4 Factors Affecting Fatigue Life .....	26
2.2 Review of the Effect of Cathodic Protection on Corrosion Fatigue Life .....	28
2.2.1 Introduction .....	28
2.2.2 Review of the Effect of Corrosion on Fatigue Life .....	30
2.2.3 Review of the Effect of Cathodic Protection (CP) on Corrosion Fatigue.....	31
2.2.4 Conclusions .....	34

2.3 Numerical Simulation of Cathodic Protection Systems .....	35
2.3.1 Introduction .....	35
2.3.2 Mathematical Background.....	36
2.3.3 Numerical Methods .....	39
2.3.4 The BEASY CP Software.....	40
2.3.5 Polarisation Diagrams .....	42
2.3.5.1 Theoretical Base of Polarisation Diagrams .....	42
2.3.5.2 Review of Parameters Affecting Polarisation Behaviour .....	46
2.4 References .....	50
<b>CHAPTER 3: Erosion-Corrosion Performance .....</b>	<b>59</b>
3.1 Introduction .....	59
3.2 Pre-Test Methodologies.....	60
3.2.1 Source of Materials.....	60
3.2.1.1 Material Investigated.....	60
3.2.1.2 Sacrificial Anode Materials .....	61
3.2.2 Surface Preparation of Test Samples .....	62
3.3 Erosion-Corrosion Testing Procedures.....	62
3.3.1 Testing Protocol .....	62
3.3.2 Flow Velocity Measurements .....	65
3.3.3 Potentiodynamic Testing .....	66
3.4 Post-Test Analysis Techniques .....	67
3.4.1 Mass loss Measurements.....	67
3.4.2 Surface Microscopy.....	67
3.4.3 Evaluation of Cathodic Protection Systems Performance .....	68
3.5 Results and Discussion .....	68
3.5.1 Mass Loss Measurements.....	68
3.5.2 Surface Microscopy.....	69
3.5.3 Cathodic Protection Systems Performance .....	71
3.5.4 Effect of Conditions Variation on CP System Performance - Polarisation Diagrams	73
3.5.4.1 Effect of Flowing Conditions.....	73
3.5.4.2 Effect of Electrolyte Salinity .....	75
3.5.4.3 Effect of Driving Voltage (Anode Material).....	76
3.6 Analytical Approach to CP System Performance Prediction.....	78
3.6.1 1-D Model for Analytical Approach .....	78

3.6.2 Sensitivity Analysis of CP System Performance .....	79
3.6.2.1 <i>Effect of increasing distance between cathode and anode</i> .....	79
3.6.2.2 <i>Effect of Anode material (Driving Voltage)</i> .....	82
3.6.2.3 <i>Effect of Electrolyte Salinity</i> .....	83
3.6.2.4 <i>Effect of Flowing Conditions</i> .....	85
3.7 Conclusions .....	87
3.8 References .....	89
<b>CHAPTER 4: Corrosion-Fatigue Performance</b> .....	<b>91</b>
4.1 Introduction .....	91
4.2 Pre-Test Methodologies.....	93
4.2.1 Source of Materials .....	93
4.2.1.1 <i>Material Investigated</i> .....	93
4.2.1.2 <i>Sacrificial Anode Materials</i> .....	93
4.2.2 <i>Design and Manufacturing of Test Samples</i> .....	94
4.2.2.1 <i>Fatigue Specimens</i> .....	94
4.2.2.2 <i>Sacrificial Anodes</i> .....	95
4.2.3 <i>Environmental Chamber</i> .....	96
4.3 Fatigue Testing Procedures.....	98
4.3.1 Testing Protocol .....	98
4.3.1.1 <i>In-Air Fatigue Testing</i> .....	98
4.3.1.2 <i>Corrosion - Fatigue Testing</i> .....	98
4.3.1.3 <i>Corrosion-Fatigue with Cathodic Protection Testing</i> .....	100
4.3.2 Flow Rate Measurements .....	101
4.5 Post-Test Analysis Techniques .....	102
4.5.1 Construction of S-N Curves .....	102
4.5.2 Fractography .....	102
4.5.3 Evaluation of Cathodic Protection Systems Performance .....	103
4.6 Results and Discussion .....	103
4.6.1 Corrosion Fatigue.....	103
4.6.1.1 <i>Effect of Corrosion on Fatigue Life</i> .....	103
4.6.1.2 <i>Effect of Cathodic Protection on Corrosion Fatigue Life</i> .....	106
4.6.2 Fractographic Investigation .....	109
4.6.3 Cathodic Protection Systems Performance .....	112
4.6.3.1 <i>Corrosion Potential</i> .....	112

4.6.3.2	<i>Closed Circuit Potential of Fatigue Specimens</i> .....	113
4.7	Conclusions .....	117
4.8	References .....	118
	<b>CHAPTER 5: Guidelines for Analytical Design and Simulation of SACP Systems for Pipelines and GEHO Positive Displacement Pumps</b> .....	122
5.1	Introduction .....	122
5.2	Guidelines for Analytical Design of Cathodic Protection Systems .....	123
5.2.1	Polarisation Data .....	123
5.2.1.1	<i>Experimental Set-Up</i> .....	123
5.2.1.2	<i>Polarisation Scanning Methodology</i> .....	124
5.2.1.3	<i>Results and Discussion</i> .....	124
5.2.2	Conceptual Design .....	127
5.2.3	Detailed Design .....	130
5.3	Guidelines for Prediction of Cathodic Protection Systems Performance Using Modelling Techniques .....	135
5.3.1	Introduction to Cathodic Protection Modelling .....	135
5.3.2	Model Creation .....	135
5.3.2.1	<i>Model Geometry</i> .....	135
5.3.2.2	<i>Normal Vectors to Surfaces</i> .....	136
5.3.2.3	<i>Anodic, Cathodic and Insulated Surfaces</i> .....	136
5.3.2.4	<i>Mesh Generation</i> .....	136
5.3.2.5	<i>Polarisation Data</i> .....	137
5.3.3	Solver Launching .....	138
5.3.4	Simulation Results .....	139
5.4	Conclusions .....	139
5.5	References .....	140
	<b>CHAPTER 6: Analytical Design and Simulation of SACP Systems for Pipelines and GEHO Positive Displacement Pumps</b> .....	142
6.1	Introduction .....	142
6.2	Design of Pipeline Cathodic Protection System .....	143
6.2.1	Analytical Design of SACP System for Pipeline Test Rig .....	143
6.2.1.1	<i>Conceptual Design</i> .....	143
6.2.1.2	<i>Detailed Design</i> .....	143
6.2.2	Simulation of Pipeline Cathodic Protection System .....	147
6.2.2.1	<i>Model Creation</i> .....	147

6.2.2.2 <i>Simulation Results</i> .....	150
6.3 Analytical Design and simulation of GEHO Positive Displacement Pump Cathodic Protection System .....	152
6.3.1 Analytical Design of GEHO PD Pump Cathodic Protection System .....	152
6.3.1.1 <i>Conceptual Design</i> .....	152
6.3.2 Simulation of GEHO PD Pump Cathodic Protection System .....	156
6.4 Conclusions .....	165
6.5 References .....	166
<b>CHAPTER 7: Concluding Remarks and Recommendations for Future Work</b> .....	168
7.1 Introduction .....	168
7.2 Concluding Remarks.....	168
7.3 Recommendations for Future Work .....	171

# Acknowledgements

Firstly, I would like to express my sincere gratitude to my supervisors Prof. Alexander Galloway and Prof. Donald MacKenzie for their inspired supervision and continuous support throughout my Ph.D. study. I could not have imagined having completed my Ph.D. thesis without their invaluable help.

I would like to thank my WEIR project champion Dr Ralph van Rijswijk (Director Venlo Technology Group, WEIR Minerals Netherlands) and also Dr Trevor Hodgkiss (Honorary Research Fellow, University of Glasgow), Jordy Brouwers (Materials Engineer, WEIR Minerals Netherlands) and Dr Stephan Hannot (Chief Engineer, WEIR Minerals Netherlands) for their insightful comments and encouragement.

My sincere thanks also goes to Christopher Lynch (Engineering Manager, Corrpro Companies Europe), Zolt Ronafalvi (Director of Sales and Marketing, Corrpro Companies Europe), Tim Froome (Managing Director, BEASY) and Robbie Ashby (Software Engineer, BEASY) for their excellent support to conduct this research.

Furthermore, I thank my fellow labmates and colleagues; George Karafyllias, Frazer Brownlie, Athanasios Anagnostakis, Marta Morgantini, Volodymyr Okorokov, Francesco Rizzuto, Blazej Polakiewicz, James Kelly, James Gillespie and Hans Slaats for their help, friendship and stimulating discussions.

Last but not least, I would like to thank my parents and sister for supporting me spiritually throughout my Ph.D. study and my life in general.

# Abstract

The current study comprises an extensive investigation of the effect of cathodic protection on the fluid erosion-corrosion and corrosion fatigue performance of a low alloy steel grade used for the manufacturing of pump components and pipelines, designed to work in severe environmental conditions. The experimental investigation showed that factors such as electrolyte salinity and flowing conditions significantly affect the performance of the material and the behaviour of cathodic protection systems. The adoption of the proper cathodic protection strategies has been seen to eliminate the effect of corrosion and extend the fatigue life to levels observed in dry conditions. The implementation of sacrificial anode cathodic protection using Magnesium alloy sacrificial anodes in low salinity and Zinc alloy sacrificial anodes in high salinity aqueous environments, proved to be successful strategies in mitigating corrosion. The development of a 1-D mathematical model enabled the sensitivity analysis of the behaviour of sacrificial anode cathodic protection systems used in various working conditions. Moreover, design rules have been developed for sacrificial anode cathodic protection systems aimed for the elimination of the effect of fluid erosion-corrosion on the fatigue life of pipelines and positive displacement pumps. The systems designed, based on these rules, were modelled using commercial simulation tools for the prediction of their performance. The findings demonstrate that sacrificial anode cathodic protection can be successfully used for the corrosion protection of such industrial equipment. Finally, the effect of current drain on the performance of sacrificial anode cathodic protection systems, used in positive displacement pumps, due to their electrical connection to pipelines, was investigated using modelling techniques. The results showed that proper design of such systems may dramatically decrease this effect and so enable the designer to avoid the use of electrical insulation systems that would increase the production cost.

# List of Abbreviations

<b>BEM</b>	Boundary element method
<b>CF</b>	Corrosion fatigue
<b>CFS</b>	Corrosion fatigue strength
<b>CP</b>	Cathodic protection
<b>CSE</b>	Copper-copper sulphate electrode
<b>DC</b>	Direct current
<b>EMF</b>	Electromotive force
<b>FDM</b>	Finite differences method
<b>FEC</b>	Free erosion corrosion
<b>FEM</b>	Finite element method
<b>ICCP</b>	Impressed current cathodic protection
<b>MIC</b>	Microbiologically-influenced corrosion
<b>PD</b>	Positive displacement
<b>SACP</b>	Sacrificial anode cathodic protection
<b>SCC</b>	Stress corrosion cracking
<b>SCCP</b>	Sacrificial coating cathodic protection
<b>SCE</b>	Saturated calomel electrode
<b>SEM</b>	Scanning electron microscopy
<b>SHE</b>	Standard hydrogen electrode
<b>SSC</b>	Silver-silver chloride electrode
<b>TML</b>	Total mass loss

# List of Symbols

<b>A</b>	Surface area
<b>A<sub>a</sub></b>	Anode surface area
<b>A<sub>c</sub></b>	Cathode surface area
<b>C</b>	Pure electrochemical deterioration
<b>C<sub>a</sub></b>	Anode current capacity
<b>D</b>	Anode material density
<b>d<sub>a,core</sub></b>	Anode core diameter
<b>d<sub>a,u</sub></b>	Final anode diameter
<b>E</b>	Pure mechanical degradation
<b>E<sub>a</sub></b>	Closed circuit anode potential
<b>E<sub>c</sub></b>	Design protective potential
<b>E<sub>corr</sub></b>	Corrosion potential
<b>E<sup>o</sup></b>	Standard potential
<b>F</b>	Faraday's constant
<b>f<sub>c</sub></b>	Coating breakdown factor
<b>I</b>	Electrical current
<b>i</b>	Electrical current density
<b>I<sub>a</sub></b>	Anode current output
<b>I<sub>a,u</sub></b>	Final anode current output
<b>i<sub>c</sub></b>	Design current density
<b>I<sub>c</sub></b>	Current demand
<b>I<sub>corr</sub></b>	Corrosion current
<b>L</b>	Length
<b>M</b>	Metal
<b>M<sub>a</sub></b>	Atomic weight
<b>m<sub>a</sub></b>	Anode mass
<b>N</b>	Number of fatigue cycles, number of anodes
<b>n</b>	Number of electrons, normal vector
<b>N<sub>i</sub></b>	Fatigue cycles to crack initiation
<b>N<sub>p</sub></b>	Fatigue cycles of crack propagation
<b>Q</b>	Water quantity
<b>R</b>	Electrical resistance, stress ratio
<b>r</b>	Anode radius, nozzle radius

$R_a$	Anode resistance
$R_{a,u}$	Final anode resistance
$R_e$	Yield strength
$R_m$	Ultimate tensile strength
$S$	Synergy, applied stress
$S_e$	Endurance limit
$t$	Total time, system life
$t_f$	Design life
$u$	Utilisation factor
$V$	Potential difference
$V_a, \phi_a$	Anode potential
$V_{an}$	Net anode material volume
$V_c, \phi_c$	Cathode potential
$v$	Water jet velocity
$W_t$	Total weight loss
$\Delta\sigma$	Stress range
$\epsilon$	Strain, electrochemical capacity
$\rho$	Electrical resistivity
$\sigma$	Electrical conductivity, applied stress
$\sigma_a$	Stress amplitude
$\sigma_m$	Mean stress

# CHAPTER 1

## Introduction

### 1.1 Thesis Introduction

Aqueous corrosion of metallic materials is an electrochemical reaction between the material and the aqueous environment to which it is exposed [1.1]. It causes deterioration of the material and its properties and is known to have a great impact on industry, in terms of cost, safety and environmental issues [1.2]. Flows of liquids may increase the effect of corrosion on metallic structures by eroding protective layers of corrosion products and by providing more corrosives on the metallic surfaces, keeping corrosion going at a high rate [1.3]. It has been observed that the service lives of systems, such as pipelines, pressure vessels and pumps, are decreased, under the combination of erosion, corrosion and working loads, compared to the initial design life of the equipment. It has been suggested by D. Mackenzie et al. [1.4] that erosion and corrosion can act simultaneously to increase surface damage, accelerate micro-crack initiation and increase crack growth rates.

Positive displacement pumps (PD pumps) suffer severely from the simultaneous effect of periodic stresses and the erosive-corrosive environment they are working in. These conditions have a crucial effect on the fatigue life of the system's components, made of poor corrosion resistant steel grades, leading to unexpected failures. Such failures have been observed in GEHO PD pumps, manufactured by WEIR Minerals Netherlands, designed for long life service in hostile environments. In **Figure 1-1** a GEHO PD pump, designed for mineral processing applications, is presented.

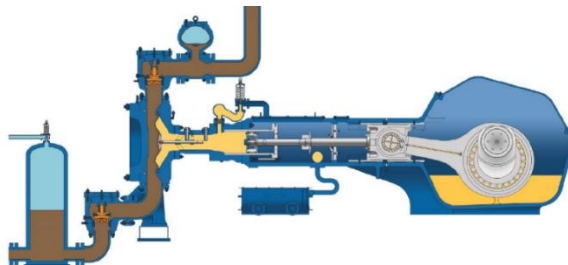


**Figure 1-1.** WEIR Minerals GEHO PD pump for mineral processing applications [1.5].

WEIR Minerals GEHO PD pump fluid end modules experience cyclic loading due to the variation in pump chamber pressure between suction and discharge pressure on every pump stroke [1.6]. These pumps are designed for continual duty in mineral processing applications with a design life of 25 years. It is of great importance to understand the mechanisms of erosion-corrosion and its impact on the corrosion fatigue lives of pump components, in order to select the proper strategies for corrosion protection and for the prolongation of the service lives of those systems. The current design method for protection against corrosion-fatigue, is limited to material selection. In cases where the chloride concentration of the pumped fluid exceeds the limit of 500ppm Cl<sup>-</sup> (824ppm NaCl), stainless steel grades are used. In the current work, alternative methods for the elimination of the effect of fluid erosion-corrosion on the fatigue life of PD pump components made of low corrosion resistant steel grades, are investigated. The use of low corrosion resistant materials in conjunction with corrosion protection techniques suggested in literature, which restore the corrosion - fatigue life of pump components to in-air levels, is proved to be an effective strategy.

Cathodic protection is a common technique used in industry to control the effect of corrosion on equipment working in corrosive environments. According to this technique, the corrosion of a metal surface is controlled by turning it into the cathode of an electrochemical cell [1.7]. There are three basic methods of applying cathodic protection, Sacrificial Anode Cathodic Protection (SACP), Sacrificial Coating Cathodic Protection (SCCP) and Impressed Current Cathodic Protection (ICCP). SACP is applied by electrically connecting the metal to be protected to a block of a more active metal (sacrificial metal) that acts as the anode of the electrochemical cell [1.8]. SCCP comprises of the application of a metallic coating on the surface of the structure under protection. This coating, being rich in a more active metal than the substrate, e.g. Zinc or Aluminum, provides a barrier between the structure and the corrosive environment. In the case of local damage, the remaining coating material acts as anode providing protective current to the structure surface area that has been exposed to the corrosive environment [1.9, 1.10]. Finally, ICCP is the method of providing cathodic (protective) current by using an external direct current (DC) electrical power source [1.11].

R. G. Ripeanu et al. [1.12] and H. Saito [1.13] suggested that CP using sacrificial anodes can be successfully applied for the protection of the internal surfaces of centrifugal pumps, used for the pumping of crude oil containing water of high sodium chloride concentration and sea water respectively. In the case of PD pumps the

working conditions of a CP system are different from centrifugal pumps. In PD pumps, compared to centrifugal pumps, the flowing conditions vary due to the motion of moving parts, such as suction and discharge valves and the reciprocation of the diaphragm that produces the pumping power. Moreover, in PD pumps the surface to be protected is not constant because of the opening and closing of the mentioned valves that may affect the performance of a CP system under certain operational conditions. Such issues must be overcome by proper design, securing the effectiveness of the CP system to be applied.

For the corrosion protection of the internal surfaces of pipelines, several CP systems have been proposed. G. Jha [1.14] suggested that metallic pipelines transporting sea water or brine water should be protected using internal lining, as primary protection, in combination with internal CP by flat bar galvanic anodes. In [1.15] S. Javia concluded that the use of specially designed wire type anode impressed current systems and SACP systems using either Zinc or Magnesium alloy flush mounted anodes, welded into the pipeline at regular intervals, are two successful methods for protecting the internal surfaces of coated, large diameter pipelines, carrying water and sea water. Furthermore, the applicability of both SACP and ICCP for the internal protection of pipelines against corrosion, has also been discussed in [1.16], where it is stated that the application of CP becomes more difficult as the diameter of the pipeline decreases. This statement should be attributed to the fact that the efficiency of a CP system decreases as the cross-section of the current-flow path becomes narrower, as has been suggested by J. Baynham and T. Froome [1.17]. Moreover, R. Johnsen et al. [1.18] refers to the restriction of the use of pencil type sacrificial anode systems, to prevent internal corrosion of carbon steel piping systems, transporting seawater, due to the high anode consumption combined with short protection distance from each anode. Finally, these issues can be overcome by the suggestion of J.H. Morgan [1.19], that concentric cylindrical anodes can be used for the internal corrosion protection of bare steel pipes carrying seawater providing uniform current distribution over the pipe surface. Taking into account the working conditions and the intended service life of the system, the geometrical characteristics of the anode can be determined accordingly in the design phase.

The scope of this work is to investigate the fluid erosion-corrosion and corrosion-fatigue performance of a low alloy steel grade, used by WEIR Minerals for the manufacturing of PD pump components, designed to work in hostile environments

and select the proper corrosion protection strategies in order to extend the service life of the systems. For this purpose, the current work consists of a comprehensive experimental approach based on fluid erosion-corrosion tests and microscopy techniques, application and monitoring of cathodic protection systems, to mitigate corrosion of a low alloy steel grade in fluid erosion-corrosion conditions, electrochemical monitoring techniques and development of an 1-D mathematical model for the investigation of the behaviour of SACP systems in various conditions. Also, the effect of cathodic protection on the corrosion-fatigue performance of the material has been investigated by conducting an experimental programme, comprising of tests in high and low conductivity aqueous environments. Consequently, design methods have been developed for CP systems aimed for the mitigation of the effect of fluid erosion-corrosion on fatigue life of pipelines and GEHO PD pumps, including also the use of numerical tools for the prediction of the performance of these systems.

The novelty of this study lies with the following:

- a) Insight into the fluid erosion-corrosion performance of a low alloy steel grade used for the manufacturing of GEHO PD pump components, working in flowing 824ppm and 35,000ppm NaCl aqueous solutions.
- b) Development of a novel method for applying and monitoring the behaviour of SACP and SCCP systems and investigation of their effect on the fluid erosion-corrosion performance of the material in the previously mentioned conditions.
- c) Insight into the behaviour of SACP systems using electrochemical monitoring methods in various flowing conditions of 824ppm and 35,000ppm NaCl aqueous solutions and development of an 1-D mathematical model for the prediction of the response of these systems in various working conditions.
- d) Insight into the corrosion-fatigue performance of the material in flowing seawater level aqueous solution and in water of lower electrical conductivity for which information in the literature is very limited.
- e) Development of novel systems for the application and monitoring of SACP systems aimed for the protection of the material in corrosion-fatigue conditions, by using pencil type anodes.
- f) Insight into the performance and effect of the previously mentioned CP systems on the corrosion-fatigue life of the material, working in flowing seawater salinity level (35,000ppm NaCl) aqueous solution, using zinc

sacrificial anodes and in an aqueous solution of low salinity level (824ppm NaCl), using Magnesium sacrificial anodes, for which there is very limited or no information in literature respectively.

- g) Development of novel methodologies for the design and simulation of SACP systems for the corrosion protection of structures, made of low alloy steel grades.
- h) Novel analytical design method and simulation of SACP systems for the protection of the internal surfaces of pipelines.
- i) Design and simulation of novel SACP systems for the protection of the internal surfaces of GEHO PD pump components.
- j) Insight into the effect of current drain on the performance of SACP systems, designed to protect the internal surfaces of GEHO PD pumps due to the electrical connection of its components to pipelines.

## 1.2 Thesis Layout

The Thesis layout is summarised as follows. In **Chapter 2**, a detailed review of the fundamentals of corrosion, corrosion control and fatigue is presented. Furthermore, it includes the outcomes of literature review concerning the effect of corrosion on fatigue life of low corrosion resistant steel grades and the effect of cathodic protection on the corrosion-fatigue life of these materials. In the final part of the Chapter, a review is presented of the mathematical background of the simulation of cathodic protection systems and the numerical methods currently used for this purpose. The polarisation characteristics of the materials involved in such systems, are used as experimental input data into the numerical models and for this reason a review of the theoretical base of polarisation diagrams and a literature review of the parameters affecting the polarisation behaviour, are also included.

**Chapter 3** discusses the experimental techniques used for the quantification of the corrosion damage and a novel approach that expands the assessments of the effect of corrosion protection methods on a low alloy steel grade working in fluid erosion-corrosion conditions. Moreover, electrochemical techniques are used for the investigation of the polarisation behaviour of materials involved in cathodic protection systems, offering an insight into the response of such systems under various environmental conditions. The Chapter concludes with the presentation of the

development and use of a 1-D mathematical model for the quantitative prediction of the performance of SACP systems, based on the outcomes of the polarisation behaviour investigation.

The experimental investigation of the effect of cathodic protection on the corrosion-fatigue performance of a low alloy steel grade is presented in **Chapter 4**. The investigation comprises of the conduction of fatigue tests in air and in corrosive aqueous environments with or without the use of a novel method for the application and monitoring of SACP. Finally, the results are presented in the form of stress-life (S-N) curves for better assessment of the effectiveness of SACP in eliminating the effect of corrosion on fatigue life.

It is **Chapter 5** which discusses novel analytical design methodologies for sacrificial anode cathodic protection systems. The designing process of such systems is very important in terms of ensuring adequate potential distribution over the entirety of the protected surfaces. The prediction of the performance of such systems, before field application, is being made possible by using numerical methods. For this reason, the use of commercial numerical tools and the method for obtaining polarisation curves to be used as input data, are presented.

**Chapter 6** presents the conceptual and detailed design, followed by simulation of novel sacrificial anode cathodic protection systems aimed for the corrosion protection of the internal surfaces of pipelines and GEHO TZPM PD pump components. The effect of current drain on the performance of SACP systems of GEHO TZPM PD pumps, due to their electrical connectivity to pipelines, is also investigated.

Finally, **Chapter 7** comprises of concluding remarks, concerning the methodologies used and the outcomes presented in this Thesis and recommendations for further investigation.

## 1.3 References

- [1.1] J. de Prey, R. W. Barrett and J. N. Wanklyn, Design and Operational Guidance on Cathodic Protection of Offshore Structures, Subsea Installations and Pipelines, The Marine Technology Directorate Limited, London, United Kingdom (1990).

- [1.2] R. W. Revie and H. H. Uhlig, Corrosion and Corrosion Control, An Introduction to Corrosion Science and Engineering, Fourth Edition, John Wiley & Sons, Inc., New Jersey, USA (2008).
- [1.3] David G. Enos and Louie L. Scribner, The Potentiodynamic Polarization Scan, Technical Report 33, Solartron Instruments a division of Solartron Group Ltd, Farnborough, Hampshire, UK (1997).
- [1.4] D. Mackenzie, W. Pan and T. Hodgkiess, Fatigue Life Design for Forgings in a Corrosive/Erosive Environment, Project G: 2011-2012, Phase 1 Literature Review, Weir Advanced Research Centre, University of Strathclyde (2012).
- [1.5] WEIR Minerals, GEHO Pumps for the Alumina Industry Brochure (2016).
- [1.6] D. Mackenzie, Audit of Material Selection & Design Criteria for GEHO PD Pumps, Rev. 2, Weir Advanced Research Centre, University of Strathclyde, Glasgow (2013).
- [1.7] Alireza Bahadori, Cathodic Corrosion Protection Systems a Guide for Oil and Gas Industries, School of Environment, Science & Engineering, Southern Cross University, Lismore, NSW, Australia (2014).
- [1.8] James B. Bushman, Galvanic Anode Cathodic Protection System Design, Bushman & Associates Inc., Ohio, USA (2010).
- [1.9] Mamdouh M. Salama, William H. Thomason, Evaluation of Aluminum-Sprayed Coatings for Corrosion Protection of Offshore Structures, Society of Petroleum Engineers of AIME, SPE 12440 (1984).
- [1.10] Herbert H. Uhlig, The Corrosion Handbook, John Wiley & Sons, Inc., New York (1948).
- [1.11] Volkan Cicek, Cathodic Protection, Industrial Solutions for Protecting Against Corrosion, Scrivener Publishing LLC, Salem, Massachusetts (2013).
- [1.12] R.G. Ripeanu, I. Tudor, F. Dinu, Research About the Efficiency of Active Anode Protection at Centrifugal Pumps, Tribology in industry, Volume 30, No. 1&2 (2008).
- [1.13] Hiroshi Saito, Cathodic Protection of Centrifugal Pump by Zinc Anodes, Hitachi Research Laboratory, Hitachi Limited (1960).

- [1.14] Gitesh Jha, Cathodic Protection System for Internal Surfaces of Piping/Pipeline, CORCON, Paper No. CAP14, Mumbai, India (2017).
- [1.15] Shailesh Javia, Impressed Current Cathodic protection System for water pipeline internal surfaces, CORCON, Paper No. ICP23, Mumbai, India (2017).
- [1.16] Tri-Star DIMET, Cathodic Protection Applications Brochure (2016).
- [1.17] J. Baynham and T. Froome, Assessment of Effects of Cavities and Narrow Channels on CP Design in the Marine Environment, NACE-2017-9275, NACE International (2017).
- [1.18] R. Johnsen, S. Valen, P.O. Gartland and J.M. Drugli, Internal Cathodic Protection of Piping System by the RCP Method: What is the experience?, NACE International, NACE 97421 (1997).
- [1.19] John H. Morgan, The Internal Cathodic Protection of Large Steel Pipes Carrying Sea Water, Corrosion – National Association of Corrosion Engineers (1958).

# CHAPTER 2

## Literature Review

### 2.1 Theoretical Background

#### 2.1.1 Corrosion Basics

##### 2.1.1.1 Corrosion of Metals

The impact of corrosion on industrial equipment is of great significance worldwide. Corrosion can cause serious problems in terms of economics, safety and environmental pollution [2.1-2.2]. Possible need for expensive overdesign and maintenance of equipment increase the cost of production. Furthermore, systems' failures may jeopardise safety and inhibit technological progress. Risks involving the loss of valuable resources not only affect the economics but the pollution of the environment as well.

Corrosion of metals is an electrochemical reaction involving the transfer of electrical charge (electrons) across the interface of a metal and a conductive solution [2.3-2.6]. The energy existing in metals, called Gibbs free energy, causes them to corrode (oxidise) spontaneously when they come in contact with such an environment, e.g. seawater. Gibbs free energy is the energy which is imparted on the metal during the refining process and is available as potential energy ( $-\Delta G^0$ ) to power the corrosion reaction.

When a metal corrodes, metal atoms pass into the electrolyte while its bonding electrons ( $ne^-$ ) are left behind, according to the following oxidation reaction [2.7-2.8]:



where n is the number of electrons.

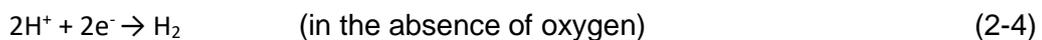
Any area where current flows in this direction is called Anodic area. The cathode is any area where the Reduction (Cathodic) reaction takes place. The cathodic reaction

depends on the environmental conditions. The pH level and the presence of oxygen in the aqueous solution can lead to the occurrence of different reduction reactions. According to [2.7-2.8], in neutral and alkaline aqueous environments, the cathodic reaction is usually the following:

Oxygen reduction reaction



Whereas, in acidic environments the cathodic reactions that are more likely to occur are the following:



In this way the entire corrosion process involves transfer of charges across the metal/electrolyte interface by both oxidation and reduction reactions forming electrochemical cells, as shown in **Figure 2-1**. The percentage of the active surface of a corroding metal is usually 5÷15% compared to the total metal surface.



**Figure 2-1.** Representation of the iron corrosion mechanism in aqueous solution.

As is stated in [2.9], in practice the rate at which the cathodic reaction can be maintained, often controls the rate of corrosion. For example, if the relevant reaction is the (2-2), the controlling factor may be the replenishment of oxygen.

### 2.1.1.2 The Corrosion Potential

The potentials established at anode and cathode interfaces, at equilibrium, are called anode open circuit potential and cathode open circuit potential respectively. The

potential difference between the anode and cathode is the electromotive force of the corrosion cell which equates to the Gibbs free energy of the metal. The charge transfer across the metal/solution interface causes the anodic and cathodic areas to polarise and is associated with a potential difference called the corrosion potential,  $E_{\text{corr}}$ . Since the anodic and cathodic reactions are different, the corrosion potential is a mixed potential. The current flowing from anodic to cathodic areas at this potential is called corrosion current,  $I_{\text{corr}}$  and is related directly to the rate of the electrode reaction [2.10]. It is not possible to determine the absolute potential across a metal/solution interface by measurement. For this reason secondary electrodes called *reference electrodes* are used. The hydrogen reference electrode is an electrode composed of a platinum wire surrounded by a solution with 1 molar concentration of hydrogen ions. Under particular conditions this electrode maintains a very stable potential. It is also called *standard hydrogen electrode* (SHE) and its potential is used as a reference from which all other electrode potentials are measured [2.3]. The most common reference electrodes suited for field use are the saturated copper-copper sulphate (CSE), the saturated calomel (SCE) and the silver-silver chloride (SSC). SSC reference electrodes are usually used for aqueous environments of high Sodium Chloride concentrations [2.11].

#### 2.1.1.3 The Pourbaix Diagram

In aqueous environments, the fundamental variables of potential and pH are particularly important [2.2]. Other variables, e.g. oxygen concentration, tend to be reflected by corrosion potential changes. E-pH or Pourbaix diagrams are a convenient way to summarise the thermodynamic behaviour of a metal and associated species at specific environmental conditions. The Pourbaix diagrams can be used to map out the occurrence of corrosion, nobility and passivity of a metal as a function of potential and pH.

#### 2.1.1.4 The Electromotive Force Series

The electromotive force series indicate the standard potentials of pure metals and relates the corrosion tendency of each, the more electronegative the potential the greater the tendency to corrode [2.3]. The standard potentials ( $E^\circ$ ) of pure metals are measured under standard conditions (temperature 25°C, solution of 1 molar concentration of the metal ions and no current is drawn from the metal specimens in the measuring circuit). The resulting table indicates the standard potentials of the pure

metals and relates the corrosion tendency of each. The most active metal in the series will be having a high negative standard potential while nobler metals possess relatively more positive standard potential. Arrangements of the standard potentials of metals, called electromotive force series (EMF series), can be found in literature [2.3, 2.12, 2.13].

As suggested by Alireza Bahadori in [2.9], the relative positions of two metals in the electromotive force series indicate their behaviour when they are electrically coupled in an electrolyte. The voltage difference between the two metals causes electrical current flow which opposes the corrosion current. The metal which is more negative acts as anode, providing sacrificial protection to the less negative (more noble) metal, which acts as cathode. This is the principle of the corrosion protection method called galvanic protection or sacrificial anode cathodic protection (SACP) that will be discussed in detail later in this Chapter.

#### 2.1.1.5 Faraday's Law

The following relationship (known also as Faraday's Law) was developed by Michael Faraday while working as Sir Humphry Davy's assistant at the Royal Institute in London, England in 1833 [2.3]. Faraday's Law is used to calculate the amount of the material lost at the anode or deposited at the cathode.

$$W_T = \frac{M_a}{nF} t I_{corr} \quad (2-6)$$

Where  $W_i$  = total weight loss at anode or weight of material produced at cathode at the cathode [g],  $n$  = number of charges transferred in the oxidation or reduction reaction,  $I_{corr}$  = Corrosion current [A],  $F$  = Faraday's constant of approximately 96,485 coulombs per equivalent weight of material (where equivalent weight =  $\frac{M_a}{n}$ ),  $M_a$  = the atomic weight of the metal which is corroding or the substance being produced at the cathode [g] and  $t$  = the total time in which the corrosion cell has operated [s].

#### 2.1.1.6 Corrosion Types

- Uniform Corrosion or Mobile Pitting Corrosion

Uniform or general corrosion is the most common form of corrosion and is a uniform etching of the metal. It can be caused by most direct chemical attacks (e.g. as by an acid). A polished surface that corrodes uniformly starts to appear dull and if the reaction is allowed to continue it becomes rough [2.14]. Examples of materials

exhibiting general attack are weathering steels and copper alloys, while stainless steels or Nickel-Chromium alloys are prone to localized attack [2.15].

- Galvanic Corrosion

When two dissimilar metals are placed in contact (electrically connected) in a corrosive solution, electrical current will flow between them, due to the difference in their potentials. In this case, the corrosion of the less corrosion-resistant metal will increase while the attack on the more corrosion-resistant metal will decrease, compared to their behaviour when not in contact [2.16]. This form of accelerated corrosion on the less corrosion resistant (more active) metal, is termed galvanic corrosion.

- Concentration Cell Corrosion

When two or more areas of the same metal surface are in contact with different concentrations of the same electrolyte, concentration cell corrosion occurs (e.g. different metal ion concentration, different oxygen concentration) [2.14].

- Pitting Corrosion

Passive metals, such as stainless steels, are likely to suffer pitting corrosion. It is localized, accelerated dissolution of metal occurring as a result of a breakdown of the otherwise protective passive film on the metal surface [2.2, 2.14]. Pitting corrosion can also occur on non-passivating metals with protective coatings after localized breakdown [2.15].

- Crevice Corrosion

Crevice corrosion is the localized form of corrosion produced at sites where metals are in contact with other metals or non-metals, usually associated with a stagnant solution on the micro environmental level (e.g. under washers) [2.14]. Crevice corrosion occurs due to changes in the local chemistry within the crevice [2.15], i.e. the surface area of the metal within the crevice is oxygen starved while the surrounding surfaces have access to dissolved oxygen [2.3].

- Intergranular Corrosion

The attack on, or adjacent to, the grain boundaries of a metal or alloy preferentially to the interior of the grain is called intergranular corrosion [2.14, 2.17]. The boundary

phase or a zone adjacent to it differing chemically from the grain, having lost the corrosion resistant element due to segregation or the formation of a compound, will become anodic relative to the remainder of the surface, when exposed to a corrosive environment. In this case Intergranular Corrosion will occur having a great impact on the structural integrity of the metallic component [2.18].

- Filiform Corrosion

This form of corrosion is observed under painted or plated metallic surfaces in the case that moisture permeates the coating [2.14]. Filiform corrosion is associated with oxygen concentration variation within the corrosion filament and results in networks of thread-like corrosion products that propagate across the surface of the metal [2.19].

- De-alloying or Selective Leaching

De-alloying or selective leaching is a form of selective corrosion of the more active component of an alloy. The more corrosion resistant component is left in a porous form on the metal surface [2.14]. An example of this form of corrosion is the removal of zinc in brass alloys, which is called dezincification [2.16].

- Microbiologically-influenced corrosion (MIC)

Microbiologically-influenced corrosion (MIC) is a mechanism of corrosion that is enhanced by the presence and activity of microbes [2.14]. Colonies of living organic matter form a biofilm on the metal surface underneath which a protective environment is created, where conditions can become very corrosive and so corrosion is accelerated. In most cases MIC takes the form of pits on the surface of the metallic structure. MIC causes serious problems in many fields, such as the oil and gas industry, water treatment systems and sewer systems [2.20]. The safety, integrity and reliability of the equipment, used in such systems, is severely affected by MIC.

#### *2.1.1.7 Stress–Corrosion Deterioration Modes*

- Erosion Corrosion

Erosion corrosion is the surface degradation mechanism of metals that is caused by the relative movement between a corrosive fluid and the metal surface [2.16]. It can result from the fast fluid flow past a stationary object (e.g. fast flow in tubes) or from

the quick motion of an object in a stationary fluid (e.g. ship's propeller) [2.14]. According to [2.21], the removal of material from the surface by a moving fluid, is termed fluid erosion. The erosion mechanism involves flow induced shear stress on the material surface that causes wear. A second failure mechanism, termed solid particle erosion, can occur when the fluid contains suspended solid particles. Many researchers [2.7, 2.8, 2.21- 2.27] use the following equation to describe the erosion corrosion phenomenon.

$$TML = E + C + S \quad (2-7)$$

where TML = total mass loss, E = pure mechanical degradation, C = pure electrochemical deterioration and S = the interaction of both that is often called synergy.

- Stress Corrosion Cracking

The simultaneous presence of tensile stress and a specific corrosive environment, can lead to Stress Corrosion Cracking (SCC) [2.28]. Residual stresses induced by the manufacturing process (e.g. residual stress due to welding), applied loads or a combination of both may lead to SCC [2.14]. When SCC occurs, small cracks form on the metal surface and propagate perpendicularly to the direction of the stress. SCC leads to extensive branching cracks gradually increasing in the metal [2.6].

- Corrosion Fatigue

Corrosion-fatigue is a frequent cause of premature failure of structural components working in corrosive environments under cyclic stressing [2.9]. Corrosive environments can promote the fatigue crack initiation in metals and increase the fatigue crack propagation rate [2.29]. Consequently, the fatigue life and corrosion-fatigue strength (CFS) decrease significantly. In corrosion-fatigue there is no Fatigue limit (or endurance limit and the S-N curve falls steeply [2.21, 2.30-2.32], as indicated in **Figure 2-2**. Corrosion-fatigue is presented and discussed in detail later in this chapter.

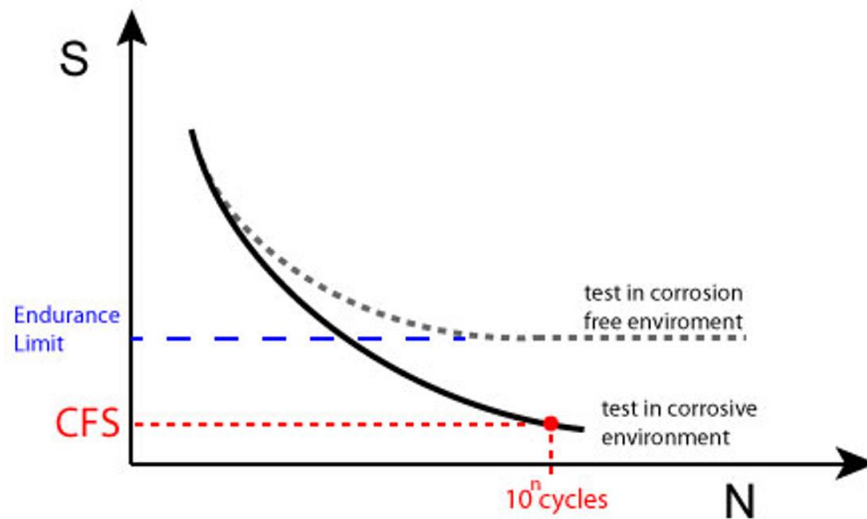


**Figure 2-2.** Form of S-N curve for corrosion free environment and corrosive environments [2.32].

- Hydrogen Embrittlement

Ingress of Hydrogen into a metallic component as a result of the reduction reaction on a metal cathode, can lead to rapid failure. The ductility and load-bearing capacity of the material decrease making it susceptible to brittle fracture even at relatively lower stresses. Vulnerable to Hydrogen embrittlement are high-strength steels, Titanium and some other metals [2.14].

## 2.1.2 Corrosion Control

### 2.1.2.1 Corrosion Prevention and Protection Methods

- Proper Design

At the design stage of structures, designing rules to prevent corrosion must be taken into account. For example, accumulation of static water must be avoided. Also, shapes must be easily accessible for cleaning and painting. Contact of dissimilar metals and alloys must be avoided in order to prevent galvanic corrosion. Moreover, structures must be designed in a way that reduces the stresses and does not lead to SCC or other stress related corrosion failures [2.6].

- Material Selection

The proper selection of the materials to be used in a project is crucial in order to prevent corrosion, after the corrosion environment has been characterised. Corrosion resistant materials (e.g. stainless steels) are more suitable for specific applications. As suggested in [2.6], the cost must always be considered, as in many cases it is not economically feasible to use more noble materials but some other measures must be applied.

- Protective Coatings

Coatings are physical barriers to corrosion that are applied on surfaces in the form of films, as is stated in [2.6, 2.33-2.34]. The coating must maintain a high degree of surface adhesion which requires some pre-application surface treatment. In many cases, the coating must not be reactive in the corrosive environment and have high resistance to mechanical damage. The efficiency of a coating depends on its permeability to the corrosive environment. The more un-permeable the coating is the more efficient it is for the specific application.

General methods of applying a corrosion protective coating are by using organic and inorganic paints, passivation of the surface via formation of a protective oxide film, hot-dipping, electro-plating, metal spraying, metal cladding and cementation [2.6]. The concept of the application of anodic coatings (sacrificial coatings), including metal-spayed Zinc, Aluminium and Magnesium, is similar to cathodic protection [2.33].

- Changing the Environmental Factors that Accelerate Corrosion

Modification of the environment may be required to reduce the corrosion rate, protecting the metal surface. By lowering the fluid temperature and/or velocity usually a reduction in corrosion rate occurs. The corrosion rate is also affected by the concentration of some species in the solution. The presence of gases like CO<sub>2</sub> and SO<sub>2</sub> in the atmosphere accelerates corrosion because they dissolve in water to form corresponding acids. As pH decreases, the evolution of hydrogen gas can replace the ionization of oxygen as the cathode reaction affecting corrosion, as is stated in [2.6]. Finally, addition of inhibiting substances or retardants in small amounts can also affect the rate of corrosion.

- Changing the Electrochemical Characteristic of the Metal Surface

By using electrochemical methods, the electrode potential of a metal can be changed. *Anodic* or *Cathodic Protection* provide methods to control corrosion in aqueous conditions, where corrosion is an electrochemical process.

*Anodic Protection* is an electrochemical method used for the corrosion protection in which an external current is applied onto the metal to passivate it [2.6, 2.30]. Thus, this method can be applied only to metals that passivate. The potential is maintained at a suitable level, which is more anodic compared to the corrosion potential, by passing a controlled current. The applied potential and current must be very carefully controlled with the help of a reference electrode, otherwise the metal can corrode very fast.

In an Anodic Protection system, the positive pole of the DC current supply is connected to the structure to be protected, while the negative side is connected to the cathode dipped in the solution. The externally applied current drives the potential of the structure in the electropositive direction until it reaches the passive region.

*Cathodic Protection* is one of the most effective means for corrosion prevention [2.6]. In this method the oxidation reaction is concentrated at the anode suppressing corrosion of the cathode in the same cell. The principles of cathodic protection are presented in detail in the next section.

The difference between the Anodic and the Cathodic Protection is that in Anodic Protection the structure to be protected is the anode, while in Cathodic Protection it is the cathode. Cathodic Protection can, in principle, be applied to any metal, but Anodic Protection can be used on only a limited number of alloys in certain restricted environments.

#### *2.1.2.2 Principles of Cathodic Protection*

The principle of Cathodic Protection is in connecting an external anode to the metallic structure to be protected and passing of an electrical DC current, in order to turn all the areas of the metal surface into a cathode and therefore mitigate corrosion. In electrochemical terms, the electrical potential between the metal and the electrolyte

solution becomes more negative, by the supply of negative charged electrons, to a level at which the anodic reactions (corrosion) are stifled and only cathodic reactions can take place [2.6, 2.13, 2.35].

There are two methods for the application of Cathodic Protection, the Impressed Current Cathodic Protection (ICCP) and the Sacrificial Anode Cathodic Protection (SACP) [2.3, 2.6, 2.9, 2.36]. The ICCP systems employ inert (zero or low dissolution) anodes and use an external electrical DC power source (rectifier) to impress a current from the external anode onto the surface of the cathode, as shown in **Figure 2-3**. Sacrificial Anode systems employ reactive metals as anodes, which are electrically connected directly to the metal to be protected. The difference in natural corrosion potentials between the anode and the structure material, as approximately indicated by their relative positions in the EMF series, causes a positive current to flow in the electrolyte, from the anode to the cathode. In this way, the whole surface of the structure becomes the cathode. A SACP system is shown in the **Figure 2-4**.

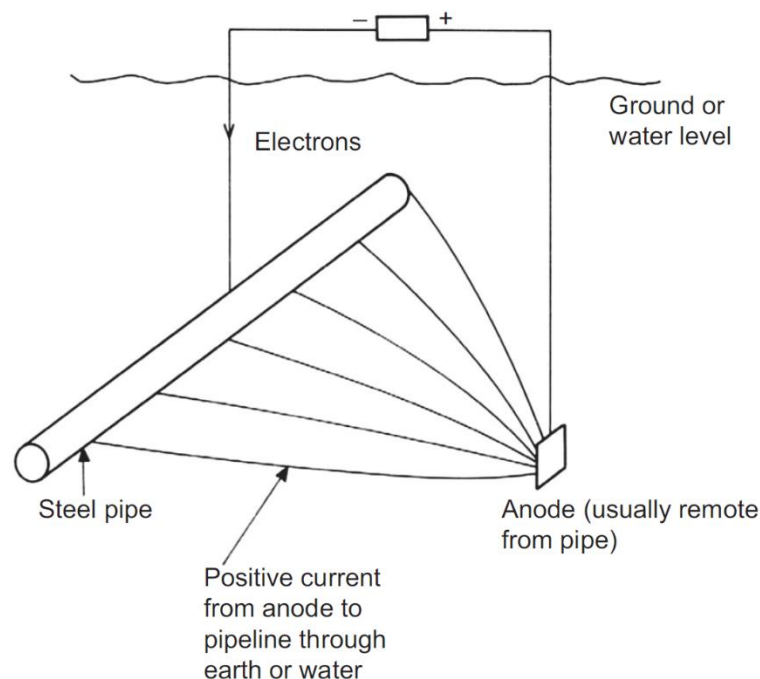


**Figure 2-3.** Application of Cathodic Protection by an Impressed Current system [2.9].

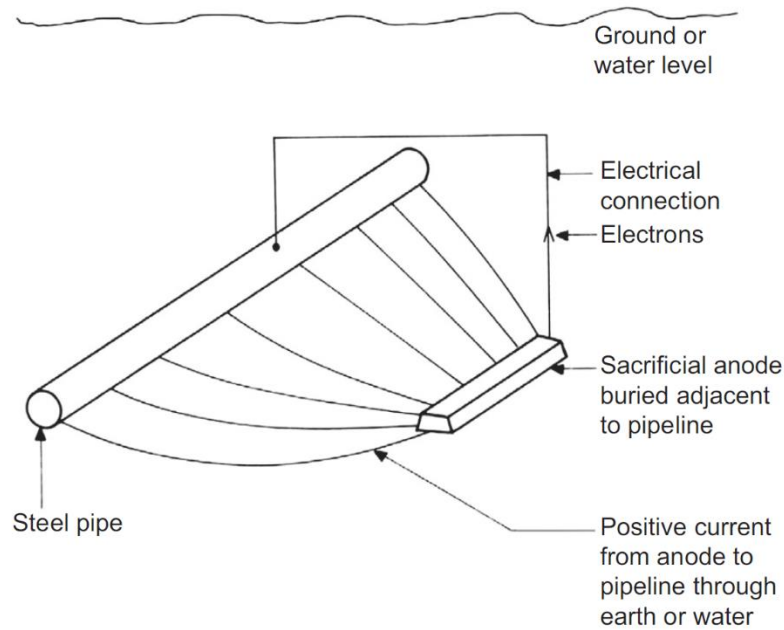


**Figure 2-4.** Application of Galvanic (Sacrificial Anode) Cathodic Protection [2.9].

Designers typically select ICCP systems for high current requirements and/or high resistivity environments. Since an external power supply is required, these systems can be electronically monitored and controlled, so that the current output and voltage can be adjusted to changes in the protection requirements of the structure. These systems have the disadvantage of increased maintenance and power costs and because of higher current output the risk of electrical interference with other metallic structure becomes more important [2.3].

Galvanic anodes have relatively small, fixed driving potentials and the consumption rate is a necessary result of CP current discharge. For these reasons SACP systems are preferred in designs where the environment resistivity is low and/or the current output is small. Also, as the current requirement for a specific case increases, the galvanic anode weight needed increases proportionally. Typical situations where SACP systems are preferable include: internal surfaces of small vessels and structures in seawater environments.

### 2.1.2.3 Cathodic Protection Criteria

The potential of steel structures under cathodic protection must be sufficiently polarised. The following criteria are commonly used to evaluate sufficient polarisation:

- The Potential Criterion

According to this criterion, the cathodic potential of the steel structure that is cathodically protected must be at specific value or more electronegative. In [2.3, 2.37-2.40] it is suggested that a potential of -800mV vs Ag/AgCl/seawater reference electrode is generally accepted as the design protective potential for carbon and low-alloy steels. For valid interpretation of this voltage measurement, voltage drops other than those across the structure to electrolyte boundary must be considered [2.41].

- The 100 mV Polarisation Shift Criterion

This criterion refers to a minimum of 100mV cathodic polarisation between the structure surface and a stable reference electrode contacting the electrolyte [2.41].

The theoretical basis of this criterion begins with the assumption that the corrosion cell is operating under cathodic control. It is also assumed that the difference in the open circuit potential of the most active anode on the structure and the corrosion potential of the structure is 100mV or less. Thus, if the structure is cathodically polarised by an external source by at least 100mV, there will be no potential difference between the anodes and cathodes on the structure and corrosion will cease [2.3].

Since it is easier to perform, the -800mV<sub>SSC</sub> criterion is usually preferred. This criterion is reliable only at pH values close to neutral pH conditions and at low temperatures and also IR ohmic potential reduction must be taken into account. The 100mV polarization shift criterion is good due to not including an ohmic IR reduction.

### 2.1.2.4 Sacrificial Anodes

Galvanic anodes are chosen among metals or alloys that are more active compared to the metal to be protected [2.6]. Anode materials should have certain electrochemical characteristics. They should have sufficiently electronegative corrosion potential and enough polarisation to allow for adequate current flow.

Furthermore, materials or alloys used as anodes must have high electrochemical capacity and also high efficiency [2.13]. The materials commonly used as sacrificial anodes are Aluminium, Zinc and Magnesium [2.3, 2.6, 2.13]. These metals are alloyed in order to improve their performance.

Magnesium has a very electronegative corrosion potential, compared to the other materials and also low polarisation. For that reason Magnesium alloys are primarily used in environments such as high resistivity soils and fresh water [2.6, 2.13]. Their use in high conductivity environments is not recommended as they may cause overprotection and also their service lives may be significantly shortened.

Aluminium alloys are not recommended as sacrificial anode materials in low conductivity soils and fresh water, where they may passivate [2.13]. They are usually used in seawater and in brackish waters that are slightly salted [2.6]. As the chloride ion content of the environment decreases below normal seawater levels, the anode potential becomes more electropositive and the current capacity decreases [2.3].

The combination of corrosion potential, high efficiency and low polarisation makes Zinc sacrificial anodes the ideal choice for seawater applications [2.13]. Although the capacity of Zinc is lower than the other sacrificial anode materials, its electrochemical capacity is relatively independent of current density. An efficiency of 90% is anticipated even at very low current density levels [2.3].

### 2.1.3 Fatigue

#### *2.1.3.1 Basic Principles of Fatigue*

Materials subjected to cyclic loads may fail under stress values much lower than those needed for fracture under static loading [2.42]. This failure mechanism is called *Fatigue*. It is caused by the simultaneous action of cyclic stress, tensile stress and plastic strain. Unless all of these three are present fatigue crack will not initiate and propagate. The plastic strain resulting from cyclic stress initiates the crack and the tensile stress promotes crack propagation. Compressive stresses will not cause fatigue but compressive loads may result in local tensile stresses, as stated in [2.43-2.44].

During fatigue micro-cracks form, coalesce or grow to macro-cracks that propagate until the fracture toughness of the material is exceeded and final fracture occurs [2.43]. Fatigue cracks, usually initiate near or at singularities that lie on or just below the surface of the metal, such as scratches, pits, inclusions, sharp changes in cross section and embrittled grain boundaries. Micro-cracks can be initially present due to heat treatment, welding and mechanical forming. Fatigue cracks may form even in a flaw-free metal with highly polished surface and no stress concentrators.

If the stress level is high enough, it may lead to slip steps on the surface due to the plastic deformation (i.e. long-range dislocation motion) that takes place [2.43, 2.45-2.46]. If the cyclic loading continues, it will lead to the initiation of one or more fatigue cracks that can be observed using modern microscopy techniques, such as Scanning Electron Microscopy (SEM). Alternately, the dislocations pile up against an obstacle (e.g. an inclusion or grain boundary), forming a slip band, a cracked particle, de-cohesion between particle and matrix or de-cohesion along the grain boundary. The micro-cracks will propagate or link up to form one or more macro-cracks, which will grow until the fracture toughness is exceeded, leading to material fracture.

### 2.1.3.2 Fatigue Cycle

Fatigue life is measured in loading cycles ( $N$ ). There are two phases in the fatigue life of a material. The first phase consists of the number of the loading cycles needed in order for the crack to initiate ( $N_i$ ), while the second phase consists of the number of loading cycles ( $N_p$ ) that will cause the crack to propagate up to the critical length, as stated in [2.42, 2.47].

$$N = N_i + N_p \quad (2-8)$$

The parameters of a fatigue loading cycle are the stress range ( $\Delta\sigma$ ), stress amplitude or alternating stress ( $\sigma_\alpha$ ), mean stress ( $\sigma_m$ ) and stress ratio ( $R$ ) [2.31, 2.42]:

$$\Delta\sigma = \sigma_{max} - \sigma_{min} \quad (2-9)$$

$$\sigma_\alpha = \frac{\Delta\sigma}{2} = \frac{\sigma_{max} - \sigma_{min}}{2} \quad (2-10)$$

$$\sigma_m = \frac{\sigma_{max} + \sigma_{min}}{2} \quad (2-11)$$

$$R = \frac{\sigma_{min}}{\sigma_{max}} \quad (2-12)$$

There are three types of cyclic loading in fatigue testing of materials. These are, the fully reversed loading, the repeated stress loading and the general case of cycling loading about a non-zero mean stress [2.31]. As illustrated in **Figure 2-5**, the test specimen is subject to a stress cycle range between equal values of tensile and compressive stress. In this type of loading the mean stress is zero and the stress ratio is equal to -1.

$$R = \frac{-\sigma}{\sigma} = -1 \quad (2-13)$$

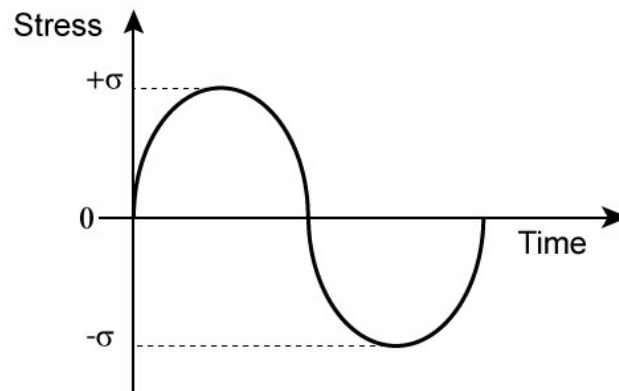


**Figure 2-5.** Fully reversed load cycle [2.31].

In the case of the repeated stress loading, the stress varies between zero and a maximum tensile stress, as shown in **Figure 2-6**.

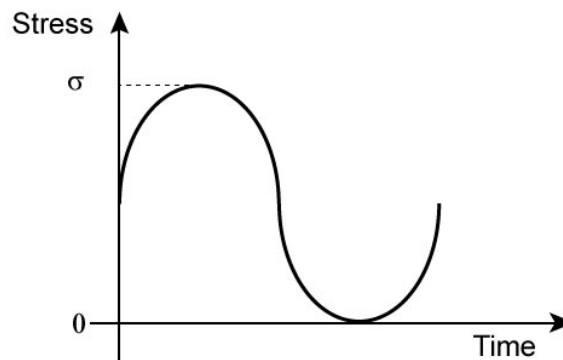


**Figure 2-6.** Repeated stress load cycle [2.31].

In this type of fatigue loading, the stress ratio is equal to zero.

$$R = \frac{0}{\sigma} = 0 \quad (2-14)$$

The general case of cycling loading about a non-zero mean stress, is illustrated in **Figure 2-7**.

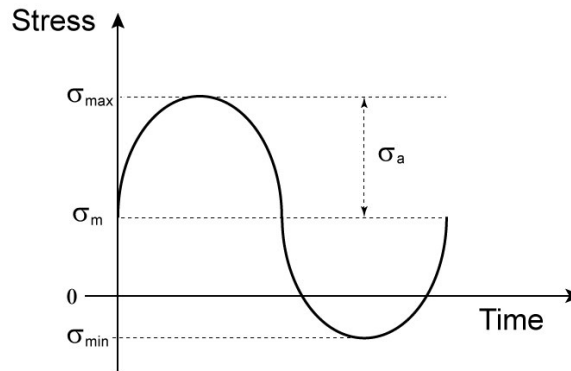


**Figure 2-7.** Load cycle about a non-zero mean stress [2.31].

#### 2.1.3.3 Fatigue Analysis Methods

Fatigue tests are classified as crack initiation or crack propagation [2.43]. In crack initiation testing, the specimens are subject to the number of stress controlled (stress-life, S-N) or strain-controlled (strain-life,  $\epsilon$ -N) cycles required for a fatigue crack to initiate and propagate enough to produce failure. The first concerns low stress levels, causing mainly elastic strains leading to a fatigue life that exceeds  $10^3$  to  $10^4$  cycles and it is also known as high cycle fatigue. In the second case, the cyclic stresses cause significant plastic strains leading to a fatigue life that does not exceed  $10^3$  to  $10^4$  cycles and it is also known as low cycle fatigue [2.42]. Crack initiation (fatigue life) testing can be further classified based on the mode of loading, such as direct (axial) stress, plane bending, rotating beam, alternating torsion and combined stress. In crack propagation testing, fracture mechanics methods are used to determine the rates of the crack growth of pre-existing cracks under cyclic loading.

The results of the stress-life fatigue testing are plotted in a diagram known as S-N plot or Wöhler curve. In this diagram, stress range (S) is plotted versus the number of cycles to failure (N), usually in a logarithmic scale [2.48]. From these diagrams, the endurance limit ( $S_e$ ), if applicable, can be measured, as shown in **Figure 2-8**. The endurance limit defines the stress amplitude, below which the material does not fail under fatigue loading, usually considered to be  $10^6$  cycles for engineering purposes.

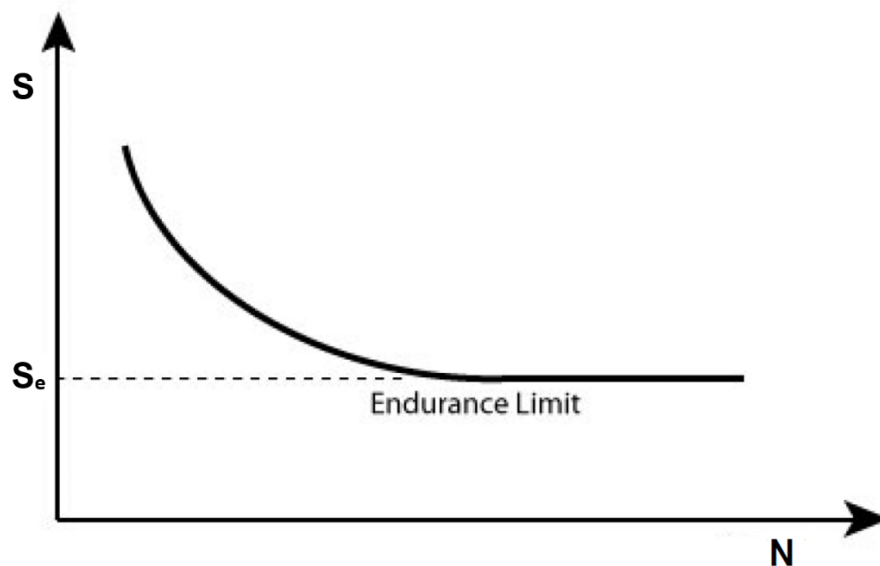


**Figure 2-8.** S-N plot with endurance limit.

A major drawback of the stress-life approach is that it does not take into account the true stress-strain behaviour and treats all strains as elastic [2.49]. Since the initiation of fatigue cracks is caused by plastic deformation, this might be important. This simplifying assumption of the stress-life approach is valid only if the plastic strains are small. Most steels, at long lives, have only a small component of cyclic strain which is plastic and the S-N approach is valid.

#### *2.1.3.4 Factors Affecting Fatigue Life*

- Surface finish

Almost all fatigue failures practically start at the surface. For types of loading, like bending and torsion, the maximum stress occurs at the surface, so it is logical that most failures should start from there. However, fatigue failure in axial loading nearly always starts from the surface also [2.50]. For this reason, surface condition has a great effect on the fatigue life of a material. Scratches, pits and machining marks on the surface add stress concentrations to the ones already present, due to a component's geometry. High strength steels, as uniform fine-grained materials, are more adversely affected by a rough surface finish compared to coarse-grained materials, such as cast iron [2.49]. The condition of surface finish has higher effect on long fatigue lives, where crack initiation dominates.

- Environment

Fatigue loading in a corrosive environment results in more detrimental effects than would be expected by considering fatigue and corrosion separately. This interaction is called corrosion-fatigue. In a corrosive environment the stress level at which a material could be assumed to have infinite life is lowered or removed completely [2.51].

In corrosion-fatigue conditions a corrosive environment attacks the surface of a metal, producing an oxide film. This oxide film usually serves as a protective layer, preventing further corrosion of the metal. Fatigue loading causes localised cracking of this layer, exposing fresh metal surface to the corrosive environment. At the same time corrosion causes localised pitting of the surface that serves as stress concentrations.

Corrosion-fatigue depends on many factors that may influence the performance of the metal. Considering the important combination of steel in water, some variables that have to be taken into account are the alloying elements of the steel, the chemical composition of the water, the temperature, the degree of aeration and the flow velocity. Another very critical variable is the loading frequency. In non-corrosive environments, fatigue tests can be run at almost any frequency and similar data will be obtained, but in corrosive environments corrosion fatigue data are greatly influenced by loading frequency [2.49]. More time for corrosion to take place is allowed in low frequency tests, resulting in shorter fatigue lives.

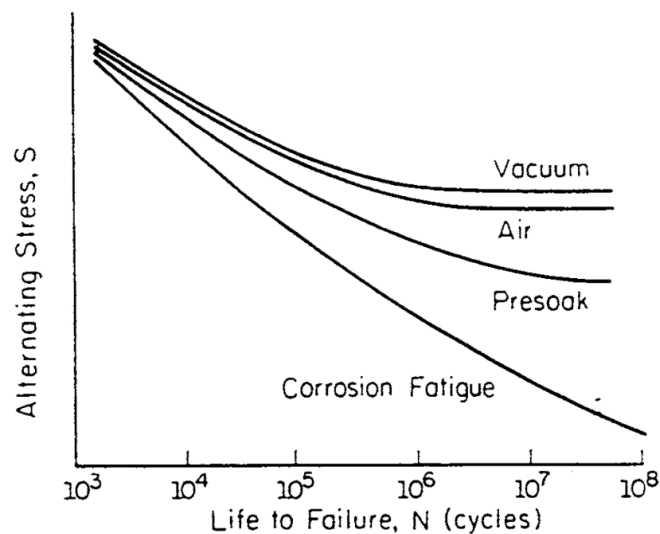


**Figure 2-9.** Effect of various environments on the S-N curve of steel [2.49].

Some general trends of corrosion fatigue are shown in **Figure 2-9**. It is observed that the curves generated in room air and in a vacuum are slightly different, due to the presence of humidity and oxygen in room air. Also, due to the rough surface caused by corrosion pitting, the curve of the pre-soaked steel indicate a reduction in fatigue properties. The corrosion-fatigue curve is significantly below the room air one, indicating also the elimination of the fatigue limit of the steel.

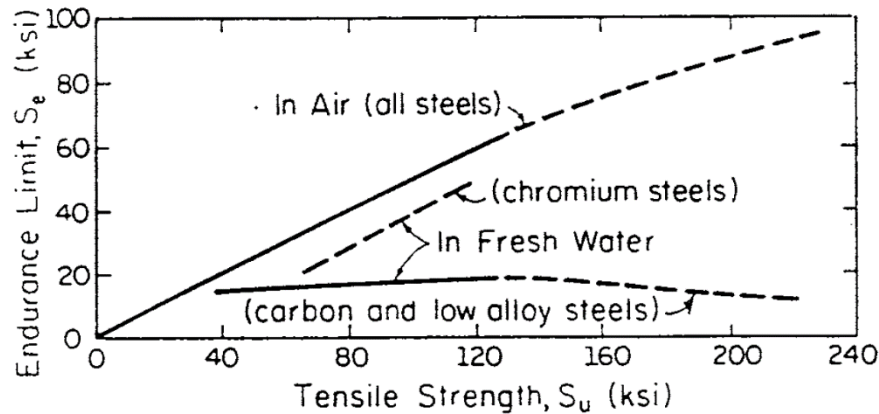


**Figure 2-10.** Influence of tensile strength and chemical composition on corrosion fatigue strength of steels [2.49].

Another important trend in corrosion-fatigue is presented in **Figure 2-10**, showing the endurance limits of various steels in room air and fresh water environments. The data for carbon and low alloy steels show that higher strength steels have no advantage in a corrosive environment. Significantly better corrosion fatigue resistance is observed for steels with a higher chromium content. It is a general trend that steels which are resistant to corrosion alone also show good corrosion-fatigue properties [2.49].

## 2.2 Review of the Effect of Cathodic Protection on Corrosion Fatigue Life

### 2.2.1 Introduction

It has already been seen that corrosion dramatically reduces the fatigue properties of steels. Corrosion-fatigue behaviour of low corrosion resistant steels has been investigated for several decades. Fatigue tests have been conducted in air and in

several corrosive environments varying from 1% to 4% NaCl aqueous solutions. The resistances against corrosion play the most important role in the corrosion-fatigue performance of materials and the corrosion potential is generally used as the measure of the corrosion resistance.

Methods for improving the corrosion-fatigue (CF) performance of steels, have been the subject of interest for many researchers. The selection of a system in order to achieve corrosion protection and minimise the influence of the environment on fatigue behaviour, is essential to secure the integrity of steel components. Cathodic protection (CP) has been found to be an effective method for protection of steels against corrosion, driving the fatigue life back to the in-air levels. Impressed current (ICCP), sacrificial anodes (SACP) and sacrificial coatings (SCCP), are cathodic protection methods that have been tested successfully.

In the following paragraphs, the effect of corrosion on the fatigue life of steels in corrosive environments, is reviewed. The factors affecting corrosion-fatigue performance of smooth (un-notched) steel specimens are analysed. Moreover, a review has been done on the effectiveness of cathodic protection in restoring the in-air fatigue properties of steels. Critical environmental parameters, influencing the function of a cathodic protection system, have to be taken into account for the successful application of this protection method.

In **Table 2-1**, the chemical compositions of the materials referred to in the review, are presented.

**Table 2-1.** Chemical composition of the steels (wt%).

Steel	C	Si	Mn	P	S	Cr	Ni	Mo	Cu	N	Al	Ref.
<b>AISI 1020</b>	0.20	-	0.46	0.005	0.020	-	-	-	-	-	-	[2.52]
<b>20</b>	0.21	0.26	0.56	Within limits	Within limits	-	-	-	-	-	-	[2.53]
<b>40</b>	0.39	0.29	0.78	Within limits	Within limits	-	-	-	-	-	-	[2.53]
<b>35</b>	0.35	0.32	0.77	0.022	0.027	-	-	-	-	-	-	[2.54]
<b>1Kh14NDL</b>	0.07	0.33	0.47	0.013	0.014	13.52	1.35	-	1.28	-	-	[2.54]
<b>ASTM A537B</b>	0.20	0.15-0.50	0.70-1.40	0.350	0.040	0.250	0.25	0.08	0.35	-	-	[2.55]
<b>S15C</b>	0.16	0.27	0.49	0.026	0.025	-	-	-	-	-	-	[2.56]
<b>S35C</b>	0.34	0.27	0.70	0.022	0.014	-	-	-	-	-	-	[2.56]
<b>SK5</b>	0.85	0.28	0.50	0.011	0.006	-	-	-	-	-	-	[2.56]
<b>C. steel "A"</b>	0.44	0.21	0.08	0.033	0.026	-	-	-	-	-	-	[2.57]
<b>C. steel "B"</b>	0.17	0.144	0.42	0.200	0.053	-	-	-	-	-	-	[2.57]
<b>C. steel "C"</b>	0.44	0.27	0.49	0.016	0.021	-	-	-	-	-	-	[2.57]
<b>AISI 4140</b>	0.41	0.27	0.81	0.012	0.015	0.990	0.10	0.16	-	0.013	0.044	[2.58]
<b>E36Z</b>	0.145	0.292	1.40	0.006	0.003	0.075	0.42	0.031	-	0.012	0.019	[2.59]
<b>HY-80</b>	0.132	0.20	0.30	0.011	0.017	1.72	2.49	0.41	-	-	-	[2.60]

## 2.2.2 Review of the Effect of Corrosion on Fatigue Life

Corrosion-fatigue is an important but complex mode of failure of steels operating in deleterious environments. At long corrosion-fatigue lives, the total number of cycles to failure reported for most small laboratory specimens is predominantly made up of crack initiation. A review [2.61] of the hypotheses of corrosion mechanisms proposed to explain the initial cracking of a metal undergoing corrosion-fatigue in aqueous solutions including but not restricted to seawater. Pitting, preferential anodic dissolution, passive film rupture, and surface adsorption were found to have some merit, but no one could explain all of the phenomena included in corrosion-fatigue failures. A more general hypothesis reflects the combined attack of the environment and cyclic stress, recognising that the mechanism of crack initiation may be slightly different for different metal/environment combinations. There are examples in the literature of the role that certain corrosion variables play in the corrosion-fatigue of steels in saline solutions and seawater. In all cases, a continuous decrease in fatigue strength, as cyclic life increased, was observed for unprotected steel. In other words, the knee or fatigue limit usually observed for constant amplitude cycling of steels in air was not present. Available corrosion-fatigue data on constant amplitude cycling of un-notched specimens are presented in the following paragraphs.

The corrosion-fatigue behaviour of steels in aqueous solutions, has been investigated by several researchers [2.52-2.57, 2.61]. In most of these studies, saltwater or synthetic seawater solutions were used. It has been reported [2.31] that a 4% NaCl tap water solution has been tested, showing a deleterious effect on corrosion-fatigue life compared to in air levels. In [2.56-2.57], a low salinity level (1% NaCl) aqueous solution was used in the experiments. Endo and Miyao [2.57] conducting tests in tap water and 1% NaCl aqueous solution, showed that even a small increase in the salinity level, has a significant effect on the corrosion-fatigue strength. The fatigue life of the material was further reduced in the 1% NaCl aqueous solution. In all cases, a continuous decrease in fatigue strength as cyclic life increased was observed for unprotected steel. In this way, the fatigue limit observed in air was eliminated.

It has been seen that dissolved oxygen content plays an important role in the degrading influence of saltwater solutions on the corrosion-fatigue resistance of AISI 4140 steel [2.58]. The fatigue resistance continued to decrease at longer lives for aerated 3% sodium chloride (NaCl) solution, but an apparent fatigue limit about the

same magnitude as that observed in air was present in deaerated 3% NaCl solution. Thus, it is obvious that oxygen content dominates the corrosion-fatigue behaviour enhancing the initiation of corrosion-fatigue damage, while its absence results in fatigue life levels similar to the in air conditions. Any corrosion variable that increases the oxygen content, raises the overall corrosion rate, attacks or disrupts calcareous deposits or corrosion products or generates a local attack that may degrade corrosion-fatigue resistance significantly.

The effect of cycle frequency has been investigated and it has been shown that corrosion-fatigue life is greatly affected by this factor. Endo and Miyao [2.57] found that decreasing from 42.5 to 4.08 Hz for corrosion-fatigue in 1% NaCl solution decreased the cyclic life by a factor of about 2.5 in the range of  $10^6$  to  $10^7$  cycles to failure. This frequency effect seems to be related to the time dependence of corrosion. Failure occurs with fewer total cycles at the lower frequencies.

Other factors affecting corrosion fatigue resistances have been reported [2.61]. It has been seen that the effect of varying pH on corrosion fatigue in saline solutions, over a broad range of pH, from about 4 to 10, has little or no effect on fatigue resistance. Very low pH values (less than 4) caused fatigue life to decrease, and very high ones (greater than 10 to 11) gave improved fatigue resistance approaching that expected in air. The effect of temperature has also been investigated and it was shown that increases in temperature over the range of 15 to 45°C caused small decreases in fatigue life for tests in artificial seawater.

### 2.2.3 Review of the Effect of Cathodic Protection (CP) on Corrosion Fatigue

A protection potential of 0.2 to 0.3V more negative than the free corrosion potential was found to reduce the corrosion rate of carbon steel by 99% [2.61]. Tests conducted on smooth steel specimens have shown that cathodic polarization to  $-730\text{mV}_{\text{SCE}}$  nullified the negative effect of aqueous solutions on the fatigue strength and the fatigue limit observed in air was practically restored [2.59]. This potential is slightly more positive compared to the generally referenced value to mitigate general corrosion in natural waters,  $-780\text{mV}_{\text{SCE}}$  or  $-850\text{mV}_{\text{CSE}}$  or  $-800\text{mV}_{\text{SSC}}$ . The experimental data showing the beneficial effect of CP on the corrosion-fatigue strength of carbon steels indicated in **Figure 2-11**, were obtained from tests conducted on E36Z steel

specimens. The fatigue life of E36Z steel in seawater increased as the applied cathodic potential became more negative than the open-circuit potential. At the potential level of  $-850\text{mV}_{\text{SCE}}$ , the lifetime was equal to that obtained in air. Similar conclusions were reached by Hudgins et al. [2.52], who tested AISI 1020 specimens in synthetic seawater, indicating that in-air fatigue performance can be attained at  $-750\text{mV}_{\text{SSC}}$ . Lyashchenko et al. [2.54] used a more negative potential of  $-1.0\text{V}_{\text{SCE}}$  to restore the in air fatigue resistance in smooth 35 steel grade specimens. Salama and Thomason [2.33] stated that the maximum fatigue strength appears to exist around the  $-900\text{mV}_{\text{SCE}}$  potential, for a high strength steel tested in synthetic seawater, as can be seen in **Figure 2-12**. According to their results this cathodic potential would be needed in order to achieve the maximum fatigue life and at the same time minimise the effect of hydrogen embrittlement, which seems to occur at potentials more negative than the optimum suggested by the authors. It may be useful at this point, to note that even at lower potentials than those suggested for complete protection, there is still some improvement in the corrosion fatigue behaviour of the materials. Thus, it seems that sufficient and even overprotection by cathodic polarisation will improve corrosion-fatigue performance of carbon steels, up to levels observed in air. Care must be given to high strength steel grades that may be vulnerable to hydrogen embrittlement when cathodically protected at very negative potentials.

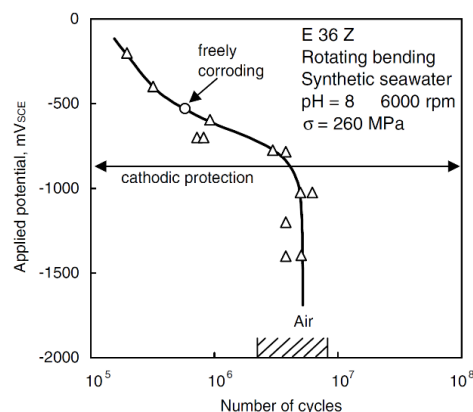


**Figure 2-11.** The effect of cathodic potential on the corrosion fatigue lifetime [2.59].

The test type used to produce the data presented in **Figure 2-11**, do not allow for separating the crack growth stage, which is of special practical interest, from the total corrosion-fatigue life that includes five stages of material failure: a) nucleation of crack/defect(s), b) initiation of crack(s) from the nucleus/defects, c) growth of small mutual cracks, d) growth of subcritical crack(s) and e) final fracture of the material.

The effectiveness of a cathodic protection system in mitigating the effect of corrosion on fatigue behaviour of steels, depends on various factors. Increased oxygen level, decreased temperatures and increased flow velocity generally will result in the need for increased current densities in order to maintain adequate protection levels [2.59].

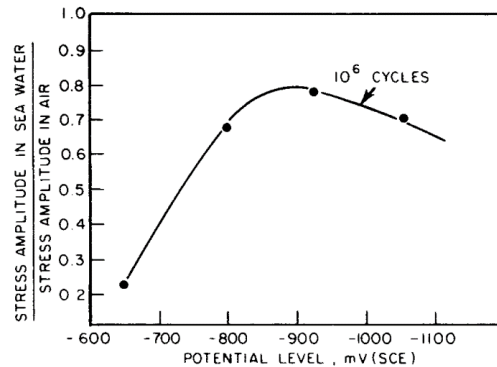


**Figure 2-12.** Effect of cathodic protection potential on the ratio between fatigue strength (stress amplitude) in seawater and that in air for 3½ Ni-Cr-Mo-V steel [2.33].

The most common cathodic protection method used in laboratory tests, for the investigation of the effect of CP on corrosion-fatigue life of steels, is the Impressed Current Cathodic Protection (ICCP). However, it has been seen that some investigators have used Sacrificial Anode Cathodic Protection (SACP) and Sacrificial Coating Cathodic Protection (SCCP). Lyashchenko et al. [2.54] used zinc and magnesium alloy anodes, that were made in the form of two half rings placed close to the gauge length of the samples. The relationship of the areas of the anode and the protected sample was 1:2 and the effectiveness of the anodes was measured on the basis of the sample potential. It was stated by the authors that the potential of  $-1.0V_{SCE}$  achieved by zinc anodes in seawater led to further increase of the fatigue limit compared to the  $-0.9V_{SCE}$  applied by an impressed current system, on 1Kh14NDL steel samples. When magnesium anodes were used, a potential of  $-1.45V_{SCE}$  was reached that decreased the fatigue limit compared to the levels achieved by zinc anodes, possibly due to hydrogen embrittlement. Moreover, zinc anodes restored the in air fatigue strength of 35 steel grade samples, eliminating the effect of corrosion. Magnesium anodes were used also by Havens and Bench [2.55] for the protection of a carbon steel in synthetic seawater. Reaching a potential more negative than  $-850mV_{CSE}$ , they showed that cathodic protection eliminated corrosion and drove the fatigue strength of the material back to the in air levels. Salama and Thomason [2.33] suggested that the use of a properly applied flame-sprayed aluminium (FSA) coating

represents the optimal corrosion protection method for providing improved corrosion fatigue performance of an offshore structural high-strength steel (3½ % Ni-Cr-Mo-V steel) and at the same time avoid hydrogen embrittlement problems. The authors considered three types of corrosion protection strategies: cathodic protection, inert coatings with cathodic protection and anodic coatings (sacrificial coating cathodic protection). A common approach for the protection of offshore structures is the use of sacrificial anodes of either zinc or aluminium alloys, but this method can possibly cause overprotection that may result in hydrogen embrittlement of the high-strength steel. The inert coatings, including conventional epoxies, fusion-bonded epoxies and heat-shrink sleeves, provide a physical barrier as long as they are continuous over the components. Cathodic protection backup protects uncoated areas or areas where the coating is damaged, but the problem of hydrogen embrittlement may still be present. Metal-sprayed zinc and aluminium anodic coatings, remain effective even when the coating is ruptured locally, acting as sacrificial anodes. Tests conducted in flowing synthetic seawater at 1/6 Hz showed that a uniform potential of around -900mV<sub>SCE</sub>, provided by flame-sprayed aluminium coating, resulted in longer fatigue lives than those of specimens protected by aluminium anodes. Aluminium anodes polarised the high strength steel to a potential level of -1050mV<sub>SCE</sub>, that may have caused hydrogen embrittlement.

#### 2.2.4 Conclusions

From this review of available data on corrosion-fatigue behaviour of low corrosion resistance steels and the effectiveness of cathodic protection methods in mitigating the effect of corrosion on fatigue life, it is concluded that CP is a successful corrosion protection method in eliminating the effect of corrosion, driving the fatigue lives back to the in air levels. Proper design and application of a CP system is expected to protect a low alloy steel grade (S355J2G3+N), that is used for the construction of PD pump components, working in severe applications.

An experimental programme has to be conducted in order to investigate the corrosion-fatigue performance of the material in a low salinity aqueous solution (824ppm NaCl), causing unexpected failures, according to the initial design. CP systems, have not yet

been applied in such a low salinity level solution and it may be proved that these methods can be used successfully.

The current WEIR Minerals design procedure suggests that when the pumps are working in a higher salinity level aqueous environment, stainless steels have to be used. These materials significantly increase the production cost of the pumps. As has been already found in the literature, this can be avoided by the use of low alloy steels, cathodically protected. Experiments are expected to prove the effectiveness of CP in high salinity water, on the sufficient protection of S355J2G3+N steel grade and restore its fatigue performance.

Sacrificial Anodes (SACP), Sacrificial Coatings (SCCP) and Impressed Current (ICCP) are corrosion protection methods that have already been tested successfully. SACP and SCCP are more cost effective methods than ICCP, because no extra equipment (rectifier) and external power supply is needed. Sacrificial anodes and sacrificial coatings are directly connected to the structure to be protected. For their application simplicity and cost effectiveness, those two methods are suggested for the experimental programme.

Finally, a sacrificial coating is expected to provide a uniform protection potential on the coated surface, while in the case of sacrificial anodes, the use of a modelling software will be useful in the optimisation of the design procedure, in terms of anode sizing, attenuation and prediction of system's service life.

## **2.3 Numerical Simulation of Cathodic Protection Systems**

### 2.3.1 Introduction

As the structures to be protected become more complex, the traditional methods for designing cathodic protection systems become less reliable [2.62]. These methods depend mostly on the individual experience and skills of a corrosion engineer and on the simple formulas that are used in designing the cathodic protection systems under the guidance of standards and criteria (e.g. DNV RP-B401). Consequently, numerical methods are often used in the design of such systems in conjunction with the traditional methods. The numerical simulation of cathodic protection provides prediction of a system's performance before in-field installation. This technique reduces the dependency on the experience of the cathodic protection engineer

enabling him to calculate critical parameters and optimize the design of the system without the need of in-field measurements that may lead to adjustments causing disrupted schedules, re-installation costs and production downtime, as is stated in [2.63]. The modelling of a cathodic protection system helps the designer forecast parameters such as:

- The degree of protection provided by the system, by calculating potential and current distributions
- The total current demand and how this may change with time
- The consumption rates of the anodes
- The expected life of the anodes
- The optimum location of the anodes

Historically, since the late seventies computers have been used in the evaluation of the design of cathodic protection systems. The activity in the exploration and production of petroleum and gas in the North Sea has been the motivation to develop these more sophisticated methods for analysing cathodic protection.

### 2.3.2 Mathematical Background

A sacrificial anode cathodic protection system can be modelled as an electrical circuit where the driving force  $V$  is the potential difference between the anode and the cathode ( $V = \Delta\phi = \phi_c - \phi_a$ ), the resistance  $R$  is the resistance of the electrolyte and  $I$  is the current flowing between the anode and the cathode.

Ohm's law can be used to calculate the current flowing in an electrical circuit. In Ohm's law the current is a function of the driving voltage and the resistance, as is shown in the **Equation 2-15**.

$$\text{Ohm's law: } R = \frac{V}{I} \Rightarrow I = \frac{V}{R} \Rightarrow I = f(V, R) \quad (2-15)$$

The polarisation behaviour of the cathode and the anode (boundary conditions), is expressed in terms of electrode potential versus current density.

$$\text{Current density, } i: i = \frac{I}{A} \Rightarrow I = i \cdot A \quad (2-16)$$

Pouillet's law can be used to calculate the resistance of the electrolyte. According to Pouillet's law, the resistance of the electrolyte is a function of the resistivity, the length and the cross section area of the electrolyte, as can be seen in **Equation 2-17**.

$$\text{Resistance (Pouillet's law), } R: R = \rho \cdot \frac{l}{A} \quad (2-17)$$

where  $l$  is the distance between the anode and cathode surfaces.

$$\text{Conductivity, } \sigma: \sigma = \frac{1}{\rho} \quad (2-18)$$

where  $\rho$  is the resistivity of the electrolyte

Substituting **Equations 2-16, 2-17** and **2-18** into **Equation 2-15**:

$$I = \frac{V}{R} \Rightarrow i \cdot A = \frac{V}{\frac{l}{\rho \cdot A}} \Rightarrow i \cdot A = \frac{V \cdot A}{\rho \cdot l} \Rightarrow i \cdot A = \frac{1}{\rho} \cdot A \cdot \frac{V}{l} \Rightarrow i = \frac{1}{\rho} \cdot \frac{V}{l} \Rightarrow i = \sigma \frac{V}{l} \Rightarrow$$

$$i = \sigma \frac{\varphi_c - \varphi_a}{l} \quad \text{or} \quad i = \frac{\varphi_c - \varphi_a}{\rho \cdot l} \quad (2-19)$$

Thus, it is obvious that current density is a function of the driving force, the conductivity and the distance between the anode and cathode surfaces.

Considering a control volume with sides  $\Delta x$ ,  $\Delta y$ ,  $\Delta z$  in an electrolyte of uniform conductivity ( $\sigma = \text{const.}$ ) and using the property of the proportionality of current density to the gradient of the electrical potential,  $\varphi$ , the continuum version of Ohm's law is obtained, as suggested in [2.64-2.65]:

$$\underline{i} = \sigma \cdot \nabla \varphi \Rightarrow \underline{i} = \begin{bmatrix} i_x \\ i_y \\ i_z \end{bmatrix} = \sigma \begin{bmatrix} \frac{\partial \varphi}{\partial x} \\ \frac{\partial \varphi}{\partial y} \\ \frac{\partial \varphi}{\partial z} \end{bmatrix} \quad (2-20)$$

where  $\underline{i} = (i_x, i_y, i_z)$  is the current density vector.

In [2.66], it is stated that during corrosion processes, there is no gain or loss of electrical charge, but just transfer of it. The continuity of electrical charge requires that the accumulated net charge in the control volume must be zero:

$$\text{div}(\underline{i}) = \frac{\partial i_x}{\partial x} + \frac{\partial i_y}{\partial y} + \frac{\partial i_z}{\partial z} = 0 \quad (2-21)$$

Substituting **Equation 2-20** into **Equation 2-21** and assuming that the medium is homogeneous, the conductivity can be eliminated and the equation reduces to the Laplace equation, which is a partial differential equation:

$$\frac{\partial}{\partial x} \left( \sigma \frac{\partial \varphi}{\partial x} \right) + \frac{\partial}{\partial y} \left( \sigma \frac{\partial \varphi}{\partial y} \right) + \frac{\partial}{\partial z} \left( \sigma \frac{\partial \varphi}{\partial z} \right) = 0 \Rightarrow \frac{\partial^2 \varphi}{\partial x^2} + \frac{\partial^2 \varphi}{\partial y^2} + \frac{\partial^2 \varphi}{\partial z^2} = 0 \Rightarrow \nabla^2 \varphi = 0 \quad (2-22)$$

In order for the model to be complete, the boundary conditions should be defined for the surfaces involved in the model. At the electrode surface, the current density is related to the potential through the polarisation curve, as is shown in **Equation 2-23** that is a Neumann type boundary condition.

Neumann Boundary Condition (at polarized electrode surfaces):

$$i_n = \frac{\partial \varphi}{\partial n} = f(\varphi) \quad (2-23)$$

where  $n$  is the normal vector to the electrode surface.

The insulated surfaces are not polarised (current density is assumed to be zero) and therefore a Dirichlet type boundary condition may be used, as is shown in **Equation 2-24**.

Dirichlet Boundary Condition (at insulated surfaces):

$$i_n = \frac{\partial \varphi}{\partial n} = 0 \quad (2-24)$$

where  $n$  is the normal vector to the insulated surface.

Summing up, in steady state and for a uniform, isotropic electrolyte system, the potential obeys the Laplace equation, which is the governing equation for electrochemical corrosion, as stated in [2.67]. The mathematical formulation of the boundary value problem for a domain  $\Omega$ , is illustrated in **Figure 2-13**:

$$\nabla^2 \varphi = 0 \quad \text{in } \Omega, \text{ Electrolyte Domain} \quad (2-25)$$

Laplace equation is solved using the following boundary conditions:

$$i_n = f_c(\varphi) \quad \text{on } \Gamma_1, \text{ Cathode} \quad (2-26)$$

$$i_n = f_a(\varphi) \quad \text{on } \Gamma_2, \text{ Anode} \quad (2-27)$$

$$i_n = 0$$

on  $\Gamma_3$ , Insulated

(2-28)

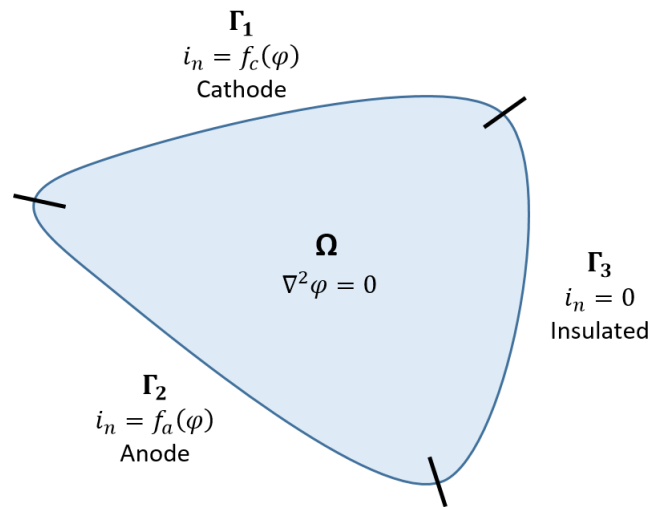


**Figure 2-13.** Mathematical formulation for a uniform, isotropic electrolyte domain  $\Omega$ .

In most cases the boundary conditions are of non-linear nature, meaning that the polarisation behaviour is not linear. Because of this, an iterative procedure must be adopted to solve such problems numerically, as is stated by N. G. Zamani et al. in [2.64]. Numerical methods that have been used to model cathodic protection systems will be discussed in the next paragraph.

### 2.3.3 Numerical Methods

The increase in the computer processing power allowed the analysis of mathematical models at a macroscopic level. This has led to intensive attempts to create reliable mathematical models that comprised of partial differential equations and the relevant non-linear boundary conditions. Due to the complexity of the geometries of the structures that need to be analysed and the non-linear nature of the boundary conditions, numerical methods have been adopted to solve the mathematical problems on computers.

Programs based on the Finite Differences Method (FDM), on the Finite Element Method (FEM) and on the Boundary Element Method (BEM) were used for modelling cathodic protection systems. These numerical methods of discretisation are combined with data bases and proceedings to work with electrochemical boundary conditions. FDM results in a well-structured and sparse system of linear equations, but is highly

inconvenient in terms of stability in complex geometries. This problem was partially solved by the use of FEM, which can easily handle irregular geometries, resulting in well-structured and sparse matrices as well. In both cases, the body of the electrolyte needs to be meshed leading to expensive and time consuming procedures. More specifically, when a structure needs to be analysed in an infinite medium (e.g. ship hulls), the structure has to be enclosed in a box in order to simulate the boundary conditions at infinity. In such cases, using FDM and FEM will lead to a great amount of information (great number of equations) generated in the body of the electrolyte that is not useful for corrosion analysis, as suggested by R. Montoya et al. in [2.68]. The Boundary Element Method is also a numerical method used to solve partial differential equations encountered in engineering and mathematical physics (e.g. Laplace's equation) [2.69-2.70]. BEM has emerged as a powerful alternative to the other numerical methods, especially in cases where better accuracy is required or in cases where the domain extends to infinity [2.71], as was mentioned earlier. The most important feature of BEM is that it requires discretisation of only the surface rather than the volume. This advantage allows the designer to generate meshes easily and make changes without the need of complete re-meshing. Compared to FDM and FEM, BEM requires the discretisation of only the anode and cathode surfaces, reducing the size of the numeric problem, resulting in better resolution and reduction in computer time, when compared to the other methods, especially for complex geometries. A drawback to this method is that the system of the linear equations is full and non-symmetric, increasing in this way the calculation cost. In the case of applications where the ratio of the electrolyte volume to the area of the surfaces involved is small (e.g. internal pipeline CP), the calculation cost is determined by the effect of the complexity of the linear equations versus the number of the equations that need to be solved. After the mathematical model is discretised, the problem is solved with a nonlinear solver such as the Newton-Raphson method [2.66]. The BEM has been the most used method in the programs developed to solve large problems always considering homogeneous conductive media [2.68].

#### 2.3.4 The BEASY CP Software

The BEASY CP is a commercial software that was developed for the purpose of analysing, designing and studying of electrodeposition, galvanic corrosion and

cathodic protection. The computational Mechanics BEASY group was the first to apply BEM to corrosion applications and also the first to develop commercial tools that were capable of modelling large scale structures. In the early eighties, the technique was applied to the Conoco TLP platform where its value was demonstrated [2.68]. BEASY CP was developed based on these early developments.

The three major stages in the process of modelling using the BEASY CP simulation software are described below:

### 1. Model Preparation

At this stage the geometry and the environmental conditions are defined. To achieve the desired results, the geometry of the model has to be defined in sufficient detail. The model requires also the conductivity of the electrolyte. Furthermore, the polarisation characteristics of each metal type in the model have to be defined. Run times can be reduced by introducing into the system only the anodic or cathodic part of the polarisation curve of a specific material based on whether the material is expected to behave anodically or cathodically respectively. Also, in order to avoid unnecessary iterations and to improve convergence, the introduced polarisation data can be restricted even further (e.g. -700mV to -1000mV). According to the results, modifications to the introduced data can be made.

### 2. Simulation

The boundary element equations that represent the electrolyte, are assembled by the computational scheme and coupled with the equations derived from the polarization data. Then, the set of equations is solved iteratively and the values of potential and current density are computed at the boundary nodes. The conditions at the nodes can be predicted at different times as requested by the user, if time dependent polarisation data are defined.

### 3. Post Processing

By the use of post-processors the results obtained can be viewed graphically. These modules can create:

- Colour plots of the potential and current density distribution.
- Geometry and results close-up viewing at areas of interest.

- Potential and current density variation with time plots at a particular position.

### 2.3.5 Polarisation Diagrams

#### 2.3.5.1 Theoretical Base of Polarisation Diagrams

Deriving the governing equation the electrode kinetics on the cathode and anode are assumed to be represented by an equation of the following form:

$$I = f(\phi) \quad (2-29)$$

The function  $f$  known as the polarisation curve describes the relationship between the current density  $I$  and the electrode potential  $\phi$  for the electrode reaction [2.72]. In order for a computer model to predict the performance of a cathodic protection system, accurate polarisation data are needed.

The method used in order to obtain polarisation curves is called “potentiodynamic test” or “polarisation scan”. In a potentiodynamic test, the current represents the rate of the anodic or cathodic reaction on the surface of the material under investigation. The results of the test are plotted in an Evans diagram (named after U. R. Evans), where the electrode potential is plotted versus the current density (current per unit area). In an Evans diagram, the potential is usually plotted on a linear scale while current on a logarithmic scale [2.3]. The anodic currents are considered to be positive and the cathodic currents are considered to be negative. However, in an Evans diagram both cathodic and anodic currents are usually plotted as positive (absolute) values.

Two different kinetic phenomena may control the reaction rate. In the case of charge transfer or activation control, the size of the driving force controls the reaction rate (as is the case in water reduction reaction and hydrogen evolution reaction). Increase in the driving force results in increase of the reaction rate. In the second mechanism, the mass transfer to the electrode surface through the electrolyte controls the reaction rate (as is the case in the oxygen reduction reaction). The rate of the reaction, controlled by diffusion, will not increase indefinitely by increasing driving force. Current density reaches a maximum value, that is called limiting current density, which depends on the diffusivity and the concentration of the chemical element of interest

in the solution. If the rate of a reaction reaches its limiting value, any additional increase in driving force will not result in further increase of the reaction rate.

A number of components should be assembled and properly prepared in order to perform a polarisation scan on a particular metal/solution system. An electrochemical cell must be acquired, that contains the environment in which the polarisation scan will be performed, the metal to be investigated and all of the equipment required for the performing of the measurements, as shown in **Figure 2-14**. Typically, three electrodes are used in the experiments, the reference electrode, the working electrode and the counter electrode [2.73]. A stable reference electrode of a known reference potential is used in the control and measurement of the surface potential of the working electrode, throughout the polarisation scan. The kind of the reference electrode that has been used in the testing must be referred with the potential values. The working electrode is the sample of the metal under investigation. Care must be given, prior to the experiment, so that the surface of the sample is prepared such that the initial condition of the measurement is well defined and does not vary from test to test. Finally, the applied current is provided by the counter electrode that has to be made of a highly corrosion resistant material, such as platinum or a platinized substrate material, so that the alteration of the solution chemistry is avoided. A typical arrangement for potentiodynamic tests is illustrated in **Figure 2-15**.

During a potentiodynamic experiment, the driving force (i.e. potential) for the cathodic and anodic reactions is controlled while the net change in the reaction rate (i.e. current) is observed [2.73]. For such kind of measurements the potentiostat must be capable of automatically varying the potential at a specific constant rate between two preset potential values. The current that must be applied to the system for achieving the desired increase in driving force, known as the applied current, is measured by the potentiostat. As a consequence, the measured or applied current will be zero at the open circuit potential (i.e. the potential at which the total anodic current equals the total cathodic current).

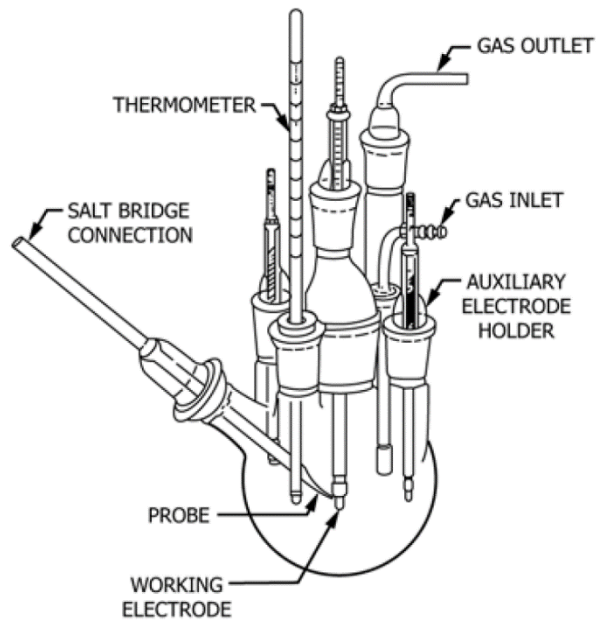


**Figure 2-14.** Schematic diagram of polarisation cell [2.73].

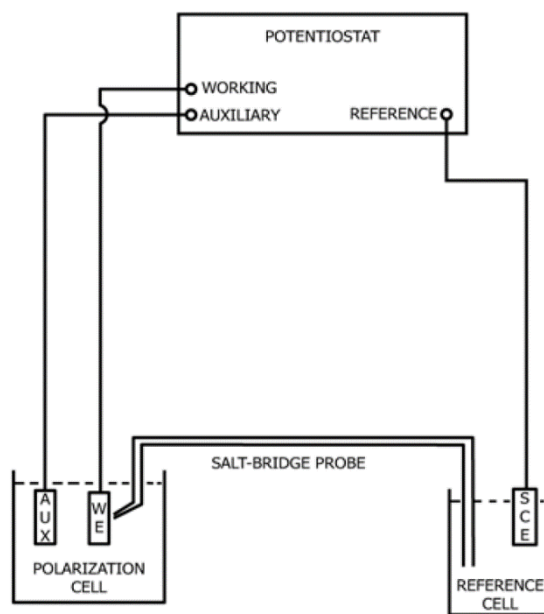


**Figure 2-15.** Arrangement for potentiodynamic experiments [2.73].

In **Figure 2-16** a theoretical anodic and a theoretical cathodic polarisation curve is presented, as suggested by David G. Enos et al. in [2.74].

The polarisation curves illustrated below are idealised representations of the features typically observed in practice. Depending on the nature of a specific system, an actual

polarisation scan may include some or all of these features. Other features may also be present that are not presented here. Knowledge of the potential anodic and cathodic reactions that may take place is essential, in order to fully understand the behaviour of a system.

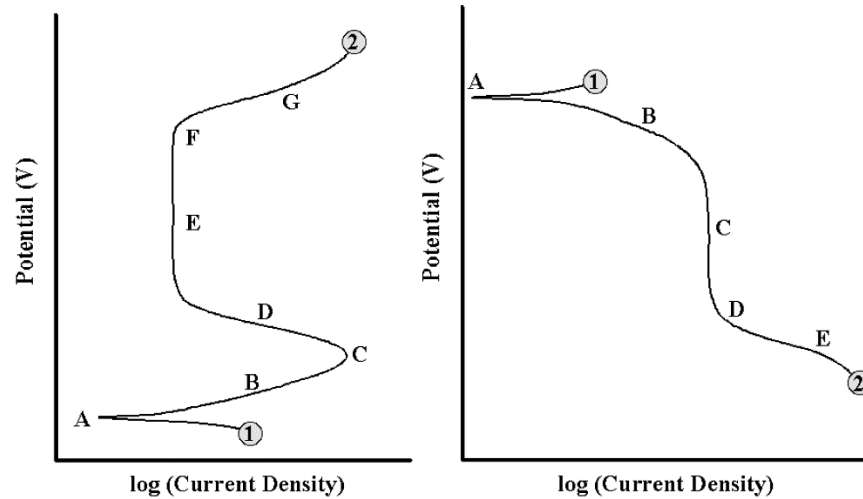


**Figure 2-16.** Theoretical Anodic (left) and Cathodic (right) polarisation curves [2.74].

In the theoretical anodic curve, the scan starting from point 1, progressively moves to the positive (potential) direction up to point 2, which is the termination point of the scan. Point A represents the open circuit potential. When the potential in moving to a more positive value, the system passes to the region B, which is called the active region. In this region the metal oxidation is the dominant reaction. Forcing potential to an even more positive value, the system passes into the region E that is called the passive region. In this region, the current density decreases with increasing (positive direction) potential up to a point (point F) that is called breakaway potential. Further, increase of the potential leads to rapid increase in the current density.

In the theoretical cathodic curve, the scan starting from point 1, progressively moves to the negative (potential) direction down to point 2, which is the termination point of the scan. As in anodic scan point A represents the open circuit potential. Depending on the system, region B may represent the oxygen reduction reaction. This reaction depends on the diffusion rate of oxygen in the solution and for this reason there will be an upper limit on the rate of this reaction that is called limiting current density. No change in the reaction rate and so the measured current occurs by further decrease in the applied potential until the system reaches point D. From this point on the potential becomes sufficiently negative for another cathodic reaction to become

operative (i.e. the thermodynamic driving force becomes sufficient for an additional cathodic reaction to start taking place). Typically, this additional reaction is the reduction of other species present in the environment, such as hydrogen evolution reaction.

#### *2.3.5.2 Review of Parameters Affecting Polarisation Behaviour*

Many factors affect the polarisation characteristics of a material. The velocity of the flow of the electrolyte over the surface of the material is a critical parameter, affecting the polarisation behaviour significantly. Furthermore, the temperature and the chemical composition of the electrolytic solution have also a great effect on the polarisation characteristics. Investigations have shown the effect of these factors on the performance of cathodic protection systems.

Generally, the motion of the electrolyte increases corrosion rates by supplying the corrosives at a faster rate. Motion is thinning quiescent layers at the metal surface so that corrosives can more easily reach the metal surface. For example, oxygen concentration is a major factor in controlling corrosion rates. In most of the cases increased velocity is expected to increase the corrosion rate by supplying more oxygen to the surface of the metal. When the velocity becomes high enough, mechanical effects may add to the damage of the metal. Protective films or layers of corrosion products can be completely removed by erosion and as a result will keep corrosion going at a high rate. N. Gantiva [2.66] stated that the growth in the corrosion rate due to the increase of flow velocity in seawater is not infinite but there comes a point where a critical velocity is reached, beyond which there is little further increase, if any at all, in the corrosion rate. H. R. Copson [2.75] suggested that the corrosion rate of steel in seawater increases up to a velocity level of at least 25ft/s (7.62m/s) and as can be seen in **Figure 2-17** at that point the curve becomes almost horizontal showing that further increase in velocity will have a small effect on the corrosion rate. In [2.3, 2.75] it is also stated that the effect of agitation increases with increasing velocity up to the point of the transition to turbulent flow conditions. This is the point where the agitation effect increases significantly, but if this point is exceeded additional velocity has little effect.

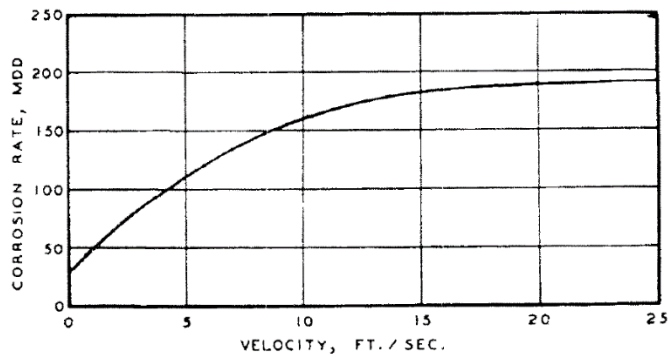


**Figure 2-17.** Effect of seawater velocity on corrosion rate of steel at atmospheric temperature (MDD: milligram per dm<sup>2</sup> per day) [2.75].

In terms of cathodic protection, the increase of the flow velocity has a great effect on the current demand for the polarisation of the structure to a sufficient negative potential level. In **Figure 2-18 (left)**, cathodic polarisation scans of mild steel, conducted in seawater flowing at different velocities, show that as the velocity increases, the curves shift to the right, as suggested by H.R. Copson [2.75]. At high velocities much more current is needed to cathodically protect the steel, compared to zero velocity, as has been suggested also in [2.76-2.77]. As is shown in **Figure 2-18 (right)**, the current that is necessary to polarise the mild steel to a potential of  $-800\text{mV}_{\text{SCE}}$  can be read from the graph for each velocity. In the case of sacrificial anode cathodic protection, this would mean that the anode must supply more current and will be consumed faster under the condition of high velocity. H.P. Hack and R.J. Guanti [2.60] showed that the current demand to polarise HY-80 steel grade to the potential of  $-800\text{mV}_{\text{SCE}}$  in natural seawater increased with velocity up to the level of around 7.5m/s. Further increase of the flow velocity that reached up to around 27.5m/s showed no significant change in the current demand.

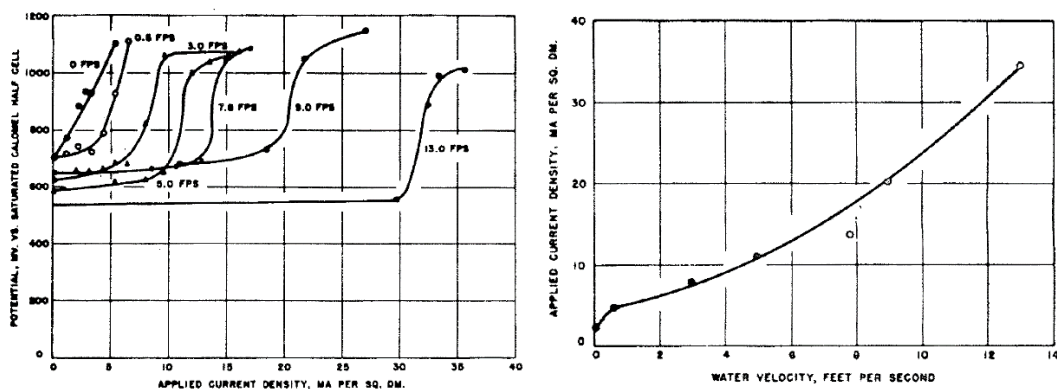


**Figure 2-18.** Cathodic polarisation curves of mild steel in seawater flowing at different velocities (left) and effect of velocity on current required to polarise steel to a potential of  $-800\text{mV}_{\text{SCE}}$  (right) [2.75].

The chemical composition of the electrolyte has a great effect on the corrosion rate. As has already been seen (**Figure 2-17**), in the presence of high concentration of  $Cl^-$  (e.g. seawater), there is no passivity established at any intermediate velocity and the corrosion rate keeps increasing up to the limiting current density. On the contrary, in natural fresh water, at sufficient high velocities, adequate oxygen may reach the surface to enable passivity to set in, as is stated in [2.78]. If passivity establishes there is a decrease in the corrosion rate after the initial increase. By further increase in velocity, mechanical erosion of passive or corrosion product films increase the rate again.

Oxygen is a cathodic reactant and therefore increases in the concentration of oxygen in the electrolyte will lead to larger current density and shift in the equilibrium potential (open circuit potential) of the cathodic reaction to more positive (i.e. noble) values. The increase in oxygen concentration results in an increase in the cathodic current needed to polarise the material to a specific negative level [2.3].

The effect of the combination of increasing oxygen concentration and velocity on corrosion rate has been shown in [2.75]. As is shown in **Figure 2-19**, the corrosion rate of steel in tap water increased with oxygen concentration and velocity. The maximum concentration shown in the figure is about 18ml/litre. At higher concentrations a protective oxide film is expected to form on the surface of the steel, decreasing the corrosion rates. Also, higher velocities would bring sufficient oxygen to the material surface for passivity to set in at oxygen concentration levels of saturation or less.

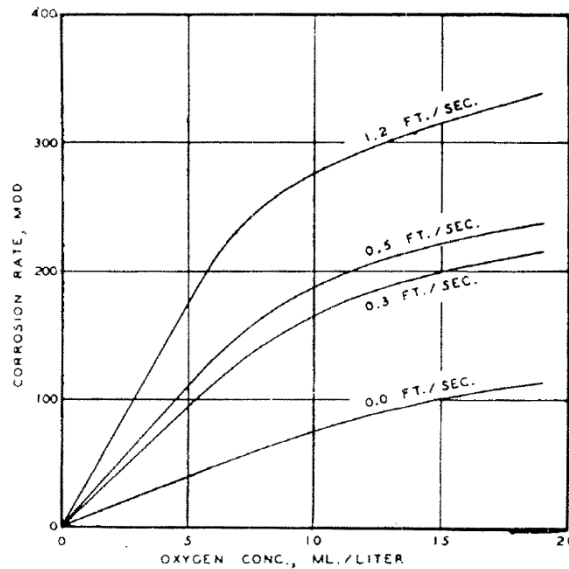


**Figure 2-19.** Effect of velocity and oxygen concentration on corrosion of steel in 23°C tap water [2.75].

Temperature is another parameter that also affects the polarisation response of structures. Increases in temperature result in depolarisation and increase in the cathodic current required for a specific polarisation level [2.3]. In some cases increases in temperature may have the opposite results. In cases where the controlling factor is the oxygen concentration in the electrolyte, a decrease in the cathodic current requirement can result by an increase in temperature. This is attributed to the decrease of the solubility of oxygen in the water by increasing temperature.

In [2.79], it is suggested that higher temperatures drive the corrosion potentials to more negative values, promoting the corrosion process. The corrosion rate of metals is affected by temperature primarily due to its effect on factors controlling the diffusion rate of oxygen, as suggested in [2.80]. Temperature affects the oxygen solubility and the oxygen diffusion coefficient. Higher temperature increases the diffusion coefficient, tending to increase the corrosion rate. In [2.81] it is stated that corrosion rate almost doubles, at a given oxygen concentration, for every 30°C rise in temperature. In [2.78-2.82] it is suggested that in the case of an open vessel, where the dissolved oxygen is allowed to escape, the corrosion rate increases with temperature up to 80°C and then, at the boiling point, it falls down to a very low value, as is indicated in **Figure 2-20**. The effect of the decrease of oxygen solubility in water above 80°C seems to overshadow the corrosion rate acceleration effect of temperature alone. On the other hand, in a closed system, oxygen is not allowed to escape and so the corrosion rate continues to increase with temperature.

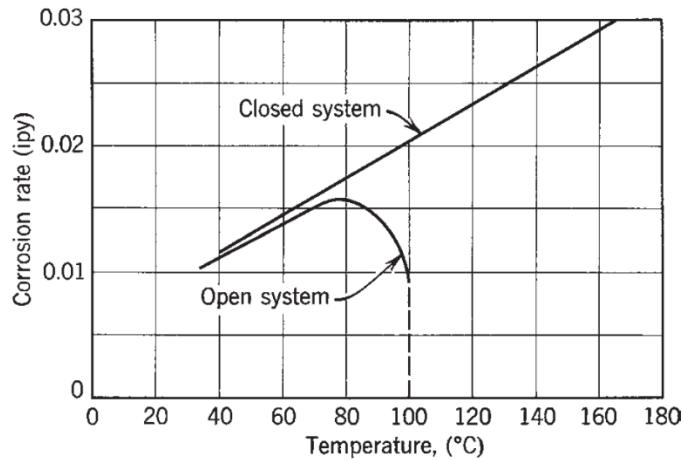


**Figure 2-20.** Effect of temperature on corrosion of iron in water containing dissolved oxygen [2.78].

Finally, it was shown by F. N. Speller [2.83] that in general the combination of the effect of increasing velocity and increasing temperature drives the corrosion rate to higher values.

## 2.4 References

- [2.1] Mohd Saiful Nizam Bin Mohamad, Cathodic Protection of Underground Steel Pipelines by Using Sacrificial Anodes, Faculty of Mechanical Engineering, University Malaysia Pahang (2009).
- [2.2] Pierre R. Roberge, Handbook of Corrosion Engineering, The McGraw-Hill Companies, Inc., USA (2000)
- [2.3] NACE International, CP3 – Cathodic Protection Technologist Course Manual, version 1 (2014).
- [2.4] Herbert H. Uhlig, The Corrosion Handbook, John Wiley & Sons, Inc., New York, USA (1948).
- [2.5] DNV (Det Norske Veritas), Erosion and Corrosion in Piping Systems for Seawater, Guidelines No. 15, Hovik, Norway (2004).
- [2.6] Volkan Cicek, Cathodic Protection, Industrial Solutions for Protecting Against Corrosion, Scrivener Publishing LLC, Salem, Massachusetts (2013).

- [2.7] L. G. Giourntas, Investigation of Erosion-Corrosion Behaviour of Pump Materials, University of Strathclyde, Department of Mechanical and Aerospace Engineering, Glasgow, UK (2016).
- [2.8] G. Karafyllias, The Effect of Acidity and Salinity Level in Erosion-Corrosion Performance of Metals, University of Strathclyde, Department of Mechanical and Aerospace Engineering, Glasgow, UK (2017).
- [2.9] Alireza Bahadori, Cathodic Corrosion Protection Systems a Guide for Oil and Gas Industries, School of Environment, Science & Engineering, Southern Cross University, Lismore, NSW, Australia (2014).
- [2.10] Christopher M. A. Brett and Ana Maria Oliveira Brett, Electrochemistry Principles, Methods and Applications, Oxford University Press Inc., New York, USA (1994).
- [2.11] NACE Standard Test Method, Measurement Techniques Related to Criteria for Cathodic Protection on Underground or Submerged Metallic Piping Systems, TM0497-2012, NACE International, Houston TX (2012).
- [2.12] Steven G. Bratsch, Standard Electrode Potentials and Temperature Coefficients in Water at 298.15 K, J. Phys. Chem. Ref. Data, Vol. 18, No.1 (1989).
- [2.13] Denny A. Jones, Principles and Prevention of Corrosion, Second Edition, Prentice-Hall, Inc., USA (1996).
- [2.14] NASA KSC Corrosion Technology Laboratory Website: [corrosion.ksc.nasa.gov](http://corrosion.ksc.nasa.gov) (2016).
- [2.15] ASM International, ASM Handbook, Volume 13: Corrosion, 9<sup>th</sup> edition (1987).
- [2.16] Mars G. Fontana, Corrosion Engineering, McGraw-Hill Book Company, Third Edition, Singapore (1987).
- [2.17] Seguin, David James, Intergranular Corrosion and Stress Corrosion Cracking of Extruded AA6005A, Dissertation, Michigan Technological University, 2013.
- [2.18] National Association of Corrosion Engineers (NACE) International Website: [www.nace.org](http://www.nace.org)

- [2.19] Patrick P. Leblanc and G. S. Frankel, Investigation of Filiform Corrosion of Epoxy-Coated 1045 Carbon Steel by Scanning Kelvin Probe Force Microscopy, *Journal of the Electrochemical Society*, Volume 151, No. 3, pp. B105-B113 (2004).
- [2.20] T. Gu, D. Xu, P. Zhang, Y. Li and A. L. Lindenberger, Microbiologically Influenced Corrosion and Its Impact on Metals and Other Materials in: *Microbiology for Minerals, Metals, Materials and Environment* edited by S. S. Abhilash, B. D. Pandey and K. A. Natarajan, ISBN 9781482257298, pp. 383-408, CRC Press, Boca Raton, Florida (2015).
- [2.21] D. Mackenzie, W. Pan and T. Hodgkiess, Fatigue Life Design for Forgings in a Corrosive/Erosive Environment, Project G: 2011-2012, Phase 1 Literature Review, Weir Advanced Research Centre, University of Strathclyde (2012).
- [2.22] L. Giourntas, T. Hodgkiess and A. M. Galloway, Comparative Study of Erosion–Corrosion Performance on a Range of Stainless Steels, *Wear*, Volumes 332-333, pp. 1051-1058 (2015).
- [2.23] N. Andrews, L. Giourntas, A. M. Galloway, A. Pearson, Effect of Impact Angle on the Slurry Erosion-Corrosion of Stellite 6 and SS316, *Wear*, Volume 320, pp. 143-151 (2014).
- [2.24] L. Giourntas, T. Hodgkiess and A. M. Galloway, Enhanced Approach of Assessing the Corrosive Wear of Engineering Materials under Impingement, *Wear*, Volumes 338-339, pp. 155-163 (2015).
- [2.25] N. Andrews, L. Giourntas, A. M. Galloway and A. Pearson, Erosion–Corrosion Behaviour of Zirconia, WC–6Co, WC–6Ni and UNS S31600, *Int. Journal of Refractory Metals and Hard Materials*, Volume 48, pp. 229-237 (2015).
- [2.26] George Karafyllias, Edward Humphries and Alexander Galloway, Erosion-Corrosion Evaluation of Two White Cast Irons under Severe Conditions for Application in the Oil Sands Industry, NACE International, Corrosion 2018 Conference & Expo, Paper No. 11405 (2018).
- [2.27] George Karafyllias, Lampros Giourntas, Alexander Galloway and Trevor Hodgkiess, Relative Performance of Two Cast Irons and Two Stainless Steels under Erosion-Corrosion Conditions, NACE International, Corrosion 2016 Conference & Expo, Paper No. 7723 (2016).

- [2.28] William Donald Needham, Stress Corrosion Cracking and Hydrogen Embrittlement of Thick Section High Strength Low Alloy Steel, Massachusetts Institute of Technology, USA (1986).
- [2.29] BS EN ISO 11782-1:2008, Corrosion of metals and alloys – Corrosion fatigue testing, Part 1: Cycles to failure testing (2008).
- [2.30] W. Von Baeckmann, W. Schwenk, W. Prinz, Handbook of Cathodic Corrosion Protection, 3rd edition, Gulf Publishing, Houston, TX Gulf Publishing (1997).
- [2.31] Donald Mackenzie, Material Selection & Design Criteria for Forgings Cyclically Loaded in a Corrosive Environment, Weir Advanced Research Centre, University of Strathclyde (2012).
- [2.32] D. Mackenzie, Audit of Material Selection & Design Criteria for GEHO PD Pumps, Rev. 2, Weir Advanced Research Centre, University of Strathclyde, Glasgow (2013).
- [2.33] Mamdouh M. Salama, William H. Thomason, Evaluation of Aluminum-Sprayed Coatings for Corrosion Protection of Offshore Structures, Society of Petroleum Engineers of AIME, SPE 12440 (1984).
- [2.34] Mehrooz Zamanzadeh, Reza Mirshams and Peyman Tahri, Cathodic Protection, Defective Coatings, Corrosion Pitting, Stress Corrosion Cracking and Soil Corrosivity Mapping and Corrosion Assessment in Aging Pipe Lines, NACE International, Corrosion Risk Management Conference 2016, Paper No. RISK16-8727 (2016).
- [2.35] Rana M. Hussain, Cathodic Protection of Storage Tank, Dissertation Project, University of Technology, Chemical Engineering Department, Iraq (2012).
- [2.36] J. de Prey, R. W. Barrett and J. N. Wanklyn, Design and Operational Guidance on Cathodic Protection of Offshore Structures, Subsea Installations and Pipelines, The Marine Technology Directorate Limited, London, United Kingdom (1990).
- [2.37] Recommended Practice DNV-RP-B401, Cathodic Protection Design (2010).
- [2.38] NORSOK Standard, Common Requirements - Cathodic Protection, M-CR-503 (1994).

- [2.39] I. Gurrappa, Cathodic Protection of Cooling Water Systems and Selection of Appropriate Materials, *Journal of Materials Processing Technology*, Volume 166, pp. 256–267 (2005).
- [2.40] NACE Standard RP0176-2003, Corrosion Control of Steel Fixed Offshore Structures Associated with Petroleum Production, ISBN 1-57590-170-6, NACE International, Houston TX (2003).
- [2.41] NACE Standard SP0169, Control of External Corrosion on Underground or Submerged Metallic Piping Systems, Houston, TX: NACE, p. 12-17 (2002).
- [2.42] Gregory Haidemenopoulos, *Physical Metallurgy (In Greek)*, Tziolas Publications, Thessaloniki, Greece (2007).
- [2.43] ASM International, *ASM Handbook, Volume 19: Fatigue and Fracture* (1996).
- [2.44] ASM International, *ASM Handbook, Volume 1: Properties and Selection: Irons, Steels, and High-Performance Alloys* (1990).
- [2.45] Hael Mughrabi, Microstructural Fatigue Mechanisms: Cyclic Slip Irreversibility, Crack Initiation, Non-linear Elastic Damage Analysis, *International Journal of Fatigue*, Volume 57, pp. 2-8 (2013).
- [2.46] K. Katagiri, A. Omura, K. Koyanagi, J. Awatani, T. Shiraishi and H. Kaneshiro, Dislocation Structures Around the Crack Tips in the Early Stage in Fatigue of  $\alpha$ -Brass, *Fracture 1977, Volume 2, ICF4*, Waterloo, Canada (1977).
- [2.47] Michael D. Sangid, The Physics of Fatigue Crack Initiation, *International Journal of Fatigue*, Volume 57, pp. 58-72 (2013).
- [2.48] Abílio M.P. de Jesus, Rui Matos, Bruno F.C. Fontoura, Carlos Rebelo, Luis Simões da Silva, Milan Veljkovic, A Comparison of the Fatigue Behavior Between S355 and S690 Steel Grades, *Journal of Constructional Steel Research*, Volume 79, pp. 140–150 (2012).
- [2.49] J.A. Bannantine, J.J. Comer, J.L. Handrock, *Fundamentals of Metal Fatigue Analysis* (1989).
- [2.50] G.E. Dieter, *Mechanical Metallurgy*, McGraw – Hill Book Company, Inc., ISBN: 07-016890-3, New York, USA (1961).
- [2.51] NACE International Website: [www.nace.org](http://www.nace.org) (2017).

- [2.52] Charles M. Hudgins, Jr., Burton M. Casad, R. L. Schroeder, Charles C. Patton, The effect of cathodic protection on the corrosion fatigue behaviour of carbon steel in synthetic sea water, Offshore Technology Conference 6200 North Central Expressway Dallas, Texas 75206, Paper No. OTC 1254 (1970).
- [2.53] E.N. Kostrov, L.A. Glikman, V. A. Orlov, Effect of cathodic protection on the corrosion fatigue strength of steels of various hardness in seawater, Fiziko-Khimicheskaya Mekhanika Materialov, Volume 2, No. 4, pp 431-436 (1966).
- [2.54] A. E. Lyashchenko, L.A. Glikman, Yu. E. Zobachev, Some features of influence of cathodic polarisation on the corrosion fatigue strength of steel samples with a notch, UDC 620.193:620.197.5 (1975).
- [2.55] Havens F. E. and Bench D. M., Fatigue Strength of Quenched and Tempered Carbon Steel Plates and Welded Joints in Seawater, Offshore Technology Conference, Paper OTC 1046, Dallas, Texas (1969).
- [2.56] Endo K., Komai K. and Nakamuro N., Estimation of corrosion fatigue strength by corrosion resistance and notch sensitivity of materials, Bulletin of the JSME, Volume 13, No 61, p. 837-849 (1970).
- [2.57] Endo K. and Miyao Y., Effects of Cycle Frequency on the Corrosion Fatigue Strength, Bulletin of JSME, Vol. 1, No 4, pp. 374-380 (1958).
- [2.58] Lee H. H. and Uhlig H. H., Corrosion Fatigue of Type 4140 High Strength Steel, Metallurgical Transactions, Vol. 3, pp. 2949–2957 (1972).
- [2.59] Sergei A. Shipilov, Iain Le May, Structural integrity of aging buried pipelines having cathodic protection, Engineering Failure Analysis Volume 13, p. 1159–1176 (2006).
- [2.60] Harvey P. Hack and Robert J. Guanti, Effect of High Flow on Calcareous Deposits and Cathodic Protection Current Demand, David Taylor Research Centre, DTRC/SME-87/82, Bethesda, Maryland (1988).
- [2.61] Jaske, C. E., Broek, D., Slater, J. E. and Anderson, W. E., "Corrosion Fatigue of Structural Steels in Seawater and for Offshore Applications", Corrosion-Fatigue Technology, ASTM STP 642, H. L. Craig, Jr., T. W. Crooker, and D. W. Hoepfner, Eds., American Society for Testing and Materials, pp. 19-47 (1978).

- [2.62] Leslie Bortels, Expert 3D Software Simulations for Cathodic Protection in Offshore and Marine Environments, NACE International, Corrosion 2009 Conference & Expo, Paper No. 09516 (2009).
- [2.63] Mohammed Al-Otaibi, The Application of BEASY Software to Simulate Cathodic Protection of Pipelines and Storage Tanks, The University of British Columbia, Vancouver (2010).
- [2.64] N. G. Amani, J. F. Porter, A. A. Mufti, A Survey of Computational Efforts in the Field of Corrosion Engineering, International Journal for Numerical Methods in Engineering, Vol. 23, p.p. 1295-1311 (1986).
- [2.65] L. Bortels and J. Deconinck, Numerical Simulation of the Cathodic Protection of Pipeline Networks under Various Stray Current Interferences, WIT Transactions on State of the Art in Science and Engineering, Volume 7 (2005).
- [2.66] Nicolas Gantiva, Design of Cathodic Protection Using BEM for Components of the Pilot Ocean Energy System, College of Engineering and Computer Science, Florida Atlantic University, Boca Raton, Florida (2010).
- [2.67] O. Abootalebi, A. Kermanpur, M.R. Shishesaz and M.A. Golozar, Optimizing the electrode position in sacrificial anode cathodic protection systems using boundary element method, Corrosion Science No 52, pp. 678–687 (2010).
- [2.68] R. Montoya, O. Rendon and J. Genesca, Mathematical simulation of a cathodic protection system by finite element method, Materials and Corrosion, No 6, pp. 406-411 (2005).
- [2.69] C. Pozrikidis, A Practical Guide to Boundary Element Methods with the Software Library BEMLIB, Chapman and Hall/CRC, Florida (2002).
- [2.70] A. B. Peratta, J. M. W. Baynham and R. A. Adey, Computational Modelling of Cathodic Protection Systems for Pipelines in Multi-Layer Soil, WIT Transactions on Engineering Sciences, Volume 65 (2009).
- [2.71] C. A. Brebbia and J. Dominguez, Boundary Elements an Introductory Course, Second Edition, WIT Press Computational Mechanics Publications, Southampton, UK (1992).

- [2.72] R. A. Adey, S. M. Niku, C. A. Brebbia and J. Finnegan, Computer Aided Design of Cathodic Protection Systems, Applied Ocean Research, vol. 8, No 4 (1986).
- [2.73] ASTM International, Standard Reference Test Method for Making Potentiodynamic Anodic Polarization Measurements, Designation: G5 – 14 (2014).
- [2.74] David G. Enos and Louie L. Scribner, The Potentiodynamic Polarization Scan, Technical Report 33, Solartron Instruments a division of Solartron Group Ltd, Farnborough, Hampshire, UK (1997).
- [2.75] H. R. Copson, Effects of Velocity on Corrosion, Northeast Region Conference, National Association of Corrosion Engineers, Boston, Massachusetts (1958).
- [2.76] Fan Fengqin, Song Jiwen, Li Chengjie and Du Min, Effect of Flow Velocity on Cathodic Protection of DH36 Steel in Seawater, Journal of Chinese Society for Corrosion and Protection, Volume 34, No. 6 (2014).
- [2.77] Yong-Sang Kim, Kyoung-Min Kim, Sangkyu Lee and Jung-Gu Kim, Effect of Temperature and Flow Velocity on the Cathodic Protection of Ships and Underwater Electromagnetic Signatures, Korean Journal of Metals and Materials, Volume 55, No. 5, pp. 348-356 (2017).
- [2.78] R. W. Revie and H. H. Uhlig, Corrosion and Corrosion Control, An Introduction to Corrosion Science and Engineering, Fourth Edition, John Wiley & Sons, Inc., New Jersey, USA (2008).
- [2.79] Wang Chun Li, Wu Jiang Hua and Yuan Man, Effect of Temperature on the Galvanic Corrosion of Cu-Ni Alloy/High Strength Steel in Seawater, MATEC Web of Conferences, Volume 67, Article No. 07039 (2016).
- [2.80] Howard A. Porte, The Effect of Environment on the Corrosion of Metals in Sea Water – A Literature Survey, Technical Note N-907, Naval Civil Engineering Laboratory, California, USA (1967).
- [2.81] G. T. Skaperdas and H. H. Uhlig, Corrosion of Steel by Dissolved Carbon Dioxide and Oxygen, Industrial and Chemical Engineering, Volume 34, pp. 748-754 (1942).

- [2.82] V. V. Gerasimov and I. L. Rozenfeld, Effect of Temperature on the Rate of Corrosion of Metals, Bulletin of the Academy of Sciences of the USSR, Division of chemical science, Volume 6, pp. 1192–1197 (1957).
- [2.83] F. N. Speller, Corrosion Causes and Prevention, An Engineering Problem, First Edition, McGraw-Hill Book Company, Inc., New York, USA (1926).

# CHAPTER 3

## Erosion-Corrosion Performance

### 3.1 Introduction

This chapter describes and discusses the techniques and outcomes of the experimental investigation of the effect of cathodic protection on the erosion-corrosion performance of the low alloy steel grade S355J2G3+N used for the manufacturing of pumping equipment. What is more, the use of electrochemical monitoring techniques for the evaluation of the cathodic protection systems behaviour in various conditions, is described. The scope of the investigation presented in this chapter is to gain important insights into the cathodic protection methods, in order to adopt the most effective strategy for controlling the corrosion-fatigue deterioration observed during the working life of WEIR Minerals PD pumps.

The major thrust of the work has been to conduct experiments, to assess the effect of application of Sacrificial Anode Cathodic Protection (SACP) and Sacrificial Coating Cathodic Protection (SCCP) in conditions mimicking the challenging circumstances that are encountered in GEHO PD pump components. In the first case, two commercial sacrificial anode materials, zinc alloy and magnesium alloy, were used for the implementation of SACP, while in the second case, a commercial zinc-rich spray coating was used as sacrificial coating, for the application of SCCP. Furthermore, the evaluation techniques comprised of mass loss measurements, electrochemical monitoring and microscopy examination.

The experimental programme consisted also of potentiodynamic tests, for the investigation of the effect of varying conditions on the performance of cathodic protection systems. The conditions that have been investigated are the flowing conditions on the surface of the cathode and anode materials, the salinity level of the electrolyte and the effect of the driving voltage, by the use of more active anode materials. Based on the results of the potentiodynamic tests, polarisation diagrams

were constructed. The presentation of the results in the form of diagrams enabled for better evaluation and understanding of the effect of those conditions on the behaviour of cathodic protection systems.

The results of the potentiodynamic testing were used in conjunction with a 1-D analytical model that has been created for the investigation of the performance of SACP systems under various environmental conditions. The polarisation curves were used as boundary conditions in the model, so as to obtain quantitative results of the response of SACP systems in varying distance between cathode and anode, electrolyte salinity, flowing conditions and the use of more active anodes.

At the end of the chapter, an assessment is being made of the methods used during the experimental programme and the results obtained from this investigation. The conclusions reached, affected the continuing of the research, concerning the effect of cathodic protection on the corrosion-fatigue performance and the design process of SACP systems that are presented later in this Thesis.

## 3.2 Pre-Test Methodologies

### 3.2.1 Source of Materials

#### 3.2.1.1 Material Investigated

The material that has been used in the erosion-corrosion investigation, is a low alloy steel grade, S355J2G3+N (hereinafter referred to as “S355 steel”) in accordance with EN 10250-2:1999, the nominal chemical composition of which is presented in **Table 3-1**.

**Table 3-1.** Nominal chemical composition of S355 steel grade.

Element	Content (wt %)
Ni	0.03
Cr	0.01
Mn	1.32
C	0.20
Mo	0.01
Si	0.34
S	0.002
P	0.009
Al	0.042
B	0.0012
Fe	remainder

The S355 was provided by WEIR Minerals Netherlands in the form of cylindrical plates of 600mm diameter and 25mm thickness, from which the specimens were extracted and machined to their final cylindrical form. The final dimensions of the specimens were 38mm diameter and 17mm thickness.

### 3.2.1.2 Sacrificial Anode Materials

The sacrificial anode materials that were used in the experimental investigation are detailed below. Specimens from these anode materials were machined to the same dimensions as the specimens of the investigated material.

- Zinc Alloy Anode Material

The Zinc alloy anode material was provided by a specialist company, MGDUFF, in the form of a rod anode (Type: ZR40, 500mm length and 40mm diameter) and its nominal chemical analysis is presented in **Table 3-2**.

**Table 3-2.** Nominal chemical composition of Zn sacrificial anode, conforming to US Mil Spec 18001K.

Element	Content (wt %)
Cu	0.0004
Al	0.46
Fe	0.001
Cd	0.035
Pb	0.001
Others (total)	0.1
Zn	remainder

- Magnesium Alloy Anode Material

The Magnesium alloy anode material was also provided by the specialist company, MGDUFF, in the form of a long flush mounted anode (Type: MD72B, length 457mm and diameter 102mm) and its nominal chemical analysis is presented in **Table 3-3**.

**Table 3-3.** Nominal chemical composition of high purity Mg sacrificial anode.

Element	Content (wt %)
Cu	0.08
Al	5.3 – 6.7
Si	0.3 max
Fe	0.005 max
Mn	0.25 min
Ni	0.003 max
Zn	2.5 – 3.5
Pb	0.03
Mg	remainder

- Zinc-rich Sacrificial Coating

The zinc-rich coating material was also provided by MGDUFF, in the form of a spray can of 500ml capacity (Type: Zinga- 500ML SPRAYCAN). The content of the spray is zinc powder, aromatic hydrocarbons and binder. When dried it contains 96% zinc in the film and it is able to resist temperatures from -40°C up to +120°C.

### 3.2.2 Surface Preparation of Test Samples

The surface preparation of the specimens comprised of the grinding of one of their flat surfaces (test surface) using 220, 500, 800 and 1200 SiC grit papers on a Struers Rotopol-21 type grinding machine.

The zinc-rich coating was sprayed on the surface of an S355 specimen which was used as an anode in the testing procedure. The spray was applied on the steel substrate in two layers, the second of which was sprayed approximately 1.5hrs after the first one. The system was left to dry for 48hrs before testing.

## 3.3 Erosion-Corrosion Testing Procedures

### 3.3.1 Testing Protocol

The tests were carried out on a submerged jet impingement, closed-loop recirculating test rig (**Figure 3-1**), which has been widely used for laboratory erosion-corrosion testing [3.1-3.8], comprising of a pump, a single nozzle system (nozzle diameter:

4mm) and a holder. The offset distance between the specimen and the nozzle was 5mm. The jet impinged at 90° onto the surface of the specimen.

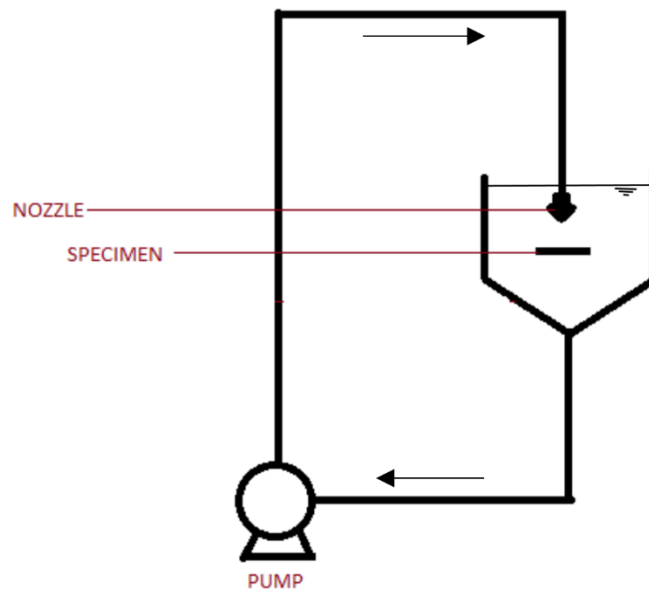


**Figure 3-1.** Schematic representation of the erosion corrosion test rig.

The holder that was used for the free erosion-corrosion testing is depicted in **Figure 3-2**. Special screw regulators were used for the positioning of the specimen at the desired angle and distance from the nozzle.

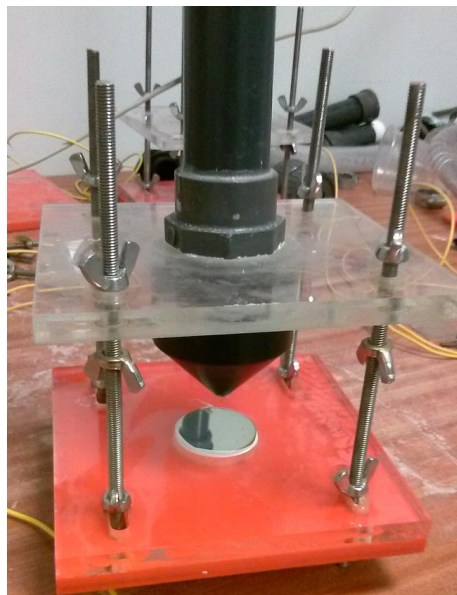


**Figure 3-2.** Nozzle and specimen holder for FEC tests.

The experimental set up, shown in **Figure 3-1**, used to undertake the experiments under free erosion-corrosion (FEC) conditions, was modified to incorporate a sacrificial anode cathodic protection system, as depicted in **Figure 3-3**.

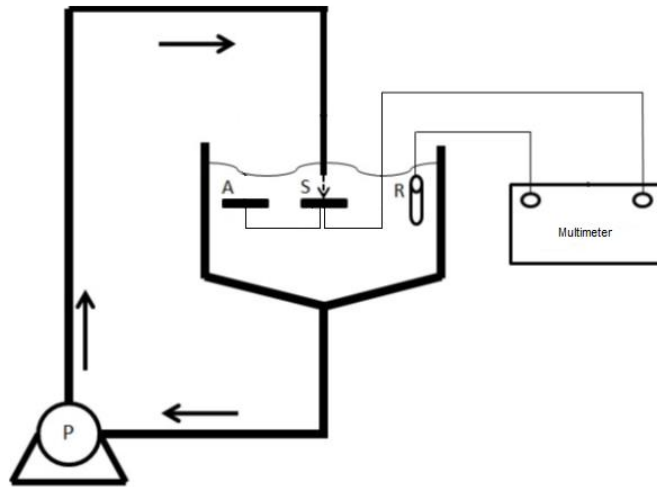


**Figure 3-3.** Schematic representation of the erosion-corrosion test rig incorporating a SACP system, P: pump, R: reference electrode, S: sample (working electrode), A: anode.

**Figure 3-4** demonstrates the set-up for the tests involving sacrificial anodes. In these, the jet impinged directly onto the test specimen while a sacrificial anode was located in a closely adjacent position. An electrical-connection wire was soldered to the base of the sacrificial anode specimens and then the specimen was encapsulated in epoxy resin. Electrical contact between the sacrificial anode specimen and the test specimen was achieved via a wire electrically connected to the base of the test specimen. This arrangement facilitated measurement of the electrode potential of the protected specimen using a voltmeter and a reference electrode. The electrode potential was measured against a Thermo Scientific Orion Ag/AgCl (silver/silver chloride) reference electrode. The anode current output was monitored using an ammeter interfered in the electrical connection between the anode and cathode samples. Both electrode potential and anode current output were measured using AIM TTi 1705 programmable digital multimeters. All tests were conducted for the duration of two hours at ambient temperature.

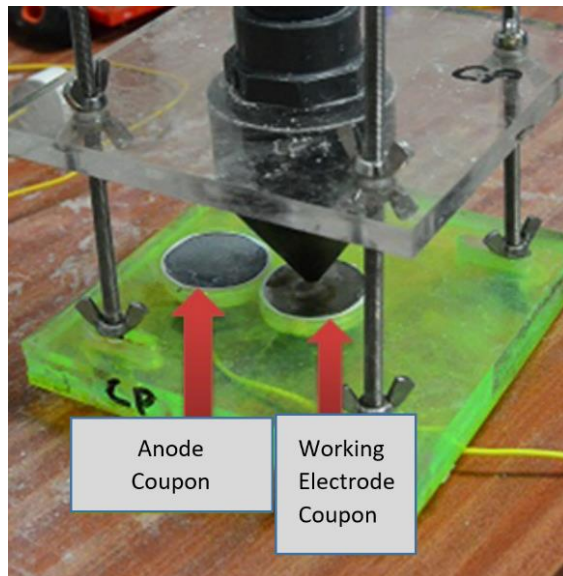


**Figure 3-4.** Nozzle and specimen holders for tests using sacrificial anodes.

Erosion-corrosion testing was carried out for two different sodium chloride concentrations of a 40lt aqueous solution (824ppm and 35,000ppm sodium chloride dissolved in tap water) and three different testing methods: FEC, SACP with the use of Zinc anode, SACP with the use of Magnesium anode and SCCP with the use of a zinc-rich coating, in flowing conditions. For all test conditions three duplicate tests were carried out.

### 3.3.2 Flow Velocity Measurements

The jet velocity was measured several times during each experimental phase of the erosion-corrosion testing programme to ensure that the flowing conditions remained constant. For this purpose a plastic hose was placed under the nozzle for 30 seconds and the water was collected in a volumetric beaker. By using the **Equation 3-1** the jet velocity was calculated.

$$v = \frac{Q}{30 \cdot \pi \cdot r^2} \left[ \frac{m}{s} \right] \quad (3-1)$$

where,

$Q$ : quantity per 30 seconds [ $m^3$ ],  $r$ : nozzle radius [ $m$ ]

The jet velocity remained constant throughout the entire duration of the experimental programme at 18m/s.

### 3.3.3 Potentiodynamic Testing

The potentiodynamic tests were carried out in a modified version of the experimental set up used for the conduction of the erosion-corrosion testing programme, as shown in **Figure 3-5**. This three electrode test set-up has been used in the past by many researchers for the investigation of the polarisation characteristics of various alloys [3.1-3.3, 3.5-3.6].

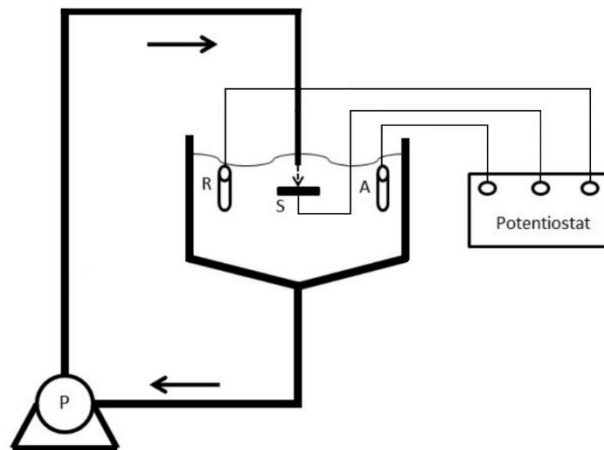


**Figure 3-5.** Schematic representation of the potentiodynamic test rig, P: pump, R: reference electrode, S: sample (working electrode), A: auxiliary electrode.

Three electrodes were used in the experiments, the reference electrode, the working electrode (sample) and the auxiliary (counter) electrode. The same reference electrode as used for the erosion-corrosion testing, was used in the control and measurement of the surface potential of the working electrode, throughout the polarisation scans. The working electrode was the sample of the metal under investigation. Finally, the applied current was provided by an MW-1033 23cm coiled Platinum (Pt) auxiliary (counter) electrode and the polarization scans were performed using ACM Instruments GillAC electrochemical equipment.

The polarisation scans were performed in the corrosive environment at ambient temperature, after pre-exposure of the samples for 55min, as suggested in [3.9], at a

scan rate of 15mV/min. The scan rate was kept low in order to allow sufficient time for the system to stabilise at each potential [3.10]. The Magnesium alloy was tested in an 824ppm NaCl tap water solution (resistivity  $\rho=584.11 \Omega \cdot \text{cm}$ ) while the Zinc alloy was tested in a 35,000ppm NaCl tap water solution (resistivity  $\rho=19.048 \Omega \cdot \text{cm}$ ). The S355 steel grade samples were tested in both solutions. Finally, all the materials were tested in both static and flowing conditions.

Cathodic scans were performed to the S355 and anodic scans to the anode alloys. All the results were printed in polarization diagrams for better assessment of the materials behaviour, as will be seen later in this Chapter.

### **3.4 Post-Test Analysis Techniques**

#### 3.4.1 Mass loss Measurements

Mass loss measurement is a widely used corrosion monitoring method, described in [3.1-3.8, 3.11-3.13]. After the conduction of each erosion-corrosion test, accurate mass loss measurements of the test coupons were performed, using a Sartorius mass balance of  $\pm 0.1\text{mg}$  accuracy, according to the following procedure. The test coupons were taken out of the test rig straight after the completion of the test and washed with water and then with methanol. Then the coupons were dried using a commercial air drier and immersed in an inhibited acid solution (Clarke's solution) for 4 seconds, in order to remove the corrosion products. The weight of the coupons was measured and the results were compared to those obtained before the testing. Finally, the average values and scatter of the results per testing condition, were used for the construction of bar charts, allowing for better evaluation of the erosion-corrosion behaviour of the material under investigation and the effectiveness of the SACP systems.

#### 3.4.2 Surface Microscopy

After the performance of the erosion-corrosion tests, coupons were examined microscopically, using an Olympus GX51 light microscope. The magnification of the

microstructural observations reached up to x200, enabling the evaluation of the effect of the erosion-corrosion testing parameters on the test surface of the specimens.

#### 3.4.3 Evaluation of Cathodic Protection Systems Performance

The evaluation of the performance of the cathodic protection systems consisted of the monitoring of the electrode potential of the low alloy steel test coupons and the anode current output, during the testing. The criterion used for the evaluation of the successful application of cathodic protection is the  $-800\text{mV}_{\text{SSC}}$ . Measurements of the electrode potential and the anode current output were taken in the beginning of each test and at 1/2hr intervals on. Finally, the results were used for the construction of charts, allowing for safer evaluation and comparison of the performance of the SACP systems used in the experimental investigation.

### 3.5 Results and Discussion

#### 3.5.1 Mass Loss Measurements

In **Figure 3-6**, the results of the erosion-corrosion performance experimental investigation of the S355 samples are presented. According to the results, it is obvious that the salinity level of the aqueous environment plays a critical role in the erosion-corrosion performance of the S355. The increase of mass loss due to the increase in salinity level observed in the results is in good agreement with the literature [3.2]. The material suffers more than double the mass losses in 35,000ppm NaCl aqueous solution compared to those in 824ppm NaCl aqueous solution. Furthermore, cathodic protection seems to have a great effect on the mass losses, recorded with all the CP variants compared to free erosion-corrosion. The significant effect of CP on the reduction of mass loss under fluid erosion-corrosion conditions, has also been reported by other researchers [3.2, 3.13]. The effect of CP seems to increase with the salinity level of the aqueous solution. Finally, the results of the lab tests in FEC conditions presented, provide qualitative and not quantitative evaluation of the erosion-corrosion performance of the S355, since the field conditions may vary

significantly, especially in terms of the flowing conditions, which are expected to have a great effect.

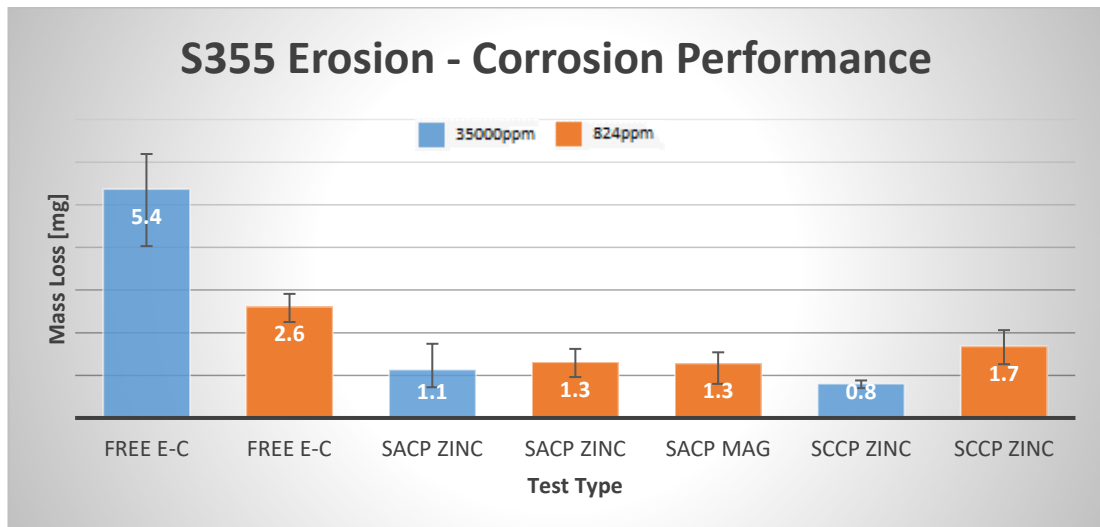


**Figure 3-6.** Average Mass losses and scatter for S355 low alloy steel in all testing conditions.

The use of zinc sacrificial anodes and zinc rich sacrificial coating, seems to reduce dramatically the effect of erosion-corrosion in both testing salinity levels. The same effect is also observed for the use of magnesium anodes in the low salinity level. Additionally, it should be noted that no signs of corrosion were observed on the surface of the S355 samples after testing with cathodic protection and so the mass losses in these tests can be regarded as negligible. These amounts of mass loss observed, can be attributed to the time needed to clean and dry the sample surfaces, after their extraction from the test rig, during which the sample is exposed to a thin layer of saline water that is highly aerated and so very corrosive. Also, the time needed for the polarisation of the working electrode to a protective electrode potential level of at least  $-800\text{mV}_{\text{SSC}}$  may contribute to this phenomenon.

### 3.5.2 Surface Microscopy

In **Figures 3-7** and **3-8**, the surface and the pits of corrosion attack after FEC testing of S355 samples, in the two NaCl aqueous solution concentrations are shown. On the left the signs of the corrosion attack, before the removal of the corrosion products, can be seen. On the right, pictures of x200 magnification of the corrosion pits have

been captured, using light microscopy, after the removal of the corrosion products from the sample surfaces.



**Figure 3-7.** S355 (left) Macroscopic view of the surface of the sample after FEC in 35,000ppm salinity aqueous solution (right) Microscopic view of the pits on the surface of the sample after corrosion attack.

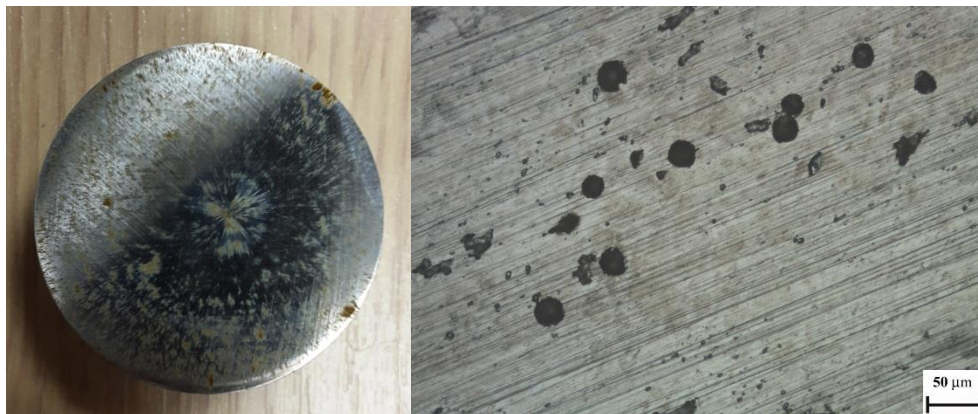


**Figure 3-8.** S355 (left) Macroscopic view of the surface of the sample after FEC in 824ppm salinity aqueous solution (right) Microscopic view of the pits on the surface of the sample after corrosion attack.

As can be observed, the corrosion pits are larger in diameter in the 35,000ppm NaCl aqueous solution. So the low alloy steel seems to have suffered more corrosion in the higher salinity level aqueous solution compared to the less corrosive environment of 824ppm NaCl aqueous solution. These results were expected also, based on the mass loss measurements that had been conducted, where the mass losses of the material in the higher salinity level were much greater.

### 3.5.3 Cathodic Protection Systems Performance

The performance of the cathodic protection systems was evaluated by measuring the electrode potential of the working electrode and the anode current output. The driving of the working electrode potential to a potential level of  $-800\text{mV}_{\text{SSC}}$  or more negative, is regarded as indication of a successful cathodic protection system. The results obtained during the tests are presented in **Figures 3-9** and **3-10**. In these figures, it is obvious that the performance of the SACP using Zinc anodes and the SCCP using Zinc rich coating have similar performances in both aqueous environments.

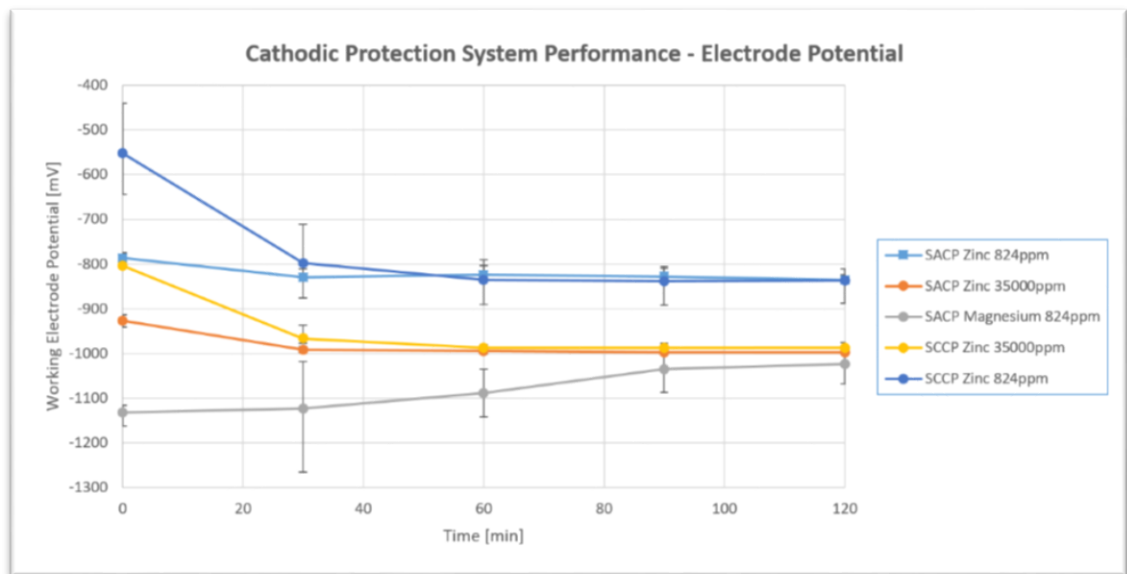


**Figure 3-9.** Electrode Potential of the S355 test specimens during testing procedure.

As can be seen in **Figure 3-9**, all of the cathodic protection methods used for the experimental investigation successfully polarised the S355 samples to the acceptable potential level of  $-800\text{mV}_{\text{SSC}}$  or more electronegative, during the testing procedure. The SACP using Zinc Anodes and the SCCP Zinc rich coating drove the potential of the working electrode down to even  $-997\text{mV}_{\text{SSC}}$ , in the 35,000ppm NaCl aqueous solution, indicating in this way that the low alloy steel samples were protected from corrosion. Moreover, the same methods proved to be successful also in the low salinity aqueous solution, but the potential achieved in this environment was not more negative than  $-837\text{mV}_{\text{SSC}}$ , a potential level slightly more negative than the accepted limit. On the contrary, the use of Magnesium anodes in the same solution enabled the driving of the potential down to  $-1023\text{mV}_{\text{SSC}}$ , an expected result as the rest potential of Magnesium anodes is much more negative than that of Zinc anodes, proving in this

way that Magnesium anodes can be used more efficiently in low salinity aqueous solutions.

In **Figure 3-10**, the current output of the anodes during the tests is indicated. In the lower salinity aqueous solution the Magnesium anodes seem to provide much more protection current to the working electrode than the Zinc anodes and the Zinc rich coating. By using Magnesium anodes 8.16mA ( $0.72\text{mA}/\text{cm}^2$  current density) protection current was provided to the sample under protection, while by the other two systems the protection current reached the value of only 2.89mA ( $0.25\text{mA}/\text{cm}^2$  current density). These values were reflected also in the potential levels achieved, as Magnesium anodes succeeded in driving the potential to more negative levels. In the 35,000ppm NaCl aqueous solution, the SACP using Zinc anodes and the SCCP using Zinc rich coating seem to exert more protective current than in the lower salinity environment reaching the value of 6.47mA ( $0.57\text{mA}/\text{cm}^2$  current density).

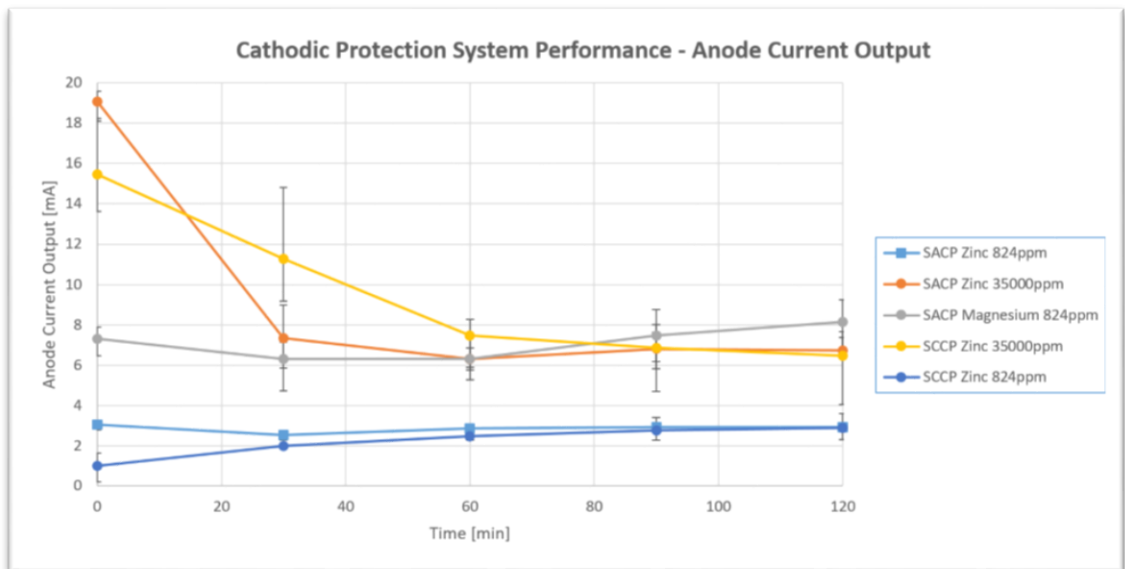


**Figure 3-10.** Anode Current Output during testing procedure.

As has been seen the SACP using Magnesium anodes proved to be the most effective method of the three, in the 824ppm NaCl aqueous solution, allowing higher anode current output and so higher polarisation of the working electrode. Thus, it can be assumed that Magnesium alloy sacrificial anodes may be used for better potential and current distribution when used as a protection method for a real scale PD pump in low salinity aqueous solutions. In the higher salinity environment, SACP using Zinc anodes and SCCP using Zinc rich coating proved to have a satisfactory performance,

but the application of such a coating and its maintenance in the protection of the internal surfaces of a PD pump may be very difficult and cost ineffective. For these reasons, the methods to be used for the experimental investigation of the effect of cathodic protection on the corrosion-fatigue performance of the S355 are the SACP using Magnesium anodes for the 824ppm NaCl aqueous environment and the SACP using Zinc anodes for the 35,000ppm NaCl aqueous environment.

#### 3.5.4 Effect of Conditions Variation on CP System Performance - Polarisation Diagrams

The effect of variation in flowing conditions, resistivity of the electrolyte and sacrificial anode material on the performance of cathodic protection systems has been investigated. The experimental investigation consisted of cathodic polarisation scans for the low alloy steel and anodic polarisation scans for the anode materials. The results of the potentiodynamic tests are presented in **Figures 3-11 to 3-16**.

##### *3.5.4.1 Effect of Flowing Conditions*

The flowing conditions tested are the static conditions where there was no flow of the electrolyte on the sample's surface and turbulent flow of the electrolyte on the sample's surface, produced by test set-up that has been presented earlier in this chapter. Tests have been performed in two salinity levels, where Magnesium anodes were used in the lower salinity level and Zinc anodes in the higher salinity level aqueous solution.

In **Figure 3-11** the effect of the flow conditions on the performance of a Magnesium Alloy Sacrificial Anode CP system, working in 824ppm NaCl tap water solution, is depicted.

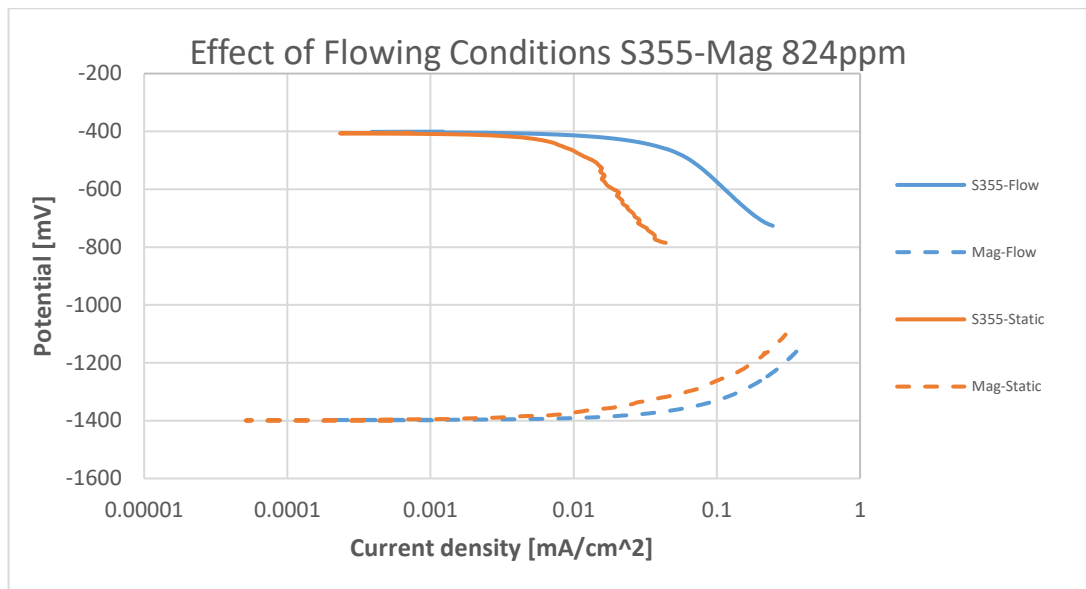


**Figure 3-11.** Effect of turbulent flow on Magnesium Alloy Sacrificial Anode CP system performance in 824ppm NaCl tap water solution.

In **Figure 3-12** the effect of the flow conditions on the performance of a Zinc Alloy Sacrificial Anode CP system, working in 35,000ppm NaCl tap water solution, is depicted.

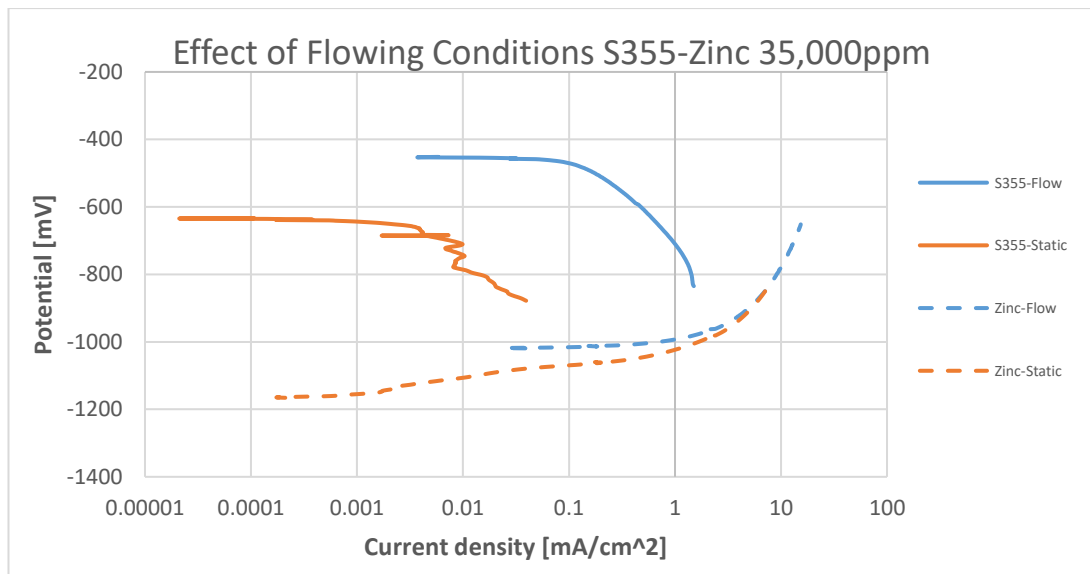


**Figure 3-12.** Effect of turbulent flow on Zinc Alloy Sacrificial Anode CP system performance in 35,000ppm NaCl tap water solution.

It is obvious that flow drives the rest potentials of the anode and cathode to more electropositive (more noble) values and increases the current density needed to polarise the steel surface to sufficient electronegative protective potential values, in

both electrolyte salinity levels. The effect of flow velocity seems to be greater in the higher salinity level aqueous solution. The increase in current demand to maintain polarisation with increasing flow velocity has been suggested in literature [3.14-3.17]. According to the results, the anodic polarisation characteristics of the anode materials seem not to be affected significantly.

#### 3.5.4.2 Effect of Electrolyte Salinity

The two salinity level aqueous solutions tested represent a resistivity of  $\rho=5.84\Omega\text{m}$  for the lower salinity (824ppm NaCl) and resistivity  $\rho=0.19\Omega\text{m}$  for the higher salinity (35,000ppm NaCl) aqueous solution. All tests have been conducted in flowing conditions, using Magnesium anodes and Zinc anodes in both salinity level aqueous solutions.

In **Figure 3-13** the effect of the salinity of the electrolyte on the performance of a Magnesium Alloy Sacrificial Anode CP system, working in turbulent flow conditions, is depicted.

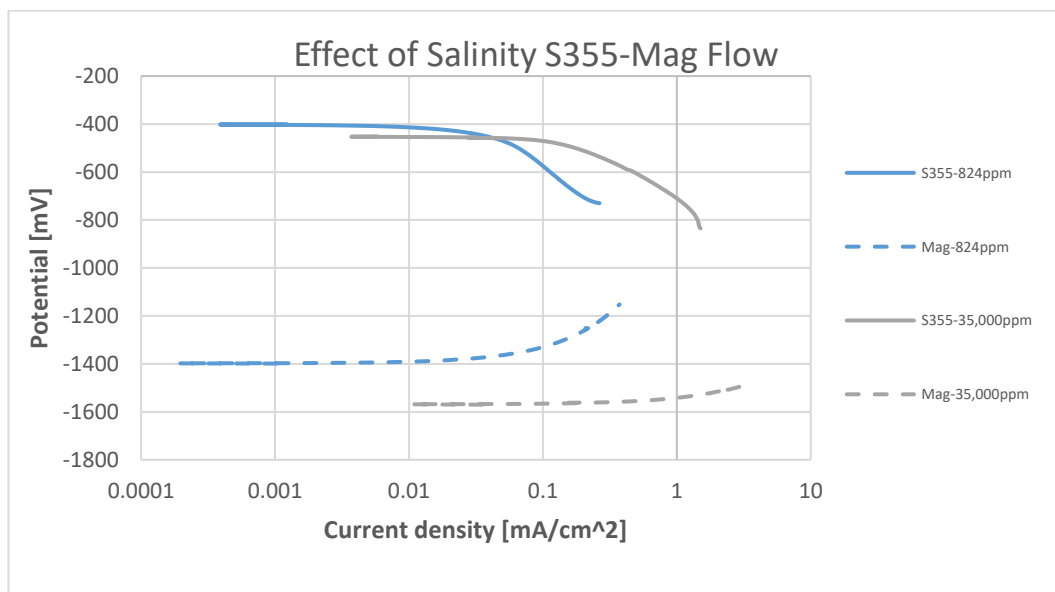


**Figure 3-13.** Effect of corrosive solution salinity on Magnesium Alloy Sacrificial Anode CP system performance in turbulent flow conditions.

In **Figure 3-14** the effect of the salinity of the electrolyte on the performance of a Zinc Alloy Sacrificial Anode CP system, working in turbulent flow conditions, is depicted.

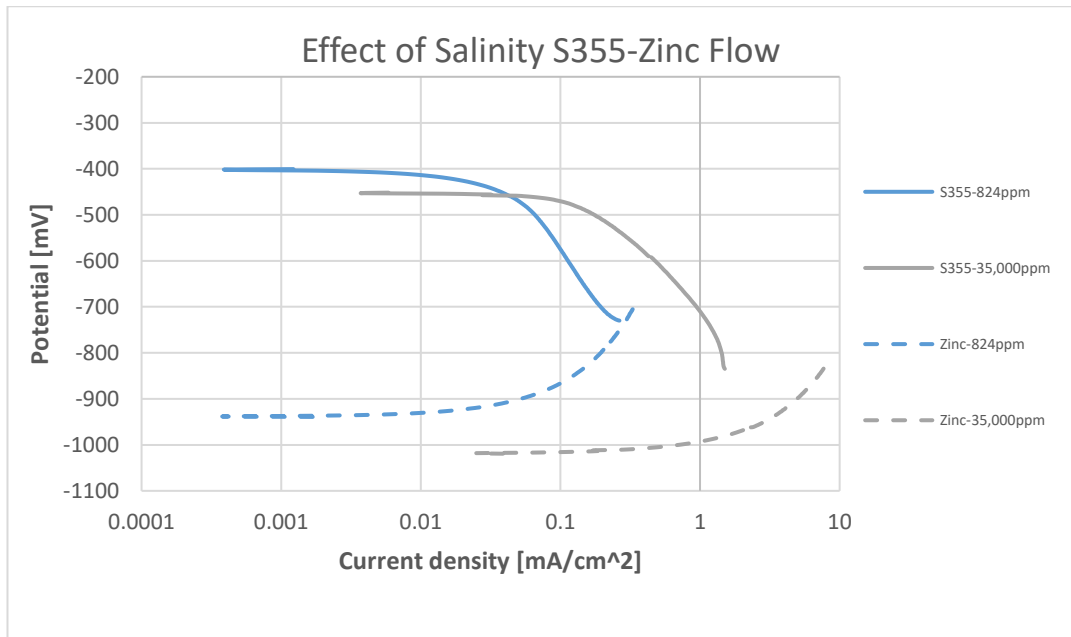


**Figure 3-14.** Effect of corrosive solution salinity on Zinc Alloy Sacrificial Anode CP system performance in turbulent flow condition.

In **Figures 3-13 and 3-14** it can be seen that, in both cases, an increase in the electrolyte salinity causes the rest potentials to become more electronegative and shifts the curves to the right, making the cathode more difficult to polarise. This means that the current density demand to achieve sufficient protective potential on the cathode surface increases. The increase in the salinity level also increases the electrical conductivity of the electrolyte allowing for more current to flow between the anode and the cathode.

#### 3.5.4.3 Effect of Driving Voltage (Anode Material)

Two different sacrificial anode materials, Zinc and Magnesium, have been tested to investigate the effect of the driving voltage on the performance of a SACP system. The tests were conducted in flowing conditions for two salinity levels (824 and 35,000ppm NaCl). The testing results are presented in **Figures 3-15 and 3-16**.

In **Figure 3-15** the effect of Anode material on the performance of a Sacrificial Anode CP system in high resistivity electrolyte, working in turbulent flow conditions, is depicted.

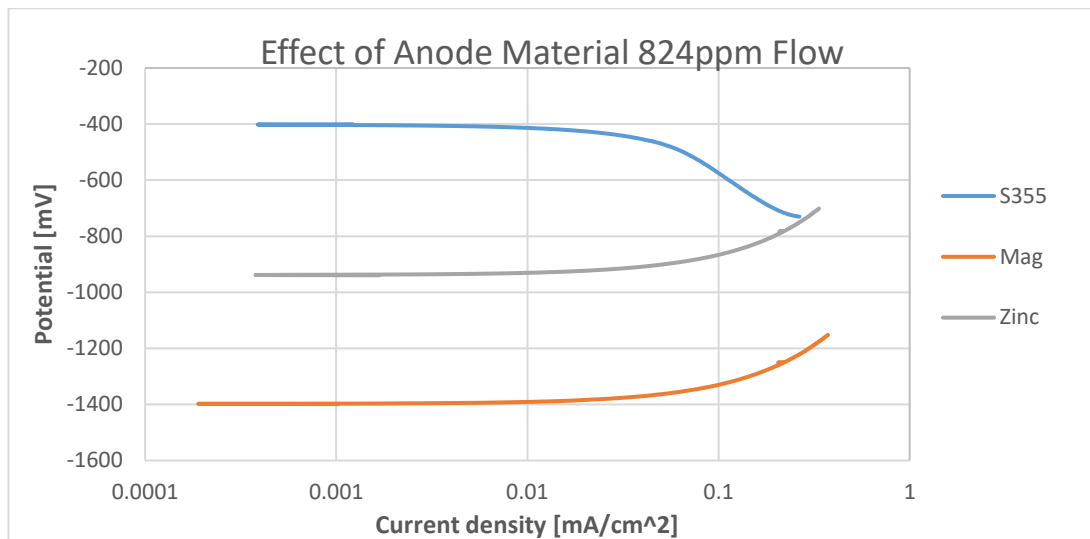


**Figure 3-15.** Effect of anode material on the performance of a Sacrificial Anode CP system in high resistivity solution under turbulent flow conditions.

In **Figures 3-16** the effect of Anode material on the performance of a Sacrificial Anode CP system in low resistivity electrolyte, working in turbulent flow conditions, is

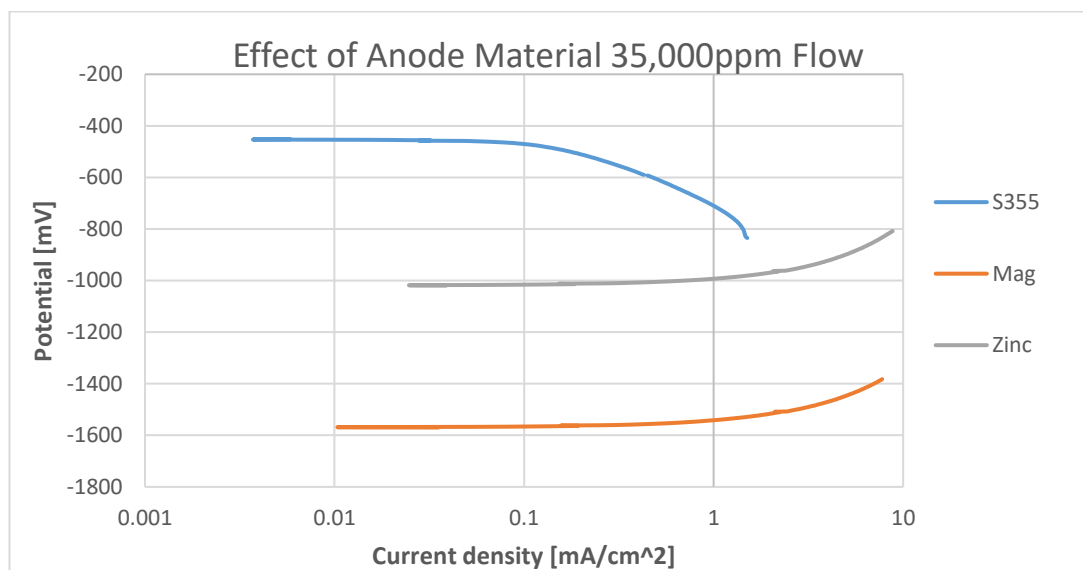


**Figure 3-16.** Effect of anode material on the performance of a Sacrificial Anode CP system in low resistivity solution under turbulent flow conditions.

According to the results, in both cases, the use of a more active anode shifts the anodic polarisation curves of the anode downwards resulting in higher driving voltage between the anode and the cathode. The increased driving voltage leads to the increase of the current flowing from the anode to the cathode. This will have a significant effect on a SACP system performance, as it will allow for the cathode to be polarised down to more electronegative potential levels.

## 3.6 Analytical Approach to CP System Performance Prediction

### 3.6.1 1-D Model for Analytical Approach

In order to predict the effect of various conditions on the behaviour of a sacrificial anode cathodic protection system, a 1-D mathematical model has been created, based on the analysis outcomes of the mathematical background review regarding the simulation of cathodic protection systems, presented in Paragraph 2.3. Ohm's law is used in combination with the boundary conditions on the surfaces of the polarized electrodes. In **Figure 3-17**, the 1-D sacrificial anode cathodic protection mathematical model is indicated.

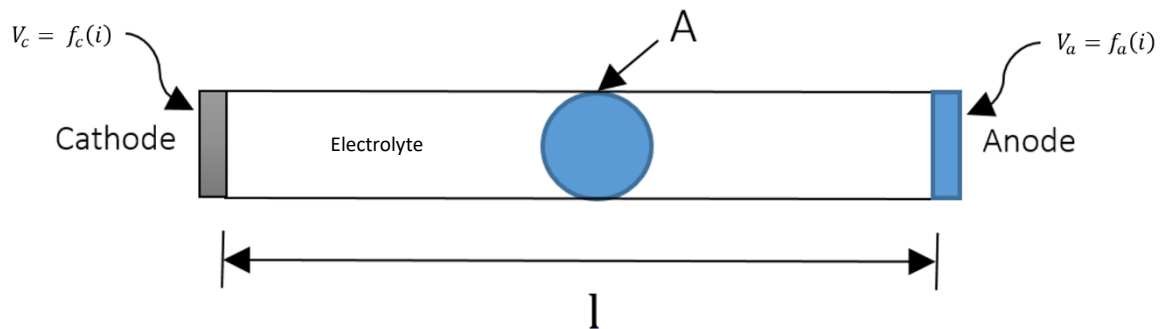


**Figure 3-17.** 1-D sacrificial anode cathodic protection mathematical model.

The scope of this model is to calculate the current flow in the system and the potentials of the anode and cathode using the boundary conditions that were obtained experimentally (polarization curves), as has already been described.

$$i = \sigma \frac{V_c - V_a}{l} \text{ or } \sigma \frac{\varphi_c - \varphi_a}{l} \Rightarrow i = \frac{V_c - V_a}{\rho l} \quad (\text{Ohm's law})$$

$$f_c(i) = V_c \quad (\text{Boundary conditions on cathode})$$

$$f_a(i) = V_a \quad (\text{Boundary conditions on cathode})$$

Substituting the equations of the boundary conditions into Ohm's law:

$$i = \sigma \frac{V_c - V_a}{l} \Rightarrow i = \sigma \frac{f_c(i) - f_a(i)}{l} \rightarrow i = f(\sigma, l) \quad (3-2)$$

or

$$i = \frac{V_c - V_a}{\rho l} \Rightarrow i = \frac{f_c(i) - f_a(i)}{\rho l} \rightarrow i = f(\rho, l) \quad (3-3)$$

From equations (3-2) and (3-3) it is obvious that the current flow is a function of the distance between electrodes' surfaces and the conductivity or the resistivity of the electrolyte, respectively. By substituting the current into the boundary conditions equations, the potential on the surface of each electrode can be calculated.

### 3.6.2 Sensitivity Analysis of CP System Performance

The effect of the distance between anode and cathode, anode material, electrolyte salinity and flowing conditions has been investigated using the 1-D mathematical model, presented in the previous section. Polarisation curves (boundary conditions), based on the experimental data have been used in the models. The scope of this investigation is the prediction of the sensitivity of a sacrificial anode cathodic protection system behaviour under the variation of these parameters.

#### 3.6.2.1 Effect of increasing distance between cathode and anode

The effect of increasing distance between the anode and the cathode has been investigated. The boundary conditions used for this investigation, based on the experimental results of the polarisation testing of S355 and Magnesium anode alloy, working in flowing 824ppm NaCl aqueous solution, are shown below.

Boundary conditions:

$$f_c(i) = V_c = -1541i - 406.78 \quad (3-4)$$

$$f_a(i) = V_a = 659.46i - 1396.1 \quad (3-5)$$

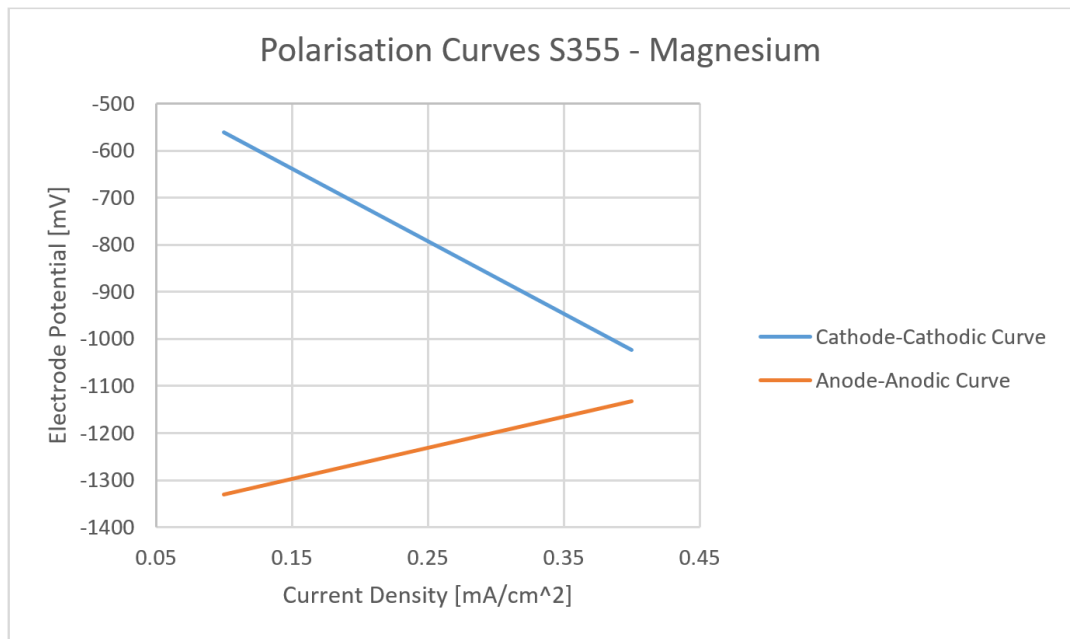


**Figure 3-18.** Polarization curves for the investigation of increasing distance between cathode and anode.

Assuming that the resistivity of the electrolyte is uniform and substituting the boundary conditions (3-4) and (3-5) into the equation (3-3):

$$i = \frac{f_c(i) - f_a(i)}{\rho l} = \frac{-1541i - 406.78 - (659.46i - 1396.1)}{\rho l} \Rightarrow$$

$$i = \frac{989.32}{2200 + \rho l} \quad (3-6)$$

where  $\rho = \text{constant} = 584.11 \Omega \cdot \text{cm}$ .

The distance between the anode and cathode is increased by 1cm increments from 1cm up to 10cm. The results of the calculations are shown in **Table 3-4**.

**Table 3-4.** Calculation results for increasing distance between anode and cathode.

l (cm)	i (mA/cm <sup>2</sup> )	Ec (mV)	Ea (mV)
1	0.3553	-954	-1162
2	0.2937	-859	-1202
3	0.2503	-793	-1231
4	0.2181	-743	-1252
5	0.1932	-705	-1269
6	0.1734	-674	-1282
7	0.1573	-649	-1292
8	0.1439	-629	-1301
9	0.1327	-611	-1309
10	0.1230	-596	-1315

According to the results of the 1-D mathematical model, as the distance between the anode and cathode surfaces increases, the resistance of the system increases causing the current flow to decrease. As a result, the current density on the electrode surfaces decreases causing the polarisation to decrease as well. In this way the cathode and anode potentials are driven to more electropositive and electronegative values respectively and so the level of protection is lower.

In **Figure 3-19** the decrease in the polarisation level on the electrodes' surfaces with the increasing distance is shown graphically.

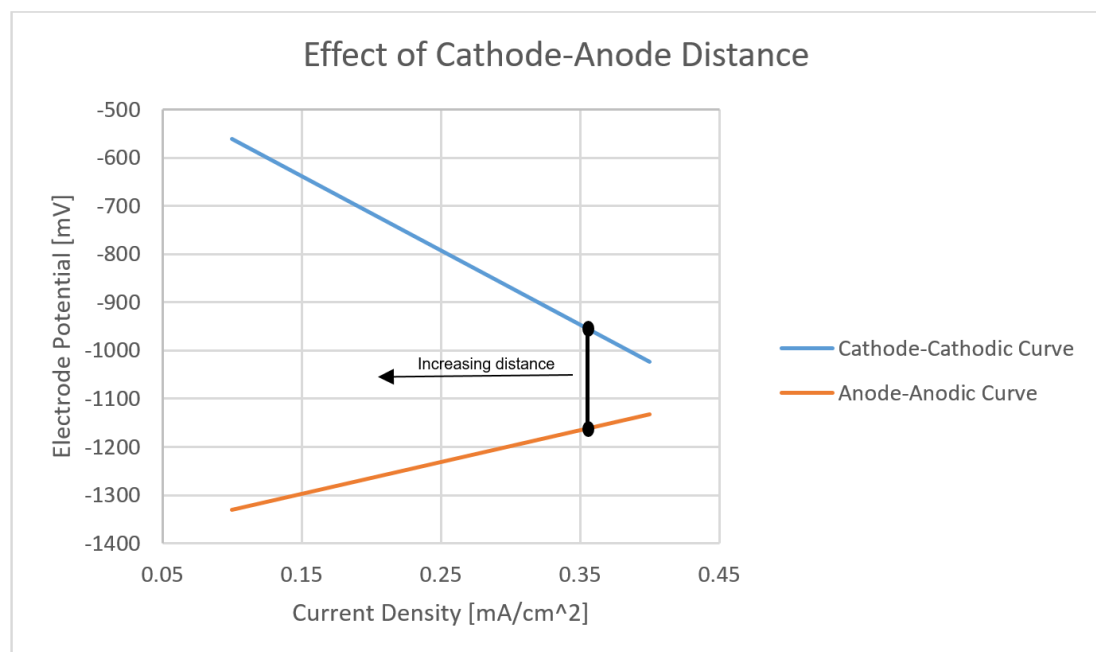


**Figure 3-19.** Graphical representation of the effect of increasing distance between cathode and anode on a SACP system performance (S355-Magnesium).

### 3.6.2.2 Effect of Anode material (Driving Voltage)

The effect of the use of a more active anode in a sacrificial anode cathodic protection system has been investigated. The boundary conditions used for this investigation, based on the experimental results of the polarisation testing of S355, Magnesium and Zinc anode alloys, working in in flowing 824ppm NaCl aqueous solution, are shown below.

Boundary conditions:

$$f_c(i) = V_c = -1541i - 406.78 \quad \text{Cathode} \quad (3-7)$$

$$f_a(i) = V_a = 530.16i - 2245.02 \quad \text{Less active anode - Zinc} \quad (3-8)$$

$$f_a(i) = V_a = 659.46i - 1396.1 \quad \text{More active anode - Magnesium} \quad (3-9)$$

Assuming that the resistivity of the electrolyte is uniform and substituting the boundary conditions (3-7) - (3-8) and (3-7) - (3-9) respectively into the equation (3-3):

$$i = \frac{f_c(i) - f_a(i)}{\rho l} \Rightarrow$$

$$i = \frac{530.16}{2245.02 + \rho l} \quad \text{Less active anode - Zinc} \quad (3-10)$$

$$i = \frac{989.32}{2200 + \rho l} \quad \text{More active anode - Magnesium} \quad (3-11)$$

where  $\rho = \text{constant} = 584.11 \Omega \cdot \text{cm}$  and  $l = \text{constant} = 2 \text{cm}$ .

The results of the calculations are tabulated in the following Table.

**Table 3-5.** Calculation results for increasing driving voltage in the system due to the use of more active anode material.

Anode	$i$ (mA/cm <sup>2</sup> )	$E_c$ (mV)	$E_a$ (mV)
Zinc Anode	0.1553	-646	-828
Magnesium Anode	0.2937	-859	-1202

According to the results of the 1-D mathematical model, if a more active anode is used for a specific sacrificial anode cathodic protection system, the driving voltage in the system will increase and so will the current flow. This will result in higher current

density on the electrodes' surfaces and increased polarisation, driving the cathode to more electronegative potential levels. This phenomenon has been seen in the erosion-corrosion tests, in the case of using of Magnesium alloy instead of Zinc alloy sacrificial anodes in low conductivity aqueous solution.

In **Figure 3-20** the increase in the polarisation level on the cathode surface with the increasing driving voltage, due to the use of more active anode material, is shown graphically.

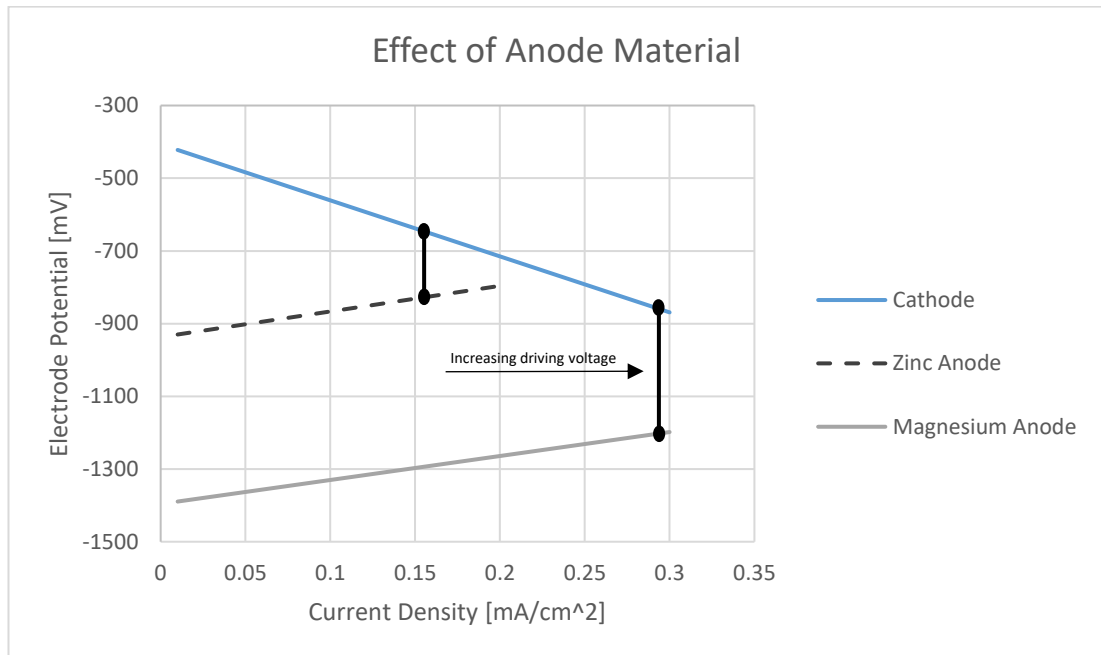


**Figure 3-20.** Graphical representation of the effect of increasing driving voltage on a SACP system performance.

### 3.6.2.3 Effect of Electrolyte Salinity

The effect of increasing salinity in a sacrificial anode cathodic protection system has been investigated. The polarisation curves used in the investigation are based on the experimental results of the polarisation scans of S355 and Magnesium anode alloy, working in flowing 824ppm (electrolyte resistivity  $\rho=584.11\Omega\cdot\text{cm}$ ) and 35,000ppm (electrolyte resistivity  $\rho=19.048\Omega\cdot\text{cm}$ ) NaCl aqueous solutions. The boundary conditions used for this investigation are shown below.

Boundary conditions:

$$f_c(i) = V_c = -1541i - 406.78 \quad \text{Cathode lower salinity} \quad (3-12)$$

$$f_a(i) = V_a = 659.46i - 1396.1 \quad \text{Anode lower salinity} \quad (3-13)$$

$$f_c(i) = V_c = -235.85x - 472.52 \quad \text{Cathode higher salinity} \quad (3-14)$$

$$f_a(i) = V_a = 25.026x - 1567.1 \quad \text{Anode higher salinity} \quad (3-15)$$

Assuming that the resistivity of the electrolyte is uniform and substituting the boundary conditions (3-12) - (3-13) and (3-14) - (3-16) respectively into the equation (3-3):

$$i = \frac{f_c(i) - f_a(i)}{\rho l} \Rightarrow$$

$$i = \frac{989.32}{2200 + \rho l} \quad \text{Lower salinity electrolyte, } \rho = 584.11 \Omega \cdot \text{cm} \quad (3-16)$$

$$i = \frac{1094.58}{260.87 + \rho l} \quad \text{Higher salinity electrolyte, } \rho = 19.048 \Omega \cdot \text{cm} \quad (3-17)$$

where  $l = \text{constant} = 10 \text{cm}$ .

The results of the calculations are shown in **Table 3-6**.

**Table 3-6.** Calculation results for increasing salinity of the electrolyte.

Salinity Level	$i$ (mA/cm <sup>2</sup> )	$E_c$ (mV)	$E_a$ (mV)
Lower	0.123	-596	-1315
Higher	2.43	-1044	-1506

According to the results of the 1-D mathematical model, in a higher salinity solution the resistance will decrease and so the current flow will increase. The increase of the current flow will lead to increased polarisation of the cathode. In this way the potential of the cathode will be driven to more electronegative values (higher level of protection).

In **Figure 3-21** the effect of the increase in the salinity level of the aqueous solution on the polarisation of both anode and cathode is shown graphically.

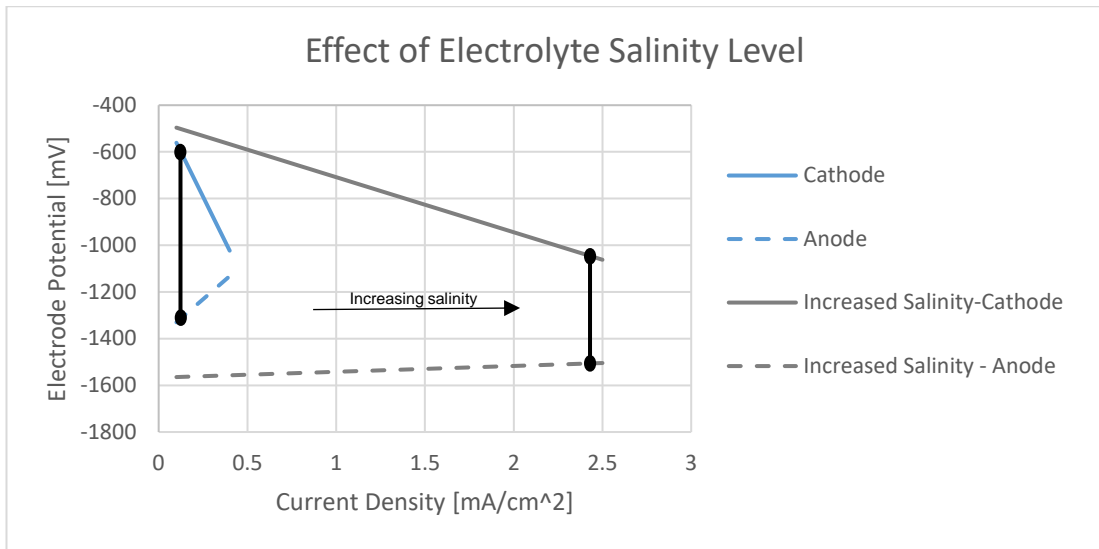


**Figure 3-21.** Graphical representation of the effect of increasing salinity on a SACP system performance.

The effect of increasing salinity level of the electrolyte on anode material is the accelerated consumption, due to the increased protection current flowing from the anode to the cathode.

The results of the 1-D model are in agreement with the findings of the erosion-corrosion tests where higher salinity levels increased the electrical current flow and drove the potential of the cathode to more protective (more electronegative) levels.

#### 3.6.2.4 Effect of Flowing Conditions

The effect of the flowing conditions in a sacrificial anode cathodic protection system has been investigated. The investigation is based on the experimental results of the polarisation scans of S355 and Magnesium anode alloy, working in static and flowing 824ppm NaCl aqueous solution. The boundary conditions used for this investigation are shown below.

$$f_c(i) = V_c = -11126x - 375.19 \quad \text{Static conditions} \quad (3-18)$$

$$f_a(i) = V_a = 915.58x - 1366.9 \quad \text{Static conditions} \quad (3-19)$$

$$f_c(i) = V_c = -1541i - 406.78 \quad \text{Flowing conditions} \quad (3-20)$$

$$f_a(i) = V_a = 659.46i - 1396.1 \quad \text{Flowing conditions} \quad (3-21)$$

Assuming that the resistivity of the electrolyte is uniform and substituting the boundary conditions (3-18) - (3-19) and (3-20) - (3-21) respectively into the equation (3-3):

$$i = \frac{f_c(i) - f_a(i)}{\rho l} \Rightarrow$$

$$i = \frac{991.71}{12041.6 + \rho l} \quad \text{Lower velocity} \quad (3-22)$$

$$i = \frac{989.32}{2200 + \rho l} \quad \text{Higher velocity} \quad (3-23)$$

where  $\rho = \text{constant} = 584.11 \Omega \cdot \text{cm}$  and  $l = \text{constant} = 10 \text{cm}$ .

The results of the calculations are shown in **Table 3-7**.

**Table 3-7.** Calculation results for increasing velocity of the electrolyte.

Flowing Conditions	$i$ (mA/cm <sup>2</sup> )	$E_c$ (mV)	$E_a$ (mV)
Static	0.0555	-992	-1316
Flowing	0.123	-596	-1315

Increasing velocity makes the cathode more difficult to polarise, as has been already seen. Thus, higher current density is needed to maintain the potential to a specific level. According to the results of the 1-D mathematical model, increases in flow velocity causes the current flow to increase, due to the fact that more reactants reach the cathode surface but the potential becomes more electropositive and so less protective. Finally, higher current densities, due to increased flow velocity, cause the anode material to consume at a higher rate.

In **Figure 3-22** the effect of the increase in the flow velocity on the polarisation of both anode and cathode is shown graphically.

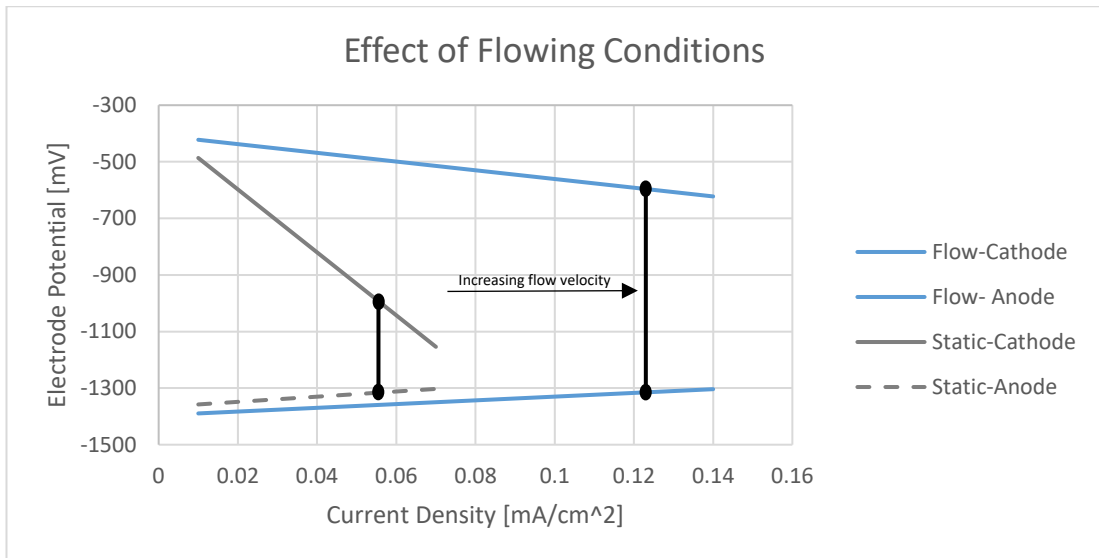


**Figure 3-22.** Graphical representation of the effect of increasing velocity on a SACP system performance.

### 3.7 Conclusions

According to the results of the experimental investigation, the level of the salinity has been found to increase the erosion-corrosion rate of the low alloy steel grade S355J2G3+N. Cathodic protection was successfully applied and was effective in both salinity levels tested in controlling erosion-corrosion. The use of Zinc alloy sacrificial anodes and Zinc rich sacrificial coating eliminated the effect of erosion-corrosion in both salinity levels, but the Magnesium sacrificial anodes proved to be more efficient in the low salinity aqueous solution, driving the potential of the test samples to more negative levels.

The use of SACP is expected to mitigate corrosion and so extend the fatigue life of WEIR Minerals pump components working in corrosion-fatigue conditions. The further experimental investigation will comprise of the use of Zinc sacrificial anodes in the higher salinity level (35,000ppm) aqueous solution and Magnesium sacrificial anodes in the lower salinity (824ppm) level aqueous solution.

SCCP using Zinc rich sacrificial coating has been shown to be a successful strategy in mitigating erosion-corrosion, but in the case of protecting the internal surfaces of GEHO PD components, it might be proved to be ineffective in several ways. The complexity of the geometry to be protected increases the risk of improper application

of the coating. By using SCCP the monitoring of the systems performance becomes very difficult and the detection of holidays almost impossible unless by performing optical survey that will mean stopping the pump operation. Also, sacrificial anodes are very easy to replace while repairing a sacrificial coating is expected to be time and cost ineffective. What is more, moving pump components such as valves, suffering severely from wear mechanisms, will be more effectively protected by SACP as the sacrificial coating applied on their surfaces is expected to wear off revealing great parts of unprotected base metal.

The conditions variation have been seen to have a critical role in the performance of cathodic protection systems. Increases in flow velocity, salinity level and the use of more active anode materials greatly affected the behaviour of a cathodic protection system. Increased flow velocity, drove the rest potentials to more electropositive values and increased the current demand for sufficient polarisation of the cathode. Increases in salinity level, drove the rest potentials to more electronegative values and increased the electrical conductivity of the electrolyte allowing for more current to flow between the anode and the cathode. The use of more active sacrificial anode materials resulted in higher driving voltage between the anode and the cathode and so increased protection current flow.

The use of the results of the polarisation testing as boundary conditions in the 1-D mathematical model allowed for quantitative predictions of the response of SACP systems to the variation of environmental conditions. The increasing distance between cathode and anode was found to have a great effect on the performance of a SACP system, as it causes the current flow to decrease, due to the increasing resistance of the system. The use of a more active anode proved to be an effective method to increase the polarisation of the cathode, driving its potential to more electronegative levels. Furthermore, the increasing salinity level of the aqueous solution was seen to increase the polarisation of the cathode as it allowed for increased protection current flow. The variation of the flow velocity of the electrolyte over the surfaces of the electrodes greatly affected the performance of the system. Increases in flow velocity increased the current flowing in the system but the potential of the cathode became more electropositive and so less protective. Increases in salinity level and flow velocity, resulting in higher current flow, cause the anode to consume at a higher rate. This means that the anodes of a SACP system should be replaced more often, increasing the cost of the system's use. Finally, the results

obtained from the use of the 1-D mathematical model, concerning the effect of the salinity level variation and the use of more active anode materials are in accordance to the results of the erosion-corrosion experiments.

### 3.8 References

- [3.1] L. G. Giourntas, Investigation of Erosion-Corrosion Behaviour of Pump Materials, University of Strathclyde, Department of Mechanical and Aerospace Engineering, Glasgow, UK (2016).
- [3.2] G. Karafyllias, The Effect of Acidity and Salinity Level in Erosion-Corrosion Performance of Metals, University of Strathclyde, Department of Mechanical and Aerospace Engineering, Glasgow, UK (2017).
- [3.3] L. Giourntas, T. Hodgkiess and A. M. Galloway, Comparative Study of Erosion–Corrosion Performance on a Range of Stainless Steels, *Wear*, Volumes 332-333, pp. 1051-1058 (2015).
- [3.4] N. Andrews, L. Giourntas, A. M. Galloway, A. Pearson, Effect of Impact Angle on the Slurry Erosion-Corrosion of Stellite 6 and SS316, *Wear*, Volume 320, pp. 143-151 (2014).
- [3.5] L. Giourntas, T. Hodgkiess and A. M. Galloway, Enhanced Approach of Assessing the Corrosive Wear of Engineering Materials under Impingement, *Wear*, Volumes 338-339, pp. 155-163 (2015).
- [3.6] N. Andrews, L. Giourntas, A. M. Galloway and A. Pearson, Erosion–Corrosion Behaviour of Zirconia, WC–6Co, WC–6Ni and UNS S31600, *Int. Journal of Refractory Metals and Hard Materials*, Volume 48, pp. 229-237 (2015).
- [3.7] George Karafyllias, Edward Humphries and Alexander Galloway, Erosion-Corrosion Evaluation of Two White Cast Irons under Severe Conditions for Application in the Oil Sands Industry, NACE International, Corrosion 2018 Conference & Expo, Paper No. 11405 (2018).

- [3.8] George Karafyllias, Lampros Giourntas, Alexander Galloway and Trevor Hodgkiess, Relative Performance of Two Cast Irons and Two Stainless Steels under Erosion-Corrosion Conditions, NACE International, Corrosion 2016 Conference & Expo, Paper No. 7723 (2016).
- [3.9] ASTM International, Standard Reference Test Method for Making Potentiodynamic Anodic Polarization Measurements, Designation: G5 – 14 (2014).
- [3.10] David G. Enos and Louie L. Scribner, The Potentiodynamic Polarization Scan, Technical Report 33, Solartron Instruments a division of Solartron Group Ltd, Farnborough, Hampshire, UK (1997).
- [3.11] Alec Groysman and Avihu Hiram, Corrosion Monitoring and Control in Refinery Process Units, NACE International, Corrosion 97, Paper No. 512 (1997).
- [3.12] WANG Chun Li, WU Jiang Hua and YUAN Man, Effect of Temperature on the Galvanic Corrosion of Cu-Ni Alloy/High Strength Steel in Seawater, MATEC Web of Conferences, Volume 67, Paper No. 07039 (2016).
- [3.13] T. Hodgkiess and L. Giourntas, Assessment of Cathodic Protection in Pumping Equipment, WARC Project No. 3.16, Final Report, University of Strathclyde, UK (2016).
- [3.14] H. R. Copson, Effects of Velocity on Corrosion, Northeast Region Conference, National Association of Corrosion Engineers, Boston, Massachusetts (1958).
- [3.15] Harvey P. Hack and Robert J. Guanti, Effect of High Flow on Calcareous Deposits and Cathodic Protection Current Demand, David Taylor Research Centre, DTRC/SME-87/82, Bethesda, Maryland (1988).
- [3.16] Harvey P. Hack, Atlas of Polarization Diagrams for Naval Materials in Seawater, Carderock Division Naval Surface Warfare Center, CARDIVNSWC-TR-61—94/44, Bethesda, USA (1995).
- [3.17] NACE International, CP3 – Cathodic Protection Technologist Course Manual, version 1 (2014).

# CHAPTER 4

## Corrosion-Fatigue Performance

### 4.1 Introduction

In this chapter, the techniques and outcomes of the experimental investigation of the effect of cathodic protection on the corrosion-fatigue life of the low alloy steel grade S355 are presented and discussed. The overall aim of this work was to utilize corrosion protection strategies in order to extend the corrosion-fatigue life of GEHO PD pump components, operating in corrosive aqueous environments.

As stated by Ralph van Rijswijk et al. in [4.1], piston diaphragm pumps, as shown in **Figure 4-1**, are used worldwide for the transportation of abrasive and/or aggressive slurries against high discharge pressures in mining, mineral processing and power industries. The function of such systems is described as follows. A crankshaft (1), which is usually driven by a frequency-controlled electric motor with a gearbox, produces the reciprocating motion of a piston (2). The motion of the piston displaces a propelling fluid (3) causing the reciprocation of a rubber diaphragm (4). In this way, the displacement of the pumped slurry (5) is achieved. The positive displacement action of the pump is generated using self-acting valves (6). Common pump configuration consists of three parallel cylinders, operating at a 120° phase shift from each other, partially evening out flow fluctuation of each individual chamber. Finally, the remaining fluctuation of the flow is absorbed by gas-filled dampeners (7), placed on the suction and discharge sides.

The fluid end modules of these pumps experience cyclic loading, due to the cyclic pump chamber pressure, varying between suction and discharge pressure on every pump stroke. Moreover, their design life is 25 years for continual duty in mineral processing applications. The GEHO design procedure is based on an infinite life approach, according to which the maximum allowable (constant) stress amplitude is

limited so as to ensure a design life of  $10^9$  cycles, based on a fixed maximum design stress of 100 MPa for pure tensile loading ( $R = 0$ ) [4.2-4.3].

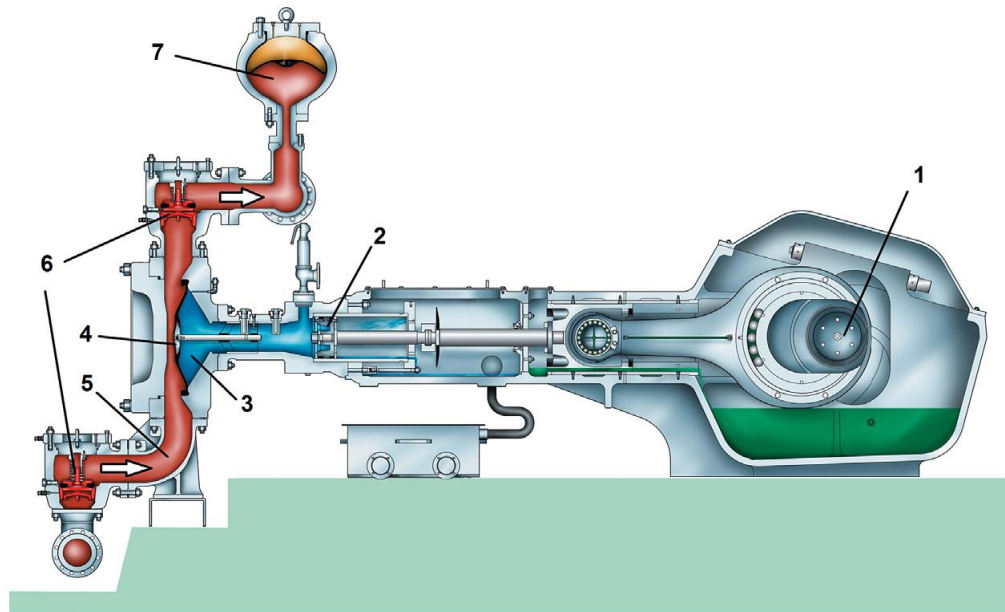


**Figure 4-1.** Cross-section of GEHO piston diaphragm pump [4.1].

The current design strategy of WEIR Minerals for protecting fluid end modules against corrosion-fatigue, resulting in unpredicted failures, dictates the use of stainless steel grades, instead of low alloy steels, in the case that chloride ( $\text{Cl}^-$ ) concentration of the pumped fluid is 500ppm (824ppm NaCl) or higher. The current work aims to prove the effectiveness of cathodic protection in eliminating the effect of corrosion on the fatigue life of the low alloy steel grade S355, used for the manufacturing of GEHO PD pump fluid end modules, working in corrosive aqueous environments of various NaCl concentrations.

A testing programme was conducted for the investigation of the effect of cathodic protection on the corrosion-fatigue performance of the material, consisting of tests in air, tests in corrosion-fatigue conditions in two salinity level aqueous solutions (824ppm and 35,000ppm) and corrosion-fatigue tests using Magnesium alloy sacrificial anodes for the lower salinity level aqueous solution and Zinc alloy sacrificial anodes in the case of the higher salinity level aqueous solution, in flowing conditions. For this purpose, a special chamber was designed and manufactured that was able to incorporate the equipment for the application of the SACP systems.

The fatigue testing aimed at the obtaining of insight into the behaviour of the material in corrosion-fatigue conditions and the effectiveness of cathodic protection in driving the fatigue life back to the in-air levels. As stated by A. Bahrami in [4.4] the in-air performance can be restored by cathodic protection only at low stresses and there is no benefit at higher stresses. Thus, focus was on the fatigue performance close to the in-air fatigue limit, which was assumed to be testing to  $10^6$  cycles without failure, according to [4.2, 4.5-4.6]. The samples, apparatus and methods used for this investigation are described in detail in the following sections.

## 4.2 Pre-Test Methodologies

### 4.2.1 Source of Materials

#### 4.2.1.1 Material Investigated

The material investigated, low alloy steel grade S355, was provided in the form of cylindrical plates, as described in Chapter 3. This material was used for the manufacturing of the fatigue specimens. Rectangular shape blocks were extracted from the cylindrical plates and machined to their final form.

The mechanical properties of the material, based on the material's manufacturing company MCC CERI Equipment Development and Manufacturing Co., Ltd., quality certificate, are as presented in **Table 4-1**.

**Table 4-1.** Mechanical Properties of the low alloy steel grade S355.

S355J2G3+N Mechanical Properties		
Yield Strength Re [Mpa]	UTS Rm [Mpa]	Elongation A [%]
295	531	34.5

#### 4.2.1.2 Sacrificial Anode Materials

The Zinc alloy and Magnesium alloy sacrificial anode materials that were used for the corrosion-fatigue testing, were manufactured from the same material blocks as for the

manufacturing of the sacrificial anodes used in the erosion-corrosion experiments. The anodes were machined to a final rod shape of circular cross section.

#### 4.2.2 Design and Manufacturing of Test Samples

##### 4.2.2.1 Fatigue Specimens

The fatigue specimens were designed and machined according to the standards ASTM E466-07 [4.7] and BS EN ISO 11782-1:2008 [4.8]. Cylindrical specimens with tangentially blended fillets between the test section and the ends, which are suitable for axial loading were employed for the tests in air, in corrosion-fatigue conditions and the tests conducted in corrosion-fatigue conditions using sacrificial anode CP. In **Figure 4-2**, the form and dimensions of the fatigue specimens are shown (all dimensions are given in mm).

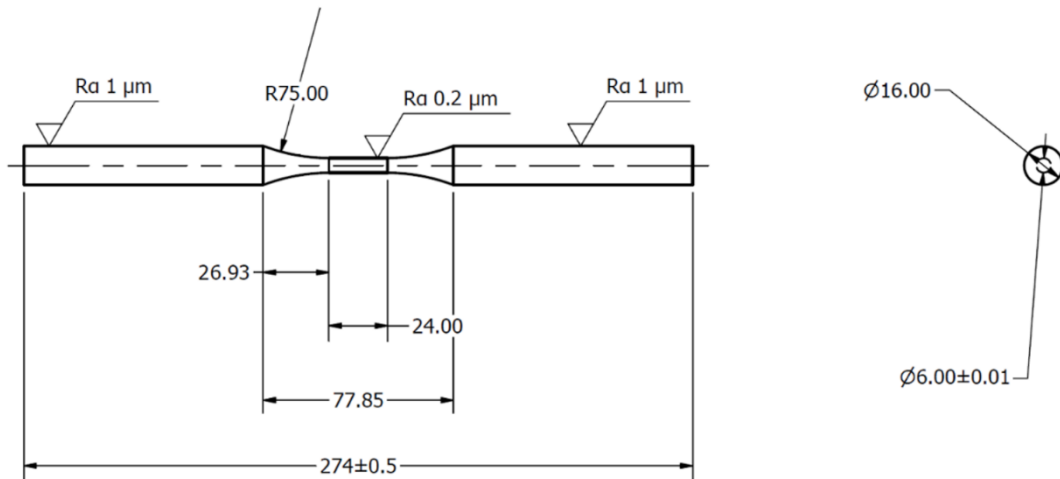


**Figure 4-2.** Fatigue test samples, manufactured according to the standards ASTM E466-07 and BS EN ISO 11782-1:2008.

The specimens were chosen to be smooth as it was assumed that no geometrical irregularities exist in the internal surfaces of GEHO pumps. The roughness of the test section of the specimens was chosen so as to represent the actual surface finish of pump components, suffering severely from corrosion-fatigue. Finally, the grip cross sectional area was designed to be larger than four times the test section area to ensure that failure occurs in the test section.

#### 4.2.2.2 Sacrificial Anodes

Special pencil type sacrificial anodes were designed and manufactured for the application of SACP in corrosion-fatigue tests. Both Zinc and Magnesium alloy anodes were manufactured according to the form and dimensions shown in **Figure 4-3** (all dimensions are given in mm).

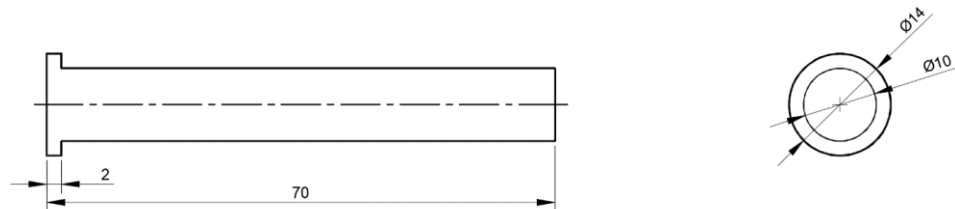


**Figure 4-3.** Pencil type sacrificial anodes, manufactured for the application of SACP in corrosion-fatigue testing.

A polymer anode holder (1) was used for the placing of the anode (2) into the corrosion-fatigue chamber. An electrical-connection wire (3) was soldered to the wider base of the sacrificial anode specimen and then the specimen was encapsulated in epoxy resin (4), as is shown in **Figure 4-4**. Electrical contact between the sacrificial anode specimen and the test specimen was achieved via a wire electrically connected to the test specimen.

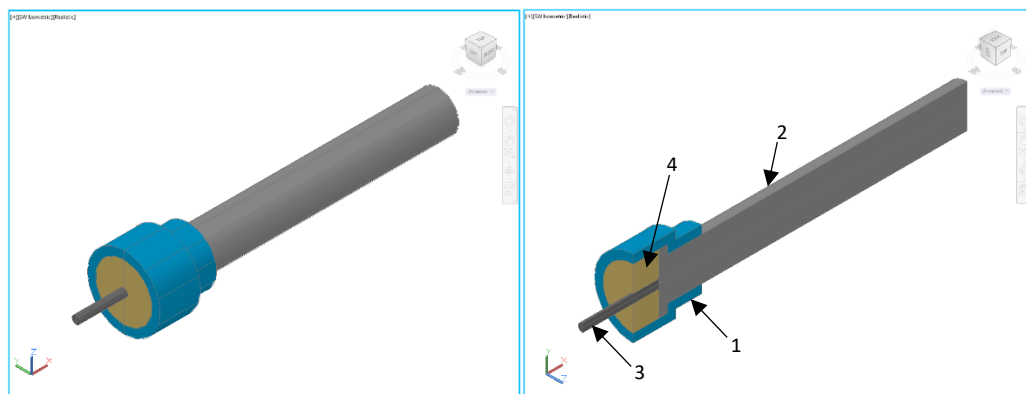


**Figure 4-4.** Isometric view (left) and cross sectional view (right) of the pencil type sacrificial anode assembly.

### 4.2.3 Environmental Chamber

A special environmental (corrosion) chamber was designed and manufactured for the conduction of the corrosion-fatigue testing of the low alloy steel grade, enabling the incorporation of a SACP system. The chamber was designed, using AutoCAD 2015 designing software, so as to completely enclose the test length of the specimen, excluding the gripped portions from contact with the corrosive environment. As is shown in **Figure 4-5**, the chamber assembly consisted of three main parts, a 3-D printed polymer cubic shape chamber (1), two acrylic plates (2) that enabled the observation of the specimen (3) during the experimental procedure and two rubber sealing parts (4) to secure that no leakage of the corrosive fluid will occur. Furthermore, the chamber comprised of two tube shape openings to act as inlet (5) and outlet (6) of the corrosive solution and circular openings on the top for the placement of the anode (7) and the same Ag/AgCl (silver/silver chloride) reference electrode (8) that was used also in the erosion-corrosion experimental programme.

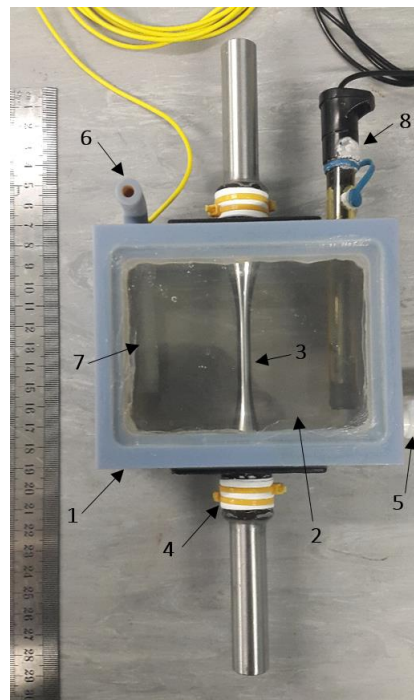


**Figure 4-5.** Corrosion-fatigue chamber assembly incorporating a SACP system.

In **Figure 4-6**, isometric views of the corrosion-fatigue chamber 3-D drawing are presented. The chamber enabled the flow of the corrosive fluid via the two tube shape openings of 5mm inner diameter and 2.5mm wall thickness. The circulation of the corrosive environment was made possible by connecting the environmental chamber

to the pump via an elastic tube of 9mm inner diameter. Another elastic tube of the same size was used for the returning of the solution back to the water tank, as will be shown in a following section of this chapter.

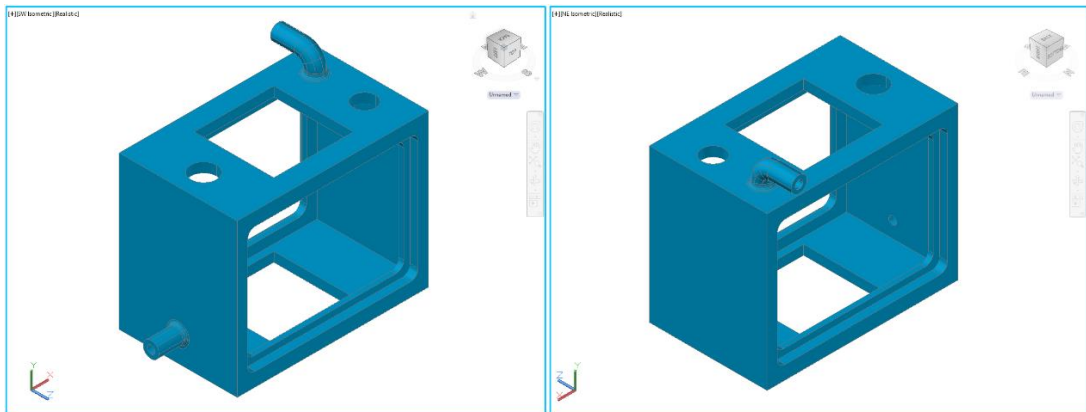


**Figure 4-6.** Isometric views of the corrosion-fatigue chamber 3-D drawing.

The rubber sealing parts were designed so as to enable complete sealing of the corrosion-fatigue chamber and at the same time absorb the specimen's deformation, without risking the chamber's tightness and integrity. Isometric view and cross sectional view of the 3-D drawing of a rubber sealing part can be seen in **Figure 4-7**.

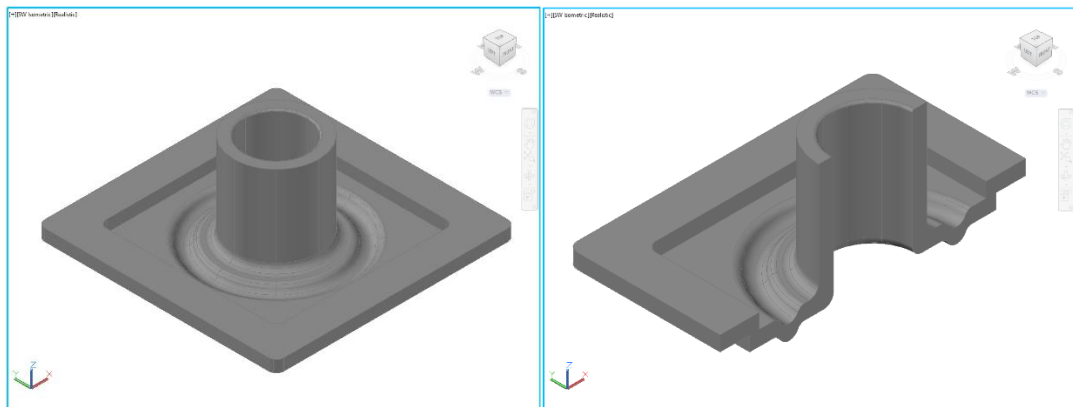


**Figure 4-7.** Isometric view (left) and cross sectional view (right) of the rubber sealing part of the corrosion-fatigue chamber set-up.

## 4.3 Fatigue Testing Procedures

### 4.3.1 Testing Protocol

#### 4.3.1.1 *In-Air Fatigue Testing*

The fatigue testing programme included tests in air at room temperature in order to determine the fatigue performance close to the fatigue limit of the material, without the effect of corrosive environments. This was achieved by adopting the method described in [4.8-4.9], which dictated that the first specimen should be tested at a high stress level, where failure is expected to occur in a relatively short number of cycles. The test stress then decreased for each succeeding specimen until a stress level, where one or two specimens did not fail within the specified number of cycles, was reached. The highest stress level at which a non-failure (runout) test is achieved, is taken as the fatigue limit. Since the runout tests were observed at a much higher stress level compared to the maximum design stress of 100MPa, for pure tensile loading ( $R=0$ ), used by WEIR Minerals, it was decided that the adoption of a more precise statistical method (e.g. staircase method) to estimate the fatigue limit, was not necessary for the purpose of this investigation.

The cycles to failure tests were conducted using an Instron 8801 fatigue testing system of up to  $\pm 100\text{kN}$  axial force capacity in conjunction with the WaveMatrix software, for the monitoring of the cyclic loading applied and the counting of the fatigue cycles. The experiments were conducted at ambient temperature with a stress ratio of  $R=0$  (pure tensile loading). The cyclic frequency was 15Hz, which is higher compared to the corrosion-fatigue testing cyclic frequency (10Hz), as in fatigue tests conducted in air, it usually has little effect, if any, according to BS EN ISO 11782-1:2008 [4.8]. For comparison reasons, the cyclic frequency was kept constant in all tests performed in corrosive environments as it influences the effect of corrosion on failure [4.10-4.11].

#### 4.3.1.2 *Corrosion - Fatigue Testing*

The effect of corrosion on the fatigue life of the material was investigated by performing tests using the environmental chamber, which was described in a previous

section. The results of this kind of testing were used as a reference point for the estimation of the effectiveness of cathodic protection in eliminating the effect of corrosion on fatigue life. Corrosion-fatigue tests were conducted at various stress levels in tap water solutions of 824ppm and 35,000ppm NaCl concentration. The apparatus used for the performance of the tests is shown in **Figure 4-8**.

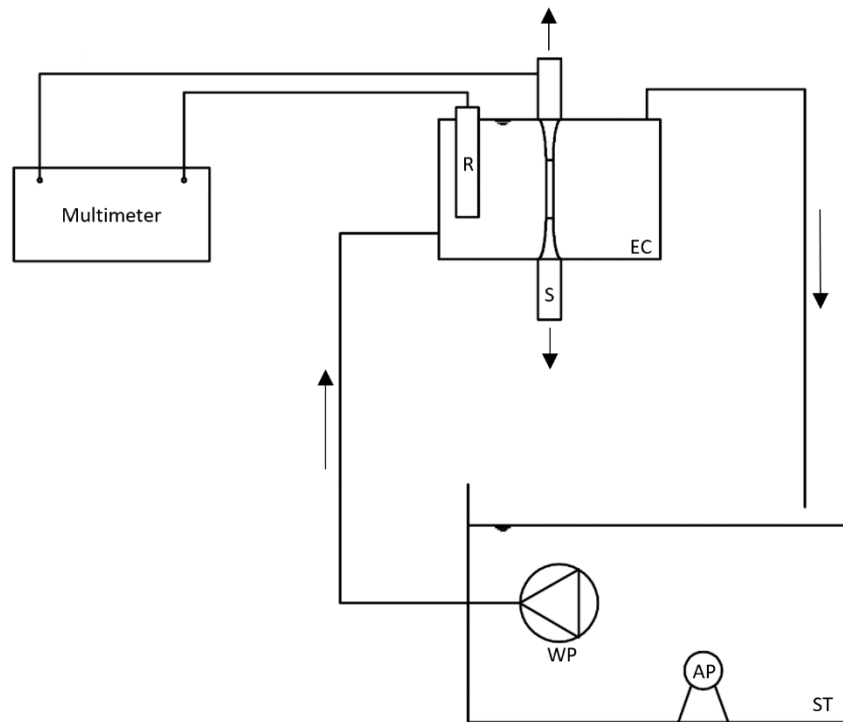


**Figure 4-8.** Schematic representation of the corrosion-fatigue test rig, S: specimen (working electrode), R: reference electrode, EC: environmental chamber, WP: water pump, AP: air pump, ST: solution tank.

The specimen was mounted on the fatigue machine grips within the environmental chamber and the testing parameters of loading and cyclic frequency, were introduced into the fatigue machine controller. The frequency of both corrosion-fatigue and corrosion-fatigue with cathodic protection tests was set at 10Hz. Aeration of the 15lt corrosive solution was maintained by bubbling air through the solution, using an EIHEIM 100 air pump. The conductivity and the concentration of the dissolved oxygen were measured by an EXTECH Instruments WQ530 water quality meter. Furthermore, the pH level was measured using a VWR pH110 ECN 662-1350 instrument. The results of the measurements are presented in **Table 4-2**. The aqueous solution was circulated by a submersible Beta 600 water pump and its temperature kept at  $25 \pm 2^\circ\text{C}$  [4.8].

**Table 4-2.** Conductivity, dissolved oxygen concentration and pH measurements.

Salinity [ppm]	Conductivity [mS/cm]	Dissolved Oxygen [mg/L]	pH
35000	52.5	4.5 - 5 (@26°C)	7 ±0.3
824	1.712	7.0 (@26°C)	

The experimental set-up facilitated monitoring of the open circuit potential of the specimen using a voltmeter and a reference electrode. The electrode potential was measured via an AIM TTi 1705 programmable digital multimeter versus a Thermo Scientific Orion single junction Cat. No 900100 Ag/AgCl (silver/silver chloride) reference electrode.

As the electrode potential will change after initial immersion and also corrosion product development will be time-dependent, the corrosive solution was introduced into the environmental chamber simultaneously with the commencement of loading. In this way, the effect of any pre-exposure period on the fatigue life of the material investigated, was eliminated.

#### 4.3.1.3 Corrosion-Fatigue with Cathodic Protection Testing

Apart from the tests conducted under open circuit conditions (corrosion-fatigue), in which the metal's electrode potential is dependent only on the specific environmental conditions, tests were carried out also with sacrificial anode cathodic protection. In order to drive the electrode potential of the metal to more electronegative levels (more negative than  $-800\text{mV}_{\text{SSC}}$ ), sacrificial anodes were used, as described in a previous section. For the protection of the low alloy steel grade S355 in 35,000ppm NaCl tap water solution, Zinc alloy sacrificial anodes were used while for the solution of 824ppm salinity, Magnesium alloy sacrificial anodes were employed. The sacrificial anode was inserted into the environmental chamber and electrically connected to the test specimen via a wire. Using an AIM TTi 1705 programmable digital multimeter, was included in the electrical connection between the anode and the test specimen, the anode current output was monitored. The experimental set-up of the corrosion-fatigue tests with sacrificial anode cathodic protection is presented in **Figure 4-9**.

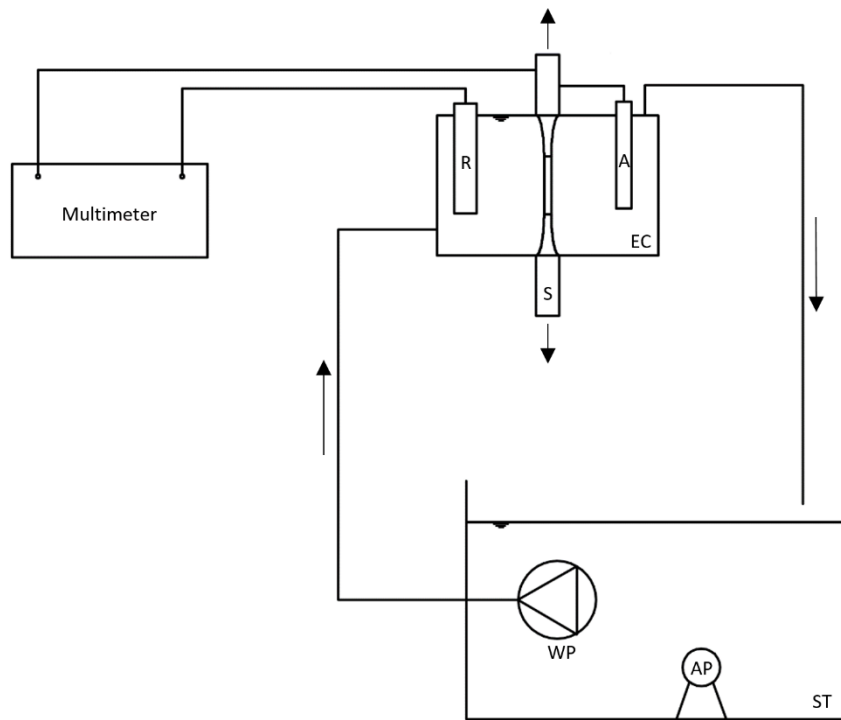


**Figure 4-9.** Schematic representation of the corrosion-fatigue test rig, S: specimen (working electrode), R: reference electrode, A: sacrificial anode, EC: environmental chamber, WP: water pump, AP: air pump, ST: solution tank.

The testing conditions, in terms of cyclic frequency, temperature, dissolved oxygen concentration, solution conductivity, pH and flow rate remained the same as in the corrosion-fatigue experiments. The loading levels were chosen close to the fatigue limit observed in tests conducted in air. In this way it should be possible to estimate the effectiveness of cathodic protection in driving the fatigue life of the material back to the in-air levels and in restoring the fatigue limit.

#### 4.3.2 Flow Rate Measurements

The flow rate was measured using the same technique as for the erosion-corrosion experimental programme. The water flowing out of the elastic tube, which was connected to the outlet of the environmental chamber, was collected in a volumetric beaker for 30 seconds. The volume of the water was then measured and by using the **Equation 3-1** the flow rate was calculated.

According to the calculations performed, the flow rate used in the corrosion-fatigue and corrosion-fatigue with cathodic protection testing was 130lt/hr.

## 4.5 Post-Test Analysis Techniques

### 4.5.1 Construction of S-N Curves

The results of the cycles-to-failure tests that have been performed were plotted in diagrams. In these diagrams the number of cycles to failure,  $N$ , have been plotted in a logarithmic scale versus the maximum applied stress,  $\sigma$ , as suggested in [4.9, 4.12].  $N$  was taken as the number of stress cycles that led to complete fracture of the specimen and as  $\sigma$  the maximum applied stress per cycle.

S-N curves were constructed based on the results of fatigue testing in air and in corrosion-fatigue conditions. These curves allowed for the estimation of the effect of various salinity levels of the corrosive environment on fatigue life. Then, the results obtained from fatigue testing in 824ppm NaCl aqueous solution were plotted separately from the results obtained in 35,000ppm NaCl aqueous solution. Each diagram included S-N curves of in-air and corrosion-fatigue conditions testing and the results of corrosion-fatigue with cathodic protection. In this way, the estimation of the effectiveness of sacrificial anode cathodic protection in eliminating the effect of corrosion and restoration of the in-air fatigue life levels, was made possible.

### 4.5.2 Fractography

For the examination of the fracture surface of the specimens, used in fatigue testing, scanning electron microscopy method was employed. For this purpose, a HITACHI S-3700 Scanning Electron Microscope (SEM) was used. The operation of an SEM involves the scanning the specimen's fracture surface with a focused beam of electrons, which interacts with the atomic structure and produces various signals which correspond to information concerning the composition and topography of the scanned area of the sample.

By using the scanning electron microscopy method, it was possible to extract useful information regarding the fatigue crack formation and growth, in relation to the working conditions. Various magnification levels enabled the examination of the fracture surfaces of the fatigue specimens. Prior to the investigation, the test section of each specimen, was immersed in an inhibited acid solution (Clarke's solution) for 4

seconds. In this way, the corrosion products were removed, enabling the examination of the fracture surfaces.

#### 4.5.3 Evaluation of Cathodic Protection Systems Performance

The evaluation of the cathodic systems performance, included the monitoring of the working electrode potential and the anode current output. Measurements of the working electrode's potential were taken versus an Ag/AgCl reference electrode, by using a voltmeter. The open circuit potential (corrosion-fatigue tests) and the closed circuit potential (corrosion-fatigue with cathodic protection tests, where the specimen's potential was under cathodic control) of the specimens were monitored throughout the experimental procedure. The measuring of the anode current output was made possible, using an ammeter that was included in the electrical connection between the anode and the cathode. The criterion of the successful application of cathodic protection was the driving of the electrode's potential to  $-800\text{mV}_{\text{SSC}}$  or more electronegative.

The results were plotted in charts (electrode potential or anode current output versus elapsed test time) that allowed for the estimation and comparison of the performance of the sacrificial anode cathodic protection systems that were used in the experimental programme.

## 4.6 Results and Discussion

### 4.6.1 Corrosion Fatigue

#### *4.6.1.1 Effect of Corrosion on Fatigue Life*

Fatigue data on S355 specimens tested in air and in corrosion-fatigue conditions, are presented in **Figure 4-10**. The fatigue curves obtained through testing in 824ppm and 35,000ppm NaCl aqueous solution are compared to the results obtained in air. In this diagram the markers with no fill indicate tests that had run out, allowing for the estimation of the fatigue limit of the material.

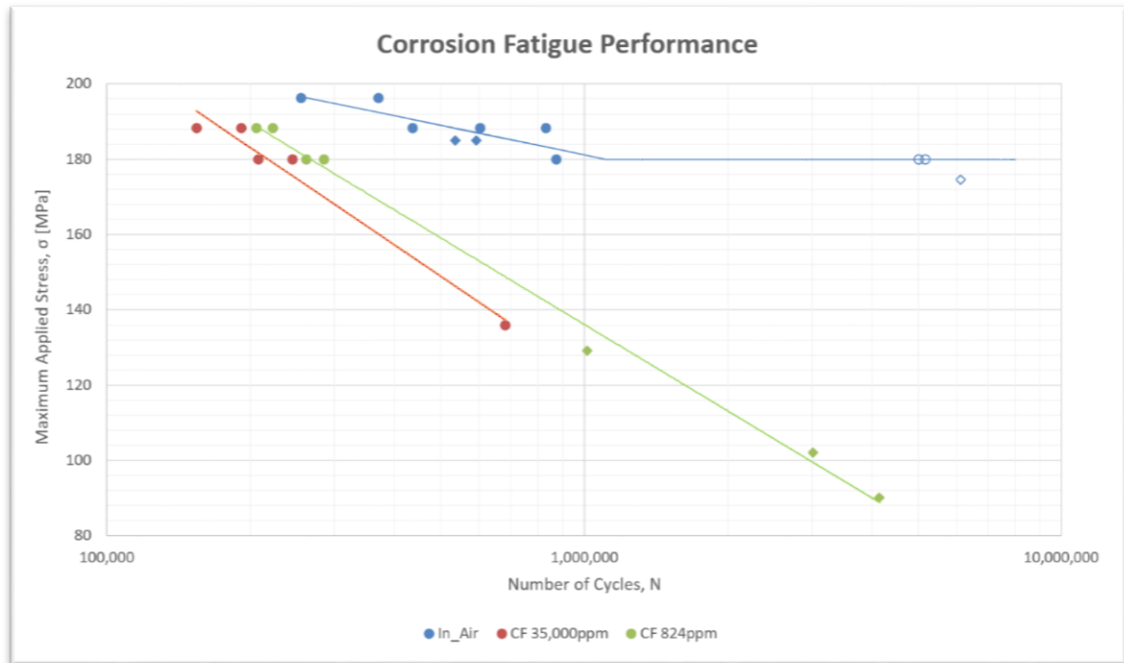


**Figure 4-10.** Fatigue performance in air and in corrosion-fatigue conditions. Results indicated by rhomboidal markers were obtained from [4.13].

As can be seen in this figure, the fatigue life of the material increases as the applied stress magnitude decreases, showing a fatigue limit at 180MPa, where two tests had run out. By introducing a corrosive environment, the fatigue life of the material seems to decrease for both salinity level aqueous solutions. The decrease in the fatigue life becomes more significant as the applied stress level decreases. The fatigue limit, observed in air testing, disappears in the case of corrosion-fatigue conditions and the curves for both salinity levels continue to descend steeply. These findings are in good agreement with the literature [4.11, 4.14-4.19].

The salinity level of the corrosive environment seems also to have an effect on the fatigue life of the material. Based on the results, it is obvious that as the salinity level increases the fatigue life is further decreased, for the whole range of stress levels tested. In the case of applied stress level close to 180MPa, where the infinite fatigue life in air is achieved, use of corrosive environment of 824ppm NaCl salinity seems to reduce the fatigue life by 75.8%. A further reduction of 80.3%, compared to in air levels, is observed when 35,000ppm NaCl corrosive solution is used. The deleterious effect of increasing salinity on the fatigue life, has also been reported in [4.11].

The effect of corrosion on the fatigue specimen surfaces was obvious even during the experimental process. In **Figures 4-11 to 4-13**, pictures taken during the experimental

investigation, show the effect of the corrosive environment on the surface of the steel specimens. As can be seen, both salinity level aqueous solutions causes extensive corrosion on the surface of the test specimens, even within relatively small testing times (2hrs). The higher corrosion damage observed, as the salinity level of the aqueous solution increases was also suggested by the erosion-corrosion testing results, presented in **Chapter 3**.



**Figure 4-11.** Corrosion-fatigue test at the beginning of the experimental process (0hrs testing).



**Figure 4-12.** Corrosion-fatigue test after 2hrs testing in 35,000 ppm NaCl aqueous solution.



**Figure 4-13.** Corrosion-fatigue test after 2hrs testing in 824 ppm NaCl aqueous solution.

According to the test results and the pictures taken during the experimental process, it is obvious that corrosion has a detrimental effect on the surface of the test specimen surfaces and so in the fatigue behaviour of the low alloy steel grade S355, in terms of reducing its fatigue life significantly and eliminating the fatigue limit. Corrosion protection strategies have been shown to successfully restore the in-air fatigue characteristics of the material, as will be seen in the next section.

#### *4.6.1.2 Effect of Cathodic Protection on Corrosion Fatigue Life*

Sacrificial anode cathodic protection using Zinc alloy sacrificial anodes was adopted for the protection of the low alloy steel grade S355 specimens tested in 35,000ppm NaCl aqueous solution, while Magnesium alloy sacrificial anodes were used in the lower salinity level of 824ppm NaCl. The sacrificial anodes were electrically connected to the test specimens, through the whole duration of the testing process. In **Figures 4-14** and **4-15**, the results of the corrosion-fatigue testing using sacrificial anode cathodic protection are presented along with the results of the in-air testing and the tests conducted in corrosion-fatigue conditions of the same salinity level corrosive environments, enabling the evaluation of the effect of cathodic protection on the corrosion-fatigue life of the material and the restoration of the fatigue limit observed in tests conducted in air. Furthermore, in these diagrams the markers with no fill

indicate tests that had run out, allowing for the estimation of the fatigue limit restoration of the material.

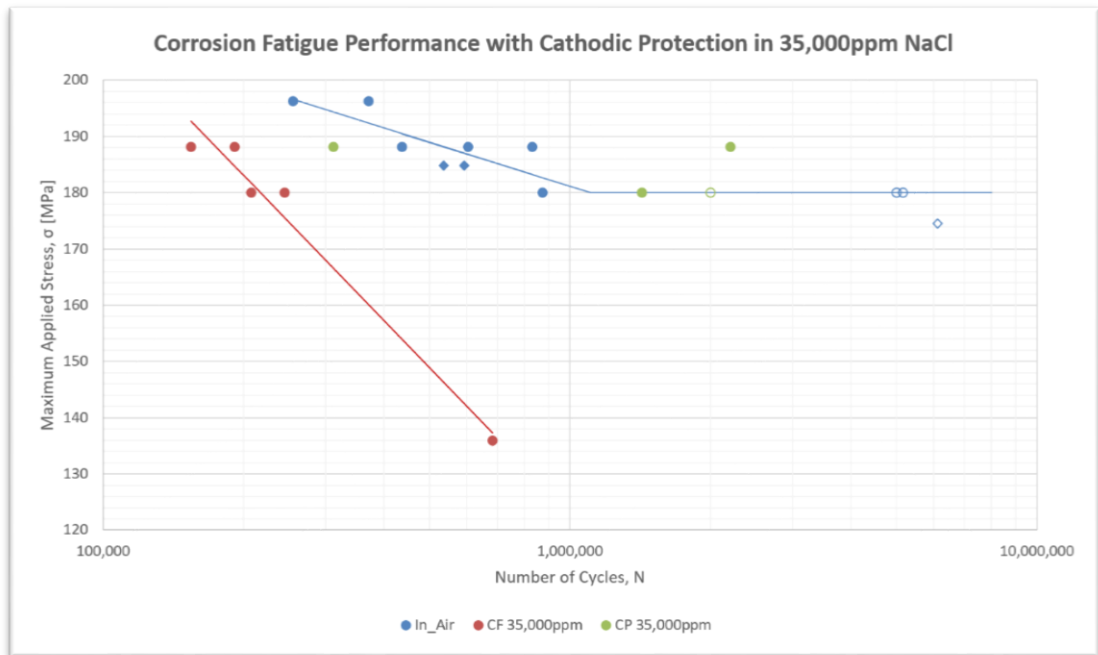


**Figure 4-14.** Fatigue performance in air, in corrosion-fatigue conditions without protection and in corrosion-fatigue conditions with sacrificial anode cathodic protection, in 35,000ppm NaCl aqueous environment. Results indicated by rhomboidal markers were obtained from [4.13].

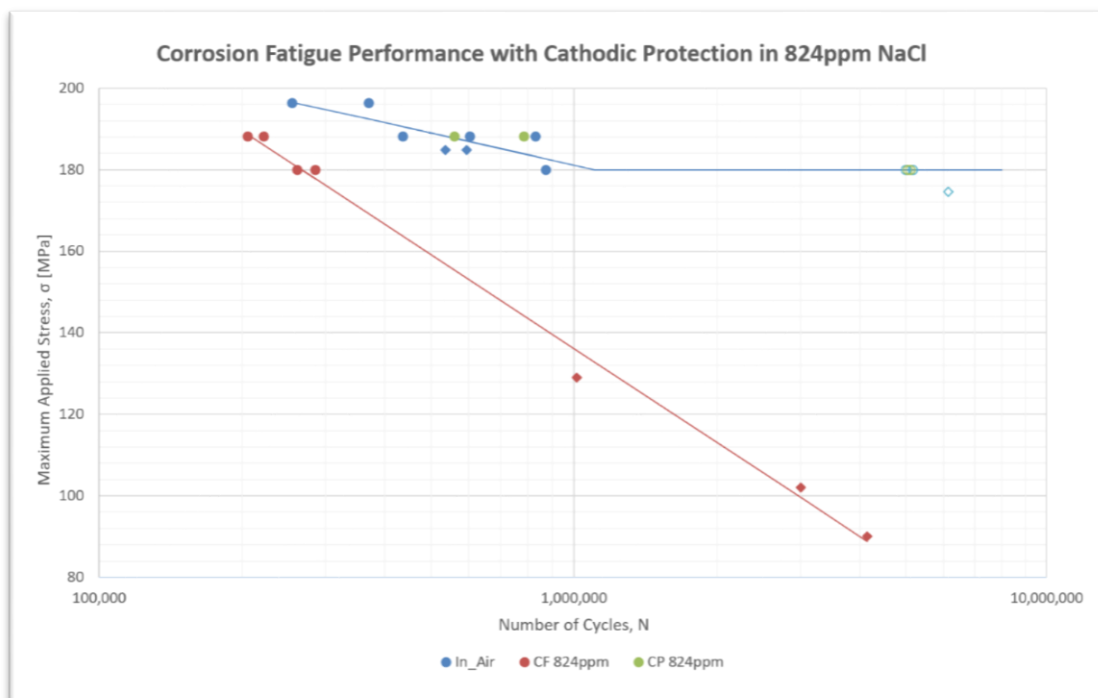


**Figure 4-15.** Fatigue performance in air, in corrosion-fatigue conditions without protection and in corrosion-fatigue conditions with sacrificial anode cathodic protection, in 824ppm NaCl aqueous environment. Results indicated by rhomboidal markers were obtained from [4.13].

The test results obtained in corrosion-fatigue with cathodic protection conditions are compared to the fatigue curve estimates based on tests conducted in air and in corrosion-fatigue without protection conditions. According to the results, it is obvious that cathodic protection greatly affected the corrosion-fatigue performance of the material, in both salinity level aqueous solutions. The beneficial effect of cathodic protection on corrosion-fatigue life has been also reported in literature [4.14, 4.16-4.17, 4.19-4.21]. At the higher stress level tested, the corrosion-fatigue life was prolonged to in air levels, while at the applied stress level of 180MPa, where the fatigue limit in air was achieved, run out test were obtained, indicating that the fatigue limit was restored. As the maximum design stress of GEHO PD pump components is 100 MPa for pure tensile loading ( $R = 0$ ), that is much lower than the estimated fatigue limit of the material, it is concluded that the effect of corrosion on their fatigue performance is securely eliminated.

In **Figures 4-16** and **4-17**, the effectiveness of sacrificial anode cathodic protection in protecting the test specimens from corrosion is shown. While extensive corrosion was observed on the surface of the specimens tested in corrosion-fatigue conditions within 2hrs of testing, by applying sacrificial anode cathodic protection, no corrosion is observed on the specimen surfaces even after 55hrs of testing in 35,000ppm NaCl concentration corrosive environment, using Zinc alloy sacrificial anodes and after 141hrs of testing in 824ppm NaCl aqueous solution, using Magnesium alloy sacrificial anodes.



**Figure 4-16.** Corrosion-fatigue test with Galvanic Protection (Zinc alloy sacrificial anode) after 55hrs testing in 35,000ppm NaCl aqueous solution.



**Figure 4-17.** Corrosion-fatigue test with Galvanic Protection (Magnesium alloy sacrificial anode) after 141hrs testing in 824ppm NaCl aqueous solution.

Based on the results, the adoption of sacrificial anode cathodic protection using Zinc and Magnesium alloy sacrificial anodes, proved to be a successful strategy for the corrosion protection of the low alloy steel grade S355 specimens tested in 35,000ppm and 824ppm NaCl aqueous solution respectively. The corrosion-fatigue life of the material was prolonged to in air levels and the fatigue limit observed in air was restored.

#### 4.6.2 Fractographic Investigation

The scope of the fractographic investigation was to determine specific aspects of the failure mechanisms of the low alloy steel grade S355 fatigue specimens. The fracture surface of the specimens that failed during testing, were examined via SEM (scanning electron microscope) in order to identify the mechanisms of crack initiation and propagation and the effect of the various testing conditions on these phenomena.

In **Figure 4-18**, the fracture surface of a specimen that failed during in air testing, is presented. As can be seen in the figure (left), the fatigue crack initiation occurred on the surface of the specimen, the crack growth damaged most of the cross section leading to the final failure. Moreover, the transgranular mode of the fatigue crack growth (right), as is the case in almost all materials compared with creep and stress corrosion cracks failures according to J. Schijve [4.22], can be observed on the fracture surface of the specimen.

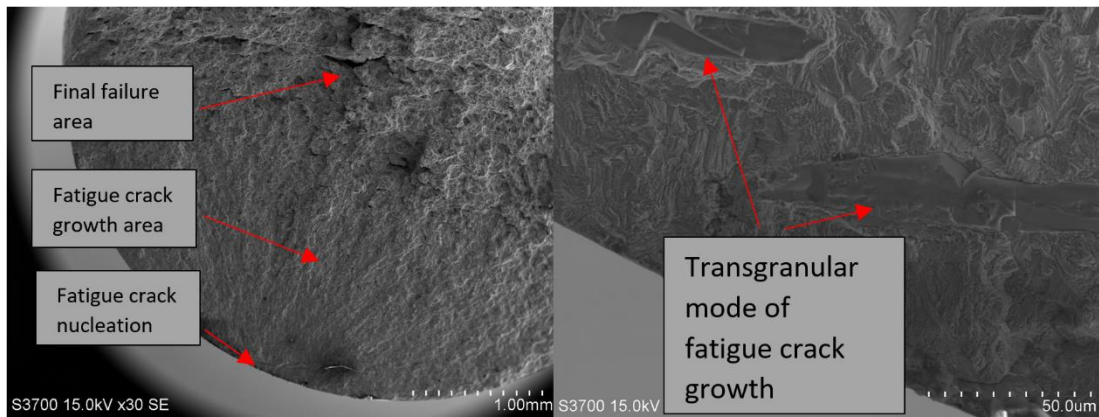


**Figure 4-18.** Lower (left) and higher (right) magnification view of the fracture surface of fatigue specimen tested in air conditions.

Corrosion can dramatically affect the fatigue performance of a low alloy steel, reducing its fatigue life and eliminating the fatigue limit observed in air, as has been seen in the previous section. Pitting corrosion is severe surface damage because the shape of a corrosion pit represents a significant stress raising geometry that promotes crack initiation. Such pits have been observed on the fracture surfaces of fatigue specimens tested in corrosion-fatigue conditions in 824ppm and 35,000ppm NaCl aqueous solutions, presented in **Figures 4-19** and **4-20** respectively.

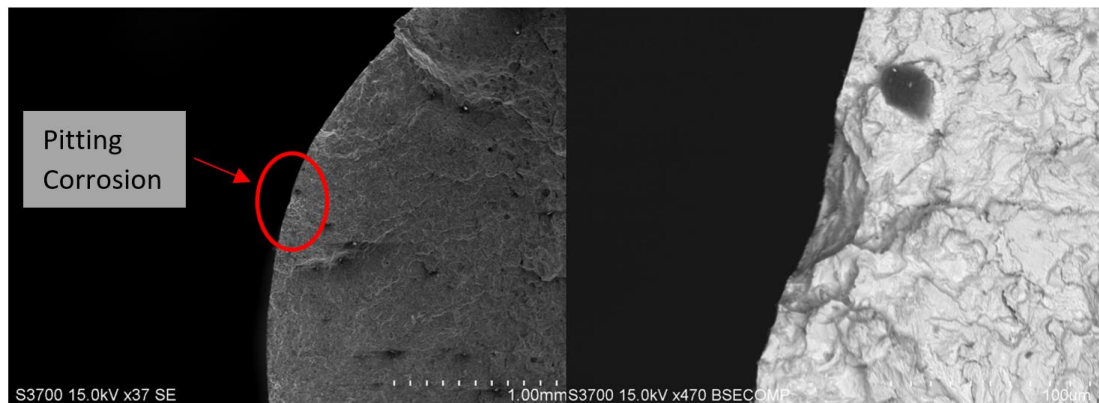


**Figure 4-19.** Lower (left) and higher (right) magnification view of a corrosion pit on the sample's fracture surface after corrosion-fatigue testing in 824ppm salinity aqueous solution.

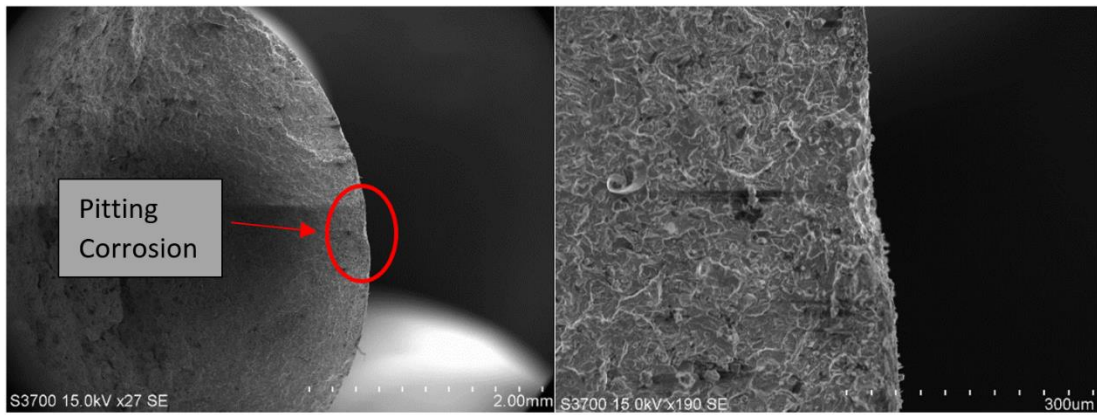


**Figure 4-20.** Lower (left) and higher (right) magnification view of a corrosion pit on the sample's fracture surface after corrosion-fatigue testing in 35,000ppm salinity aqueous solution.

In **Figure 4-21** the fracture surface of a fatigue specimen tested in 35,000ppm NaCl aqueous solution with Zinc alloy sacrificial anode cathodic protection, is shown. On the left, a higher magnification of the fracture surface topography is presented, while on the right, higher magnification revealed the fatigue crack initiation.

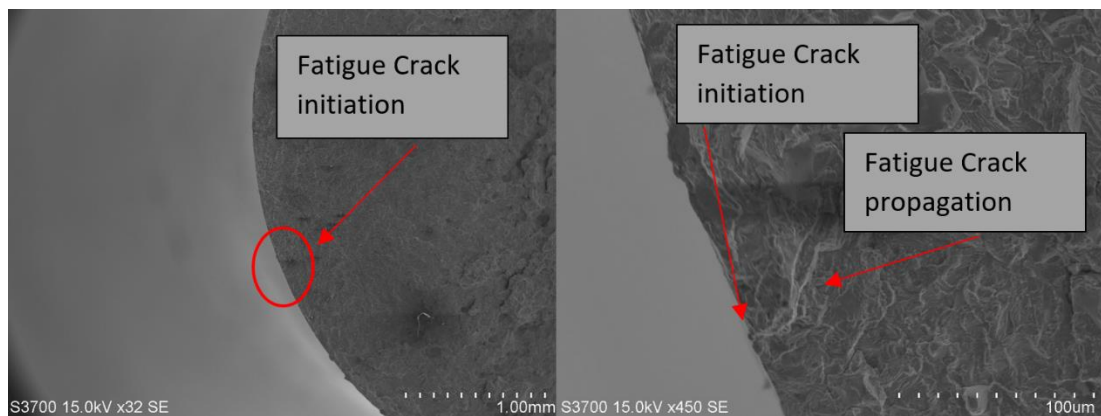


**Figure 4-21.** Lower (left) and higher (right) magnification view of the fracture surface of fatigue specimen tested in 35,000ppm NaCl solution with Zinc alloy sacrificial anode cathodic protection.

The examination of the fracture surface suggested that no corrosion pits were formed on the surface of the tested specimen, showing that sacrificial anode cathodic protection using a Zinc alloy sacrificial anode, successfully protected the material from corrosion, which would have formed stress raising geometries. In this way, the effect of corrosion was eliminated and fatigue life of the material was driven back to in air levels.

### 4.6.3 Cathodic Protection Systems Performance

The performance of the sacrificial anode cathodic protection systems was evaluated via monitoring of the electrode potential and the anode current output. The criterion of the successful application of cathodic protection was the polarisation of the working material to potential levels of  $-800\text{mV}_{\text{SSC}}$  or more electronegative. The results are presented in the form of diagrams where the electrode potential or anode current output are plotted versus testing time. Separate diagrams have been constructed for the presentation of the open circuit potential, i.e. the fatigue specimen potential working in corrosion-fatigue conditions and for the closed circuit potential, i.e. the polarised fatigue specimen potential when coupled with sacrificial anodes.

#### 4.6.3.1 Corrosion Potential

The results of the measuring of the corrosion potential of the fatigue specimens are presented in **Figure 4-22**. In this diagram, the corrosion potentials of the specimens in both salinity level aqueous solutions, has been plotted versus testing time.

As can be seen in the diagram the presence of higher ion content in the solution causes the electrode potential to become more electronegative. The higher ion content decreases the resistivity of the solution, causing higher corrosion current flow that results in increased polarisation of the anodic and cathodic areas of the material surface. Due to fact that the corrosion cell is under cathodic control, i.e. higher polarisation occurring at the cathode (as is the case for most corrosion cells of steel in contact with water), the corrosion potential is forced to more electronegative levels.

Reaction products may build up on the material surface, as the corrosion process continues with time, slowing down charge transfer reactions, reducing the corrosion current, as suggested in [4.23]. The reduction in corrosion current causes depolarisation and the corrosion potential shifts to more electronegative values in both salinity levels.

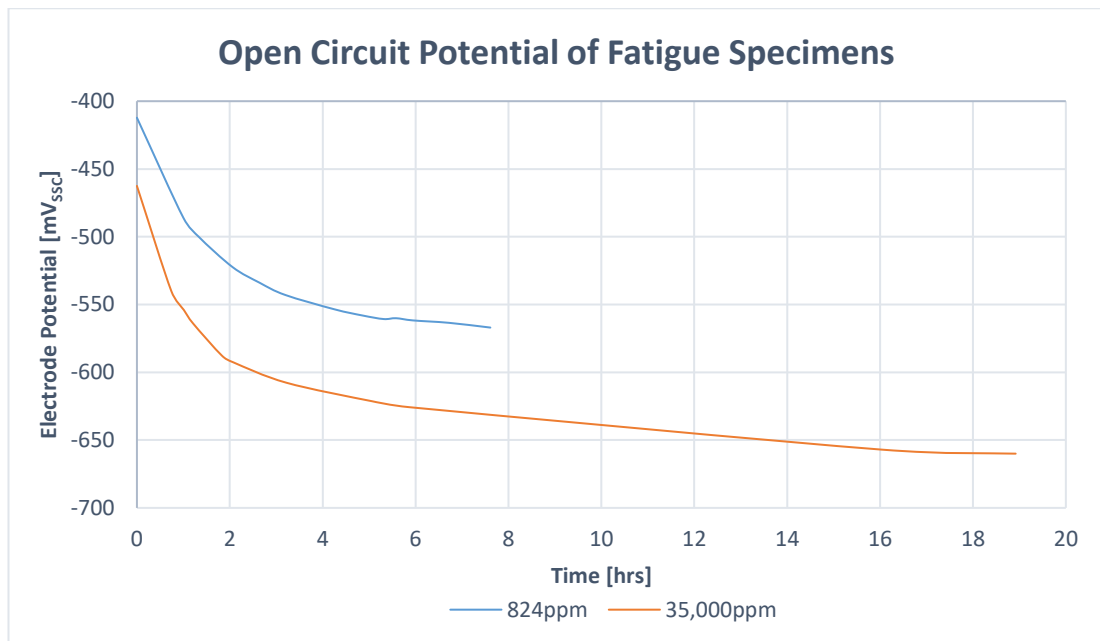


**Figure 4-22.** Open circuit potential of fatigue specimens working in corrosion-fatigue conditions.

In the lower salinity level aqueous solution, the corrosion potential of the material shifted from  $-412\text{mV}_{\text{SSC}}$  to  $-567\text{mV}_{\text{SSC}}$  after 7.6hrs of testing. In the case of the higher salinity level aqueous solution, the initial corrosion potential of the material was more electronegative and shifted from  $-462\text{mV}_{\text{SSC}}$  to  $-660\text{mV}_{\text{SSC}}$  after 18.9hrs of testing. Through the whole testing process, the corrosion potential was more negative in the case of the higher salinity, indicating that the corrosion current and so the corrosion rate would be expected to be higher compared to the 824ppm NaCl.

#### 4.6.3.2 Closed Circuit Potential of Fatigue Specimens

The electrode potential of the fatigue specimens has been monitored and plotted versus testing time for both salinity level aqueous solutions. Also, the Zinc and the Magnesium alloy anode current output has been plotted versus testing time in solutions of 35,000ppm and 824ppm NaCl concentrations respectively. The results are presented in **Figures 4-23** to **4-26**.

- Testing in 35,000ppm NaCl Concentration Aqueous Solution

In the case of testing in corrosion-fatigue conditions in 35,000ppm NaCl concentration aqueous solution, using Zinc alloy sacrificial anode cathodic protection, the electrode

potential of the specimens was shifted to  $-985\text{mV}_{\text{SSC}}$  at the beginning of the testing process and polarised rapidly to potential levels more negative than  $-1000\text{mV}_{\text{SSC}}$  reaching the value of  $-1029\text{mV}_{\text{SSC}}$  after 55hrs of testing, as shown in **Figure 4-23**. In this way the specimens were cathodically protected throughout the testing process, resulting in the prolongation of their corrosion-fatigue life.

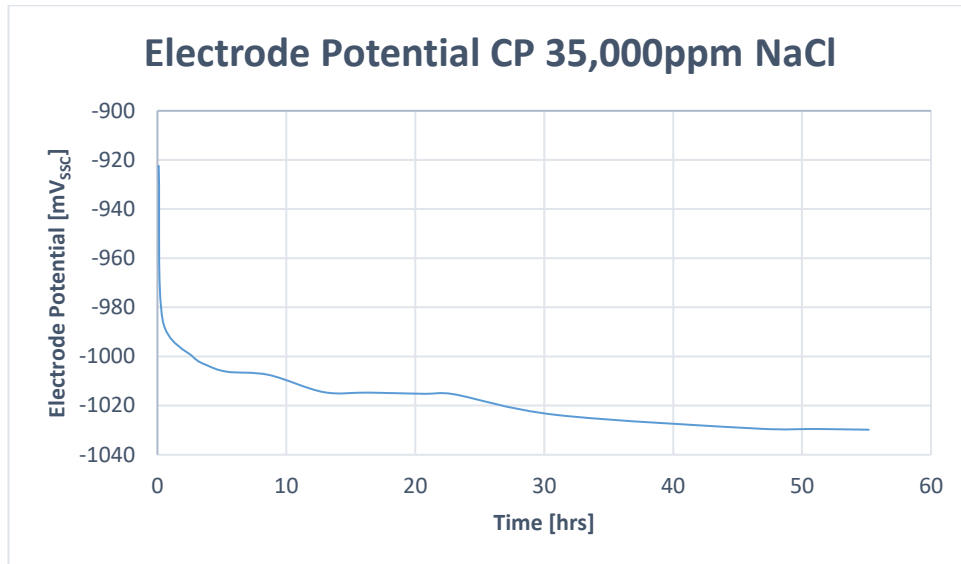


**Figure 4-23.** Closed circuit potential of fatigue specimens working in corrosion-fatigue conditions with Zinc alloy sacrificial anode cathodic protection.

The results of the current output of the anode material during the testing, are presented in **Figure 4-24**. According to the results, it can be seen that the anode current output decreased with time reaching  $0.54\text{mA}$  after 55hrs of testing but at the same time the electrode potential of the specimen continued to polarise to more electronegative values. The behaviour of the Zinc alloy anodes is similar to that observed in [4.24]. After the initial rapid decrease in current drainage for 6hrs, the anode current output seems to become steady or decrease at a very low rate.

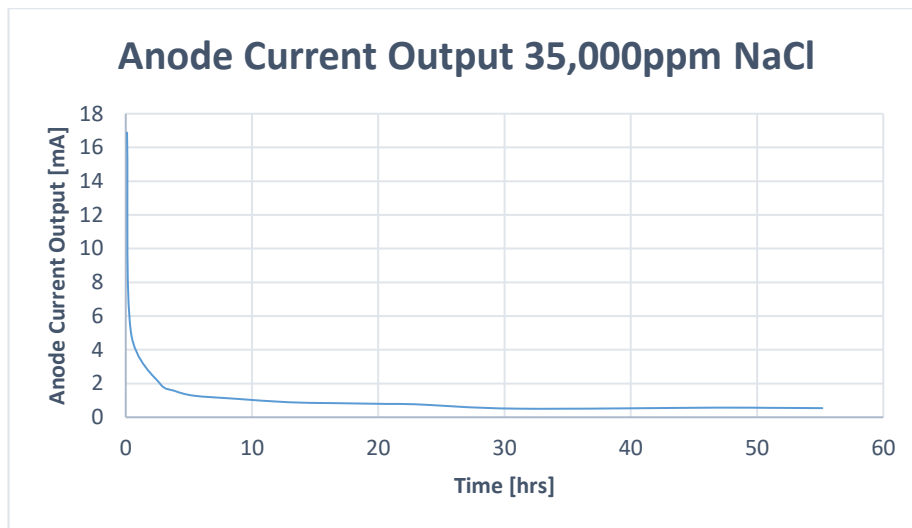


**Figure 4-24.** Zinc alloy sacrificial anode current output working in 35,000ppm NaCl aqueous solution.

- Testing in 824ppm NaCl Concentration Aqueous Solution

The application of Magnesium alloy sacrificial anode cathodic protection in 824ppm NaCl concentration aqueous solution, has been found to drive the electrode potential of the fatigue specimens to levels where they were protected from corrosion, as can be seen in **Figure 4-25**.

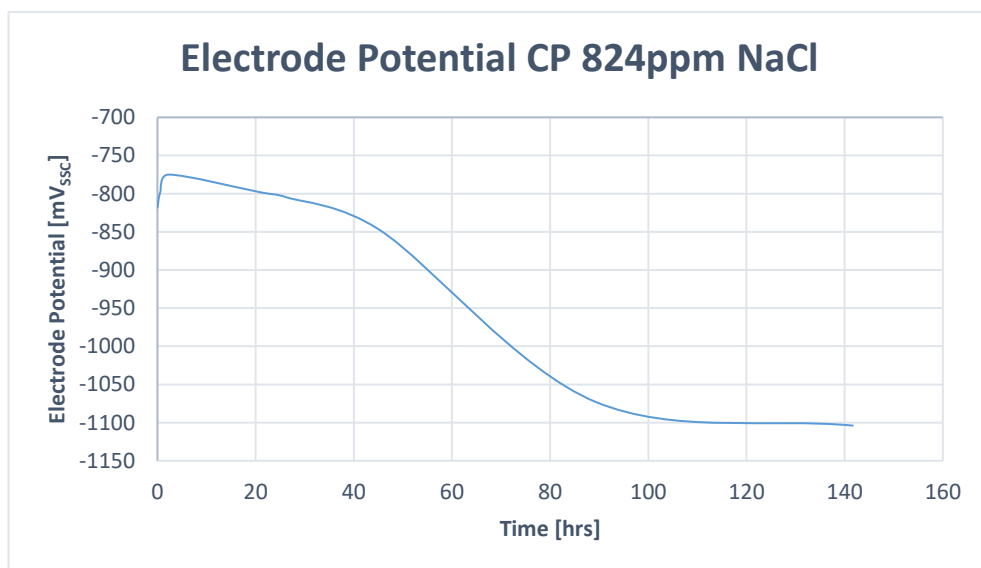


**Figure 4-25.** Closed circuit potential of fatigue specimens working in corrosion-fatigue conditions with Magnesium alloy sacrificial anode cathodic protection.

As can be seen, the electrode potential shifted from the initial  $-818\text{mV}_{\text{SSC}}$  to the more electropositive value of  $-775\text{mV}_{\text{SSC}}$  after 2.3hrs of testing. The fact that during this time, the electrode potential moved to more electropositive values while the anode

current output increased, as can be seen in **Figure 4-26**, can be attributed to increasing oxygen concentration in the solution due to the function of the air pump. The increase in oxygen concentration to the saturation point, depolarises the cathode to more electropositive levels, increasing the driving voltage and therefore the anode current output. After that point the working electrode potential was driven to more electronegative levels, reaching the value of  $-1103\text{mV}_{\text{SSC}}$  after 141.6hrs of testing. The potential seems to remain at less electronegative values than  $-800\text{mV}_{\text{SSC}}$ , for the first 20.9hrs. Since no corrosion was observed on the specimen surface and its fatigue life was driven to in air levels, it is concluded that corrosion protection was satisfactorily achieved even at potential levels slightly more electropositive than  $-800\text{mV}_{\text{SSC}}$  as has been suggested in [4.14, 4.19-4.20].

In **Figure 4-26**, the values of the anode current out plotted versus testing time, are presented.

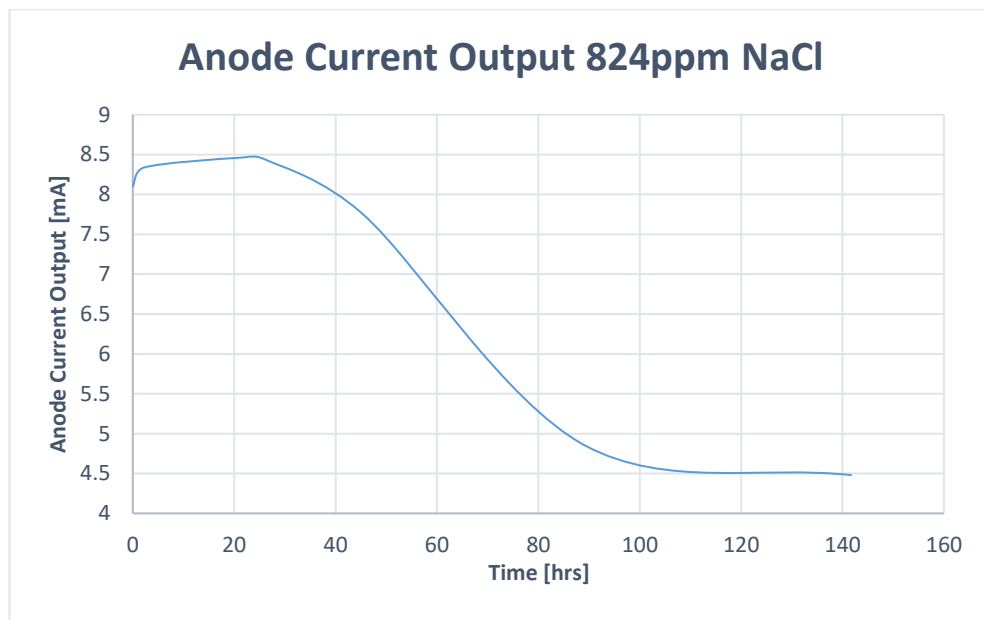


**Figure 4-26.** Magnesium alloy sacrificial anode current output working in 824ppm NaCl aqueous solution.

The anode current output increases for 20.9hrs of testing, reaching the peak value of 8.46mA. From that point on, the anode current output decreases but the specimens potential continues to polarise to more electronegative levels. After 141.6hrs of testing the value of 4.48mA is reached, driving the electrode potential to  $-1103\text{mV}_{\text{SSC}}$ .

The phenomenon of higher polarisation of the tested material to more electronegative levels with decreasing anode current output, observed in both testing conditions, has been also reported in literature [4.24-4.25]. This may be attributed to the deposition of calcareous films on the specimen surface, as suggested in [4.25-4.26]. Such films increase the oxygen concentration polarisation by restricting oxygen access to the substrate, as is suggested in [4.23]. Thus, the limiting current density decreases and as a result a significant reduction in the current required to maintain polarisation, is observed. Finally, the reduction in the current flow, due to the deposition of a (more likely) calcareous film, results in a lower consumption rate of the anode and thus in the extension of its service life.

According to the results, Zinc and Magnesium alloy sacrificial anode cathodic protection in 35,000ppm and 824ppm respectively, has been successfully applied, as the test specimens were polarised to sufficiently electronegative potential levels, eliminating the effect of corrosion and driving the fatigue life to in air levels.

## **4.7 Conclusions**

Based on the results of the experimental investigation, the application of sacrificial anode cathodic protection, has been found to have a great effect on the corrosion - fatigue performance of the low alloy steel grade S355. GEHO pump components, protected by sacrificial anode cathodic protection, may have enhanced Corrosion - Fatigue life and allow for higher stresses to be applied.

Tests conducted in 35,000ppm and 824ppm NaCl concentration aqueous solutions, showed that the effect of corrosion dramatically reduces the corrosion-fatigue life of the material and eliminates the fatigue limit that is observed in air testing. The effect of salinity level proved to be of much importance. The higher the salinity level, the greater the effect of corrosion on fatigue life, as has been observed. Topography of the fracture surface of specimens tested in corrosion-fatigue conditions, revealed the formation of corrosion pits that acted as stress concentration geometries, promoting crack initiation. Another factor that can be assumed to decrease fatigue life is the fact that corrosion reduces the available sectional working material, increasing the applied stress level.

The application of Zinc and Magnesium alloy anode cathodic protection in 35,000ppm and 824ppm NaCl concentration aqueous solutions respectively, has been found to successfully eliminate the effect of corrosion on fatigue performance of the tested material. Tests results showed that the corrosion-fatigue life was prolonged to in air levels and the fatigue limit observed in air was restored. Throughout the testing process the material remained un-corroded and according to the fractographic examination, no pitting corrosion was observed on the surface of the protected specimens.

Monitoring of electrode potential, during corrosion-fatigue testing, showed that the salinity level of the environment greatly affects the corrosion potential of the material. As the salinity level increases, the resistivity of the aqueous solution decreases, allowing for higher corrosion current flow and so higher corrosion rate. The increasing corrosion current flow forced the corrosion potential of the tested material to more electronegative levels. Furthermore, the building up of corrosion products on the specimen surfaces polarised the corrosion potential to more electronegative values in both salinity level aqueous solutions.

Sacrificial anode cathodic protection was successfully applied in both salinity levels, as the electrode potential of the fatigue specimens was driven to potential values much more electronegative than  $-800\text{mV}_{\text{SSC}}$ . During the testing process, depositions observed (more likely calcareous films) on the specimen surfaces significantly reduced the current required to maintain polarisation and the electrode potential was driven to more electronegative levels. This phenomenon improves the performance of the anode by reducing the consumption rate and extending in this way the service life of the sacrificial anode cathodic protection system.

## 4.8 References

- [4.1] Ralph van Rijswick, Arno Talmon and Cees van Rhee, Fluid Structure Interaction (FSI) in Piston Diaphragm Pumps, The Canadian Journal of Chemical Engineering, Volume 94, pp. 1116 - 1126 (2016).
- [4.2] Donald Mackenzie, Material Selection & Design Criteria for Forgings Cyclically Loaded in a Corrosive Environment, Weir Advanced Research Centre, University of Strathclyde (2012).

- [4.3] D. Mackenzie, Audit of Material Selection & Design Criteria for GEHO PD Pumps, Rev. 2, Weir Advanced Research Centre, University of Strathclyde, Glasgow (2013).
- [4.4] Amir Bahrami, 'Fatigue performance of riser girth welds for deep-water applications' Deep Water Technology Conference, Kuala Lumpur, Malaysia (2009).
- [4.5] ASM International, ASM Handbook, Volume 19: Fatigue and Fracture (1996).
- [4.6] J.A. Bannantine, J.J. Comer, J.L. Handrock, Fundamentals of Metal Fatigue Analysis (1989).
- [4.7] ASTM International, Standard Practice for Conducting Force Controlled Constant Amplitude Axial Fatigue Tests of Metallic Materials, Designation: E466 – 07 (2007).
- [4.8] BS EN ISO 11782-1:2008, Corrosion of metals and alloys – Corrosion fatigue testing, Part 1: Cycles to failure testing (2008).
- [4.9] G.E. Dieter, Mechanical Metallurgy, McGraw – Hill Book Company, Inc., ISBN: 07-016890-3, New York, USA (1961).
- [4.10] D. Mackenzie, W. Pan and T. Hodgkiess, Fatigue Life Design for Forgings in a Corrosive/Erosive Environment, Project G: 2011-2012, Phase 1 Literature Review, Weir Advanced Research Centre, University of Strathclyde (2012).
- [4.11] Endo K. and Miyao Y., Effects of Cycle Frequency on the Corrosion Fatigue Strength, Bulletin of JSME, Vol. 1, No 4, pp. 374-380 (1958).
- [4.12] ASM International, ASM Handbook, Volume 1: Properties and Selection: Irons, Steels, and High-Performance Alloys (1990).
- [4.13] Marta Morgantini, Donald MacKenzie, Tugrul Comlekci and Ralph van Rijswijk, The Effect of Mean Stress on Corrosion Fatigue Life, Procedia Engineering, Volume 213, pp. 581–588 (2018).

- [4.14] Charles M. Hudgins, Jr., Burton M. Casad, R. L. Schroeder, Charles C. Patton, The effect of cathodic protection on the corrosion fatigue behaviour of carbon steel in synthetic sea water, Offshore Technology Conference 6200 North Central Expressway Dallas, Texas 75206, Paper No. OTC 1254 (1970).
- [4.15] E.N. Kostrov, L.A. Glikman, V. A. Orlov, Effect of cathodic protection on the corrosion fatigue strength of steels of various hardness in seawater, Fiziko-Khimicheskaya Mekhanika Materialov, Volume 2, No. 4, pp 431-436 (1966).
- [4.16] A. E. Lyashchenko, L.A. Glikman, Yu. E. Zobachev, Some features of influence of cathodic polarisation on the corrosion fatigue strength of steel samples with a notch, UDC 620.193:620.197.5 (1975).
- [4.17] Havens F. E. and Bench D. M., Fatigue Strength of Quenched and Tempered Carbon Steel Plates and Welded Joints in Seawater, Offshore Technology Conference, Paper OTC 1046, Dallas, Texas (1969).
- [4.18] Endo K., Komai K. and Nakamuro N., Estimation of corrosion fatigue strength by corrosion resistance and notch sensitivity of materials, Bulletin of the JSME, Volume 13, No 61, p. 837-849 (1970).
- [4.19] Jaske, C. E., Broek, D., Slater, J. E. and Anderson, W. E., "Corrosion Fatigue of Structural Steels in Seawater and for Offshore Applications", Corrosion-Fatigue Technology, ASTM STP 642, H. L. Craig, Jr., T. W. Crooker, and D. W. Hoepfner, Eds., American Society for Testing and Materials, pp. 19-47 (1978).
- [4.20] Sergei A. Shipilov, Iain Le May, Structural integrity of aging buried pipelines having cathodic protection, Engineering Failure Analysis Volume 13, p. 1159–1176 (2006).
- [4.21] Mamdouh M. Salama, William H. Thomason, Evaluation of Aluminum-Sprayed Coatings for Corrosion Protection of Offshore Structures, Society of Petroleum Engineers of AIME, SPE 12440 (1984).
- [4.22] J. Schijve, Fatigue of Structures and Materials, Springer, ISBN: 978-1-4020-6807-2 (2009).

- [4.23] NACE International, CP3 – Cathodic Protection Technologist Course Manual, version 1 (2014).
- [4.24] Mohammed Al-Otaibi, The Application of BEASY Software to Simulate Cathodic Protection of Pipelines and Storage Tanks, The University of British Columbia, Vancouver (2010).
- [4.25] J. L. Solis and J. Genesca, Effect of Calcareous Deposit Formation on Galvanic Anode Cathodic Protection of Steel in Seawater, NACE International, Corrosion 2009 Conference & Expo, Paper No. 09520 (2009).
- [4.26] R. Johnsen and H. W. Stangeland, Cathodic Protection in Cold Seawater – Current Density Requirements, NACE International, Corrosion 2009 Conference & Expo, Paper No. 09521 (2009).

# CHAPTER 5

## **Guidelines for Analytical Design and Simulation of SACP Systems for Pipelines and GEHO Positive Displacement Pumps**

### **5.1 Introduction**

In the previous Chapter it was seen that sacrificial anode cathodic protection can be successfully applied to extend the corrosion-fatigue life of the low alloy steel grade tested, restoring the in-air fatigue performance. In the current Chapter, guidelines for the design of sacrificial anode cathodic protection systems for the protection of WEIR Minerals pumping equipment, are presented. Focus has been placed on the corrosion protection of pipelines and GEHO positive displacement pumps, working in hostile environments and so prone to corrosion-fatigue failures.

The design method comprises of two general steps. In the first step, which is called Analytical Design, the cathodic protection system is calculated so as to ensure that the anodes to be used would be able to provide adequate current to protect a structure throughout the design life of the system. In the second step, which is called Simulation, numerical methods are used to predict the performance of the system enabling the designer to ensure that the cathodic current would be distributed in such a way that all the protected surfaces of the structure are polarized to a sufficient electronegative potential.

The analytical design rules presented in this chapter are based on the standard method used in industry, as described in the literature [5.1-5.6]. The detailed design of cathodic protection systems is preceded by the conceptual design procedure. In this stage, the anode type and fastening devices should be determined, based on the expected forces exerted on anodes during installation and operation. Furthermore,

any coating system that is to be applied should be defined at this stage, in order to allow for preliminary calculations of cathodic current needed for protection and the required total net anode mass to provide adequate current throughout the design life of the system. The detailed design method of sacrificial anode cathodic protection systems, aimed for the protection of the internal surfaces of pipelines and GEHO PD pumps, presented later in this Chapter, combines the standard method and the use of experimental data (Polarisation Curves), for the accurate calculations of the system's working parameters. The methodologies used to obtain the polarization characteristics of the materials under investigation, working in various environmental conditions, are also discussed. The results, obtained from the experimental investigation, are presented in the form of diagrams.

The polarisation behaviour data are also used as input (boundary conditions) in the cathodic protection system simulation. At this stage the performance of the cathodic protection system is predicted using numerical methods, without the need of in-field measurements, as has been discussed in **Chapter 2**. In the current work, focus is on the use of the commercial software BEASY CP that applies the BEM method to model cathodic protection systems. The steps of the modelling procedure are presented and discussed.

In the next Chapter these guidelines will be followed in order to design sacrificial anode cathodic protection systems for small diameter pipelines and WEIR Minerals GEHO TZPM positive displacement pumps.

## **5.2 Guidelines for Analytical Design of Cathodic Protection Systems**

### 5.2.1 Polarisation Data

#### *5.2.1.1 Experimental Set-Up*

The experimental set-up, used for the obtaining of the polarisation characteristics of the materials to be used in the sacrificial anode cathodic protection systems, has already been described in **Chapter 3**. The scope of the testing programme is to create polarisation curves to be used for the measuring of the current density, needed to provide adequate polarisation to the low alloy steel grade S355 to potential levels of

-800mV<sub>SSC</sub> and the estimation of the anode material's closed circuit potential, as will be seen later in this Chapter. Moreover, the polarisation data of the materials will be used as boundary conditions in the modelling process, enabling the prediction of the cathodic protection system performance.

#### *5.2.1.2 Polarisation Scanning Methodology*

The polarisation scans were conducted in corrosive environments at ambient temperature and at the scan rate of 15mV/min. The scanning started 1hr after sample immersion, as suggested in [5.7]. The Magnesium alloy was tested in 824ppm NaCl tap water solution (resistivity  $\rho=5.84\Omega\text{m}$ ) while the Zinc alloy was tested in 35,000ppm NaCl tap water solution (resistivity  $\rho=0.19\Omega\text{m}$ ). The low alloy steel grade S355 samples were tested in both solutions. Cathodic scans were performed to the steel grade, beginning at corrosion potential reaching up to -1200mV<sub>SCC</sub>, while anodic scans were performed to the anode alloys, beginning at corrosion potential and continued up to -500mV<sub>SSC</sub>. Three duplicate tests were conducted per testing condition. Finally, all the results were presented in polarization diagrams for better assessment of the materials' behaviour.

#### *5.2.1.3 Results and Discussion*

The results of the polarisation scans conducted on the low alloy steel grade S355 samples are presented in **Figures 5-1 to 5-2**, while those conducted on the sacrificial anode alloy materials are presented in **Figures 5-3 to 5-4**.

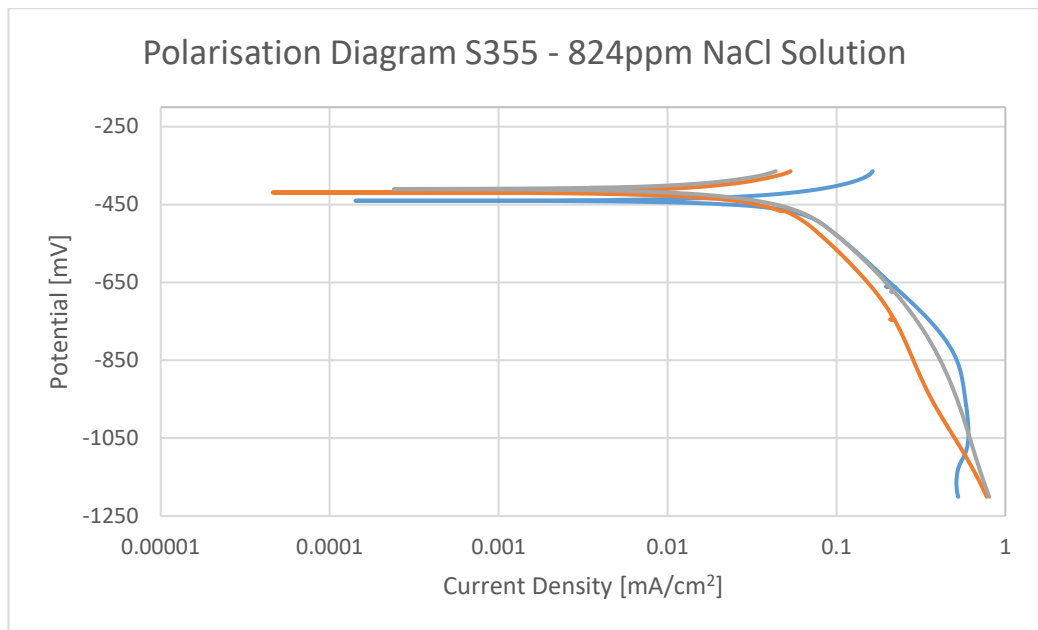


**Figure 5-1.** Cathodic polarisation scan of S355 in 824ppm NaCl tap water solution.

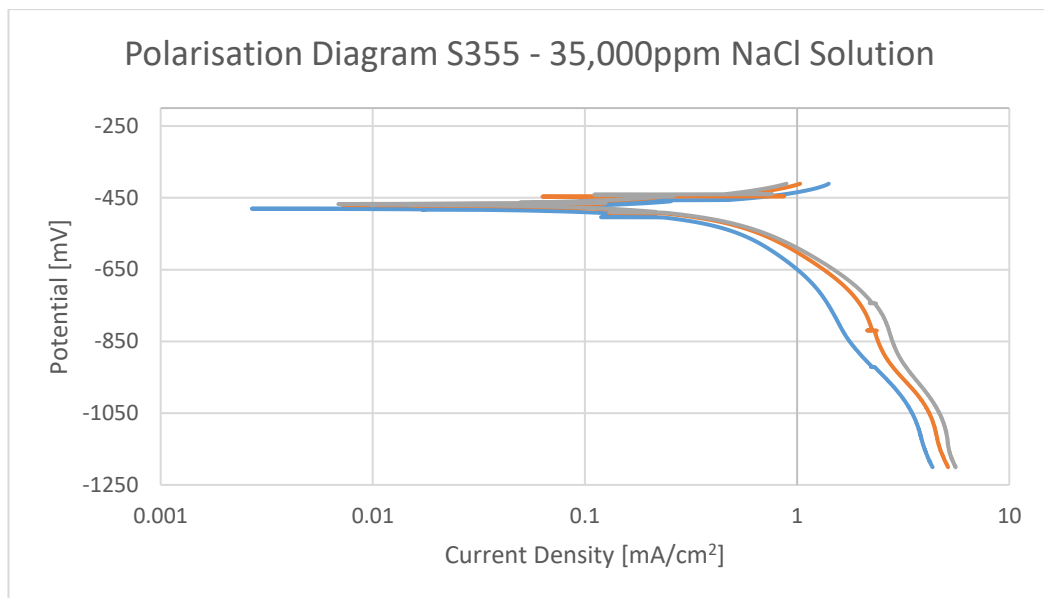


**Figure 5-2.** Cathodic polarisation scan of S355 in 35,000ppm NaCl tap water solution.

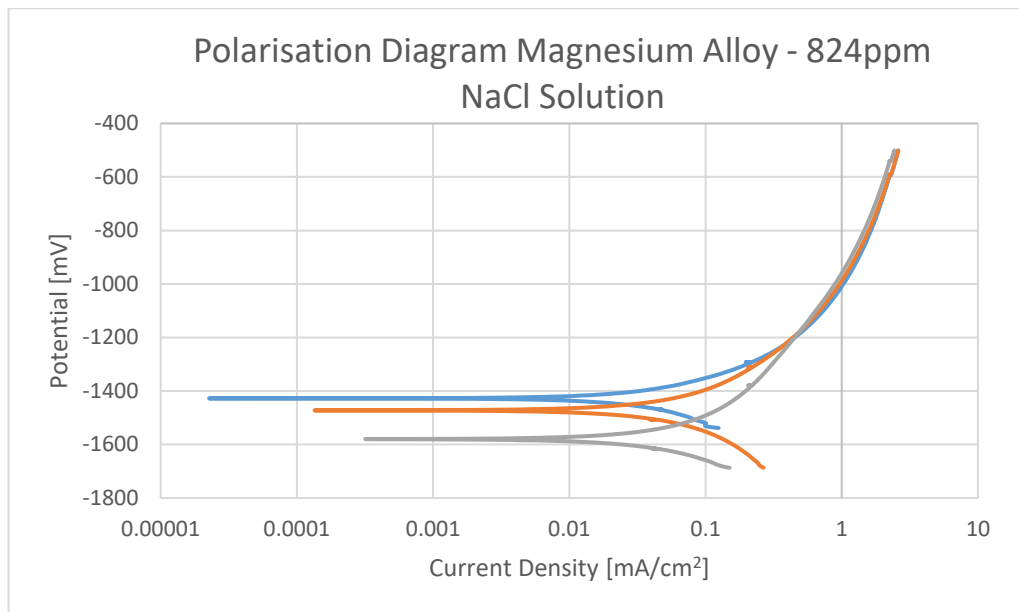


**Figure 5-3.** Anodic polarisation scan of Magnesium alloy in 824ppm NaCl tap water solution.

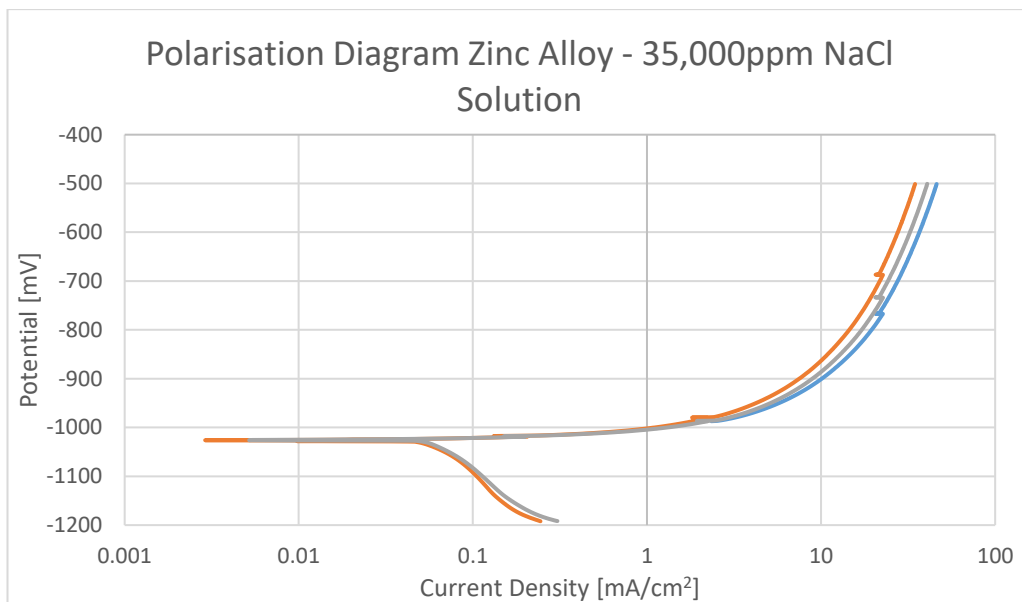


**Figure 5-4.** Anodic polarisation scan of Zinc alloy in 35,000ppm NaCl tap water solution.

The results of the potentiodynamic testing performed on the low alloy steel grade and Zinc alloy anode material in the high salinity aqueous solution, are in good agreement with the literature [5.8]. However, making quantitative predictions by short-term exposures is inaccurate because polarisation curves are time dependent. Calcareous deposits and anode material electrodeposition may significantly affect the polarisation characteristics of a cathodically protected steel surface [5.9-5.10]. In order to predict the current demand for a structure under cathodic protection, potentiostatic tests should be conducted. In potentiostatic tests the potential of the working electrode is maintained at a specific value and the reduction of current needed to maintain the

polarisation level is monitored [5.8, 5.11]. As has been seen by Harvey P. Hack in [5.8], this reduction can be up to two orders of magnitude over an exposure period of 120 days. Values of current densities for cathodic protection based on long-term exposures, can be found in literature, but as they are not complete polarisation curves, they are not adequate for computer modelling. In order to make more accurate predictions, polarisation curves from short-term exposures can be adjusted to the protection current density values obtained from literature, for long-term exposures. According to [5.8], potentiostatic tests performed on Zinc alloy anode grade, ranging from 1 day to 120 days of exposure, showed negligible effect of time on the anodic polarisation characteristics of the material. Since the performance of Magnesium alloy anodes, in the corrosion-fatigue testing, showed effective polarisation of the cathode, throughout the testing process, it is assumed that the effect of time is also negligible on the behaviour of Magnesium alloy sacrificial anodes and that polarisation data obtained from short-term exposures can be used in the cathodic protection system design process.

### 5.2.2 Conceptual Design

The conceptual design is the first stage of the cathodic protection system design procedure. At this stage, various working conditions of the system should be taken into account, such as the solution chemical composition, the fluid flowing conditions and the geometrical characteristics of the protected structure, in order to determine the material, type, and fastening devices of the sacrificial anodes and the need of the application of coating systems.

The current work focuses on the design of sacrificial anode cathodic protection systems for the corrosion protection of the internal surfaces of small inner diameter pipelines and WEIR Minerals GEHO PD Pump components, working in 824ppm NaCl aqueous solution, which has led to unexpected failures of the equipment. The methodologies presented could also be used for cathodic protection design in 35,000ppm NaCl aqueous solution, making the use of higher corrosion resistant materials unnecessary.

Pipelines of 0.1071m internal diameter, made of low alloy steel grade S355, is to be protected by sacrificial anode cathodic protection. Since the use of discrete anodes is

restricted due to the high anode consumption combined with short protection distance from each anode, the use of axially continuous anodes may be more practical, as suggested in [5.3]. Thus, it was decided that a continuous rod shape anode should be placed in the pipeline concentrically, centralised by a specially designed polymer anode holder, as can be seen in **Figure 5-5**. Should the performance of the pumping system be significantly affected from the placement of the anode and the anode holder, directly into the flow, larger diameter pipelines may be used and the sacrificial anode cathodic protection system should be recalculated.

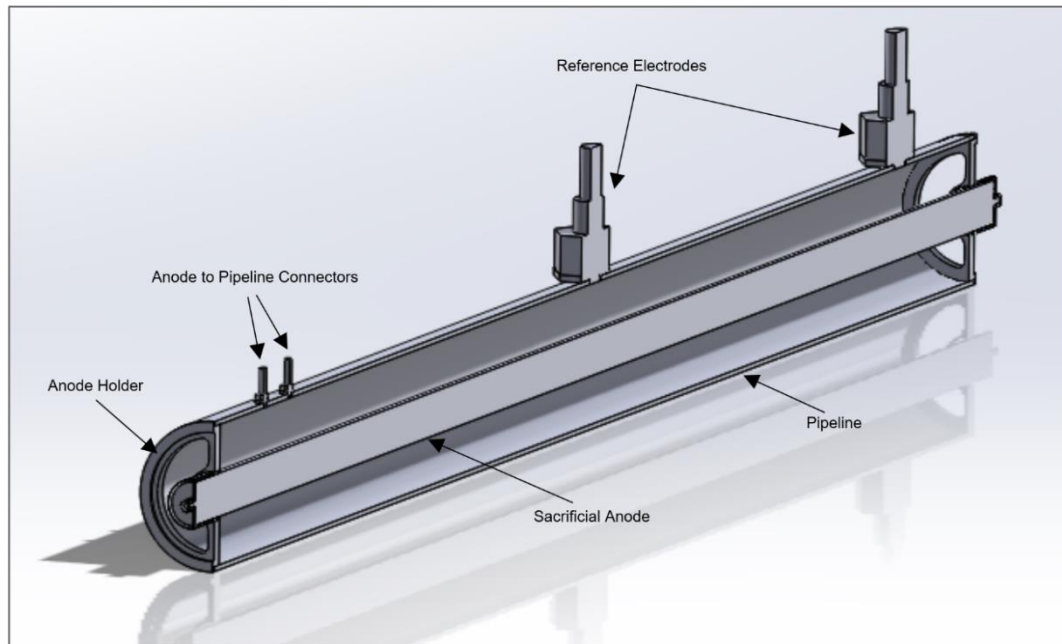


**Figure 5-5.** Cross sectional view of the sacrificial anode cathodic protection system aimed for the protection of the internal surfaces of pipelines.

Due to the relatively high resistivity of the aqueous solution, Magnesium alloy anode material should be used. By including adjustable electrical resistors in the electrical connection of the sacrificial anode to the pipeline, the anode current output may be controlled prolonging the service life of the system.

Based on the results of the corrosion-fatigue testing, it was decided that no coating system should be applied, and the decrease in the cathodic current demand would rely on the film formation and maintenance of calcareous deposits and anode material electrodeposition.

In the case of WEIR Minerals GEHO TZPM PD pumps, the sacrificial anode cathodic protection system is aimed for the corrosion protection of the internal surfaces of

pump components, working in corrosive aqueous environments. These pumps consist of three main components: the suction valve housing, the discharge valve housing and the diaphragm housing, as shown in **Figure 5-6**. According to [5.1, 5.4], it is convenient to divide large and/or complex protected structures. This division may be based on e.g. changes in working conditions and physical interfaces of the protected object such as retrievable units. Also, electrical isolation of the protected components must be considered when electrically connected to non-protected facilities [5.5]. In the case of a GEHO PD pump, the valves open and close at a high rate (1Hz) during operation and for this reason the sacrificial anode cathodic protection system will be designed and modelled assuming that both valves are open, allowing for the protection current to flow through the pump main components.

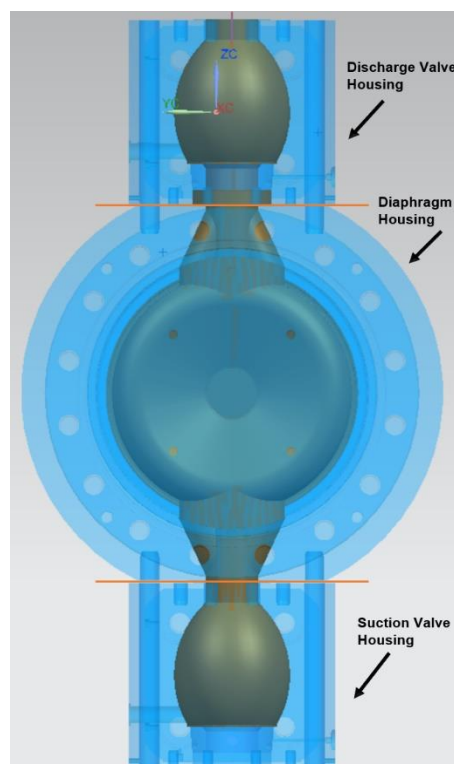


**Figure 5-6.** Internal surfaces of GEHO TZPM PD pump components to be protected from corrosion by sacrificial anode cathodic protection.

The anodes will be arrayed in such a way that ensures the adequate protection of the entirety of the internal surface of the pump components under protection. The diaphragm housing will be protected using two flush-mounted anodes that will be screwed on the housing cover insert. Each valve housings will be protected using two disc anodes; one screwed on the valve cover and the other on the valve housing opposite the valve housing cover. Four bracelet anodes will be placed to the inlet and outlet of the valve housings in order to obtain uniform current and potential distribution

on the protected surfaces. No coating system is to be applied on the internal surfaces of the pump. Finally, the performance of the system should be monitored by the use of reference electrodes placed in such locations where the protection level (Electrode Potential) is expected to be lowest (less electronegative).

### 5.2.3 Detailed Design

The analytical design methodology for the calculation of sacrificial anode cathodic protection systems, aimed for the protection of the internal surfaces of pipelines and GEHO TZPM PD pumps, is presented. These guidelines are to be used as general rules for the design of such systems but the procedure may vary according to the application, as will be seen in the next Chapter.

- Surface Area Calculations

The total surface area of the pipeline or pump components to be protected shall be calculated. For objects with complex geometries it is convenient to apply some simplifications, but the overall result should be conservative. Narrow geometries must be avoided by either insulation or redesigning, because in such parts the resistance is too high and so very difficult to obtain adequate current distribution.

- Current Demand Calculations

The current demand is calculated by multiplying the protected surface area,  $A_c$  [ $m^2$ ] by the design current density,  $i_c$  [ $A/m^2$ ] and the coating breakdown factor,  $f_c$ , as can be seen in **Equation 5-1**.

$$\text{Current Demand: } I_c = A_c \cdot i_c \cdot f_c \text{ [A]} \quad (5-1)$$

For uncoated surfaces the coating breakdown factor,  $f_c$  is set 1. The design current density  $i_c$  shall be taken from data found in the literature or from relevant polarisation diagrams if such diagrams are available. The polarization behaviour is time dependent so data from potentiostatic tests are more accurate for the prediction of the current demand than potentiodynamic tests from short-term exposures, as has already been discussed. The current density needed to polarise the material to the design protective potential,  $E_c$  [V] which is set to be  $-800\text{mV}_{\text{SSC}}$ , can be obtained from polarization curves, as shown in the **Figure 5-7**.

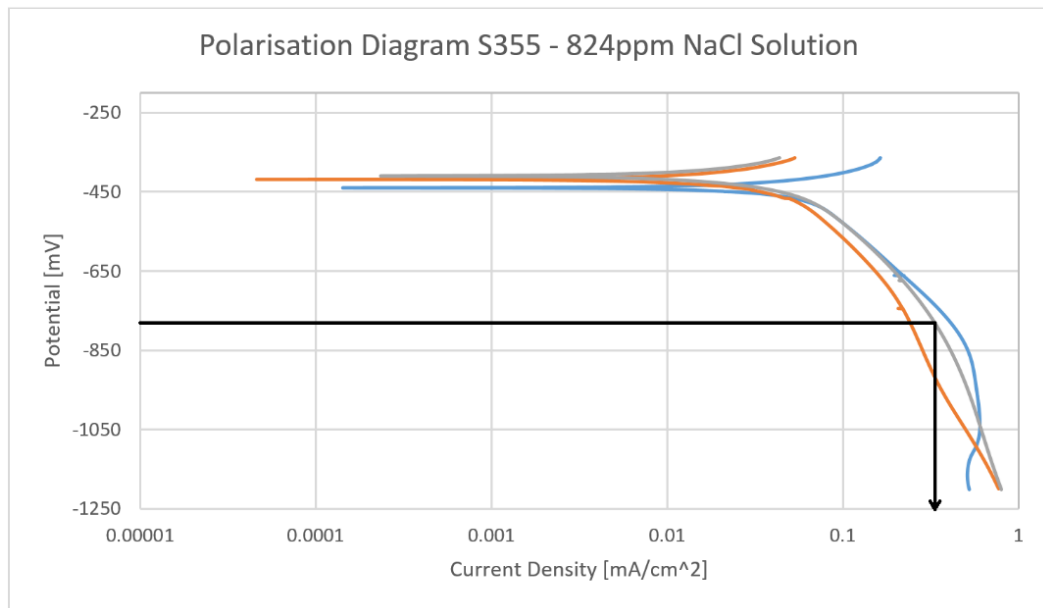


**Figure 5-7.** Measurement of the current density needed to polarize the S355 cathode to the design protective potential.

- Current Drain Calculations

All the items that may be electrically connected to the cathodic protection system should be taken into account. The calculations of the current drain shall respect the same calculation procedure for items to be cathodically protected. It is recommended that items, not to be protected by cathodic protection, should be electrically isolated from the protected parts. If this is not possible, the system should be designed in such a way as to ensure adequate current distribution on the protected surfaces, taking into account the decrease in the service life of the anodes, due to current drain.

- Anode Mass Calculations

In order to calculate the anode mass, the design life of the system,  $t_f$  [yrs] the anode utilisation factor,  $u$  and the design anode electrochemical capacity,  $\varepsilon$  [Ah/Kg] need to be defined.

The utilization factor is the fraction of the anode material, of specific design, that can be used for the calculation of the net anode mass, needed to maintain protection throughout the design life of the system. When the anode is consumed to its utilization limit, the anode current output and so its polarizing capacity becomes unpredictable. This happens due to loss of support of the anode material or the rapid increase in anode resistance. The electrochemical capacity of an anode material is the current

that can be produced from a specific anode material per mass unit, in a time unit. The total net anode mass can be calculated using **Equation 5-2**.

$$m_a = \frac{I_c \cdot t_{[yrs]} \cdot 8760}{u \cdot \varepsilon} = \frac{I_c \cdot t_{[months]} \cdot 720}{u \cdot \varepsilon} = \frac{I_c \cdot t_{[hrs]}}{u \cdot \varepsilon} \text{ [Kg]} \quad (5-2)$$

- Calculation of Number of Anodes and Individual Anode Current Output

Ohm's law is used in order to calculate the individual anode current output,  $I_a$  [A]. The sum of the individual anode current outputs needs to meet the current demand,  $I_c$  [A].

$$I_c = N \cdot I_a = \frac{N(E_c - E_a)}{R_a} = \frac{N \cdot \Delta E}{R_a} \text{ [A]} \quad (5-3)$$

Where  $E_a$  [V], is the closed circuit anode potential which is the potential of the anode when connected to the structure under protection. The value of the closed circuit anode potential can be measured from the polarisation curves as shown in **Figure 5-8**.  $E_c$  [V] is the design protective potential, which is  $-800\text{mV}_{\text{SSC}}$ .  $R_a$  [ $\Omega$ ], is the anode resistance. The anode resistance is a function of the geometric characteristics and the electrolyte resistivity. Formulas for the calculation of the anode resistance of specific anode geometries can be found in the literature. Some examples of formulas for the calculation of anode resistance are given below.

For short flush mounted and bracelet anodes the anode resistance is calculated using the following formula (McCoy's formula), which is suggested in [5.2]:

$$R_a = \frac{0.315 \cdot \rho}{\sqrt{A}} \text{ [\Omega]} \quad (5-4)$$

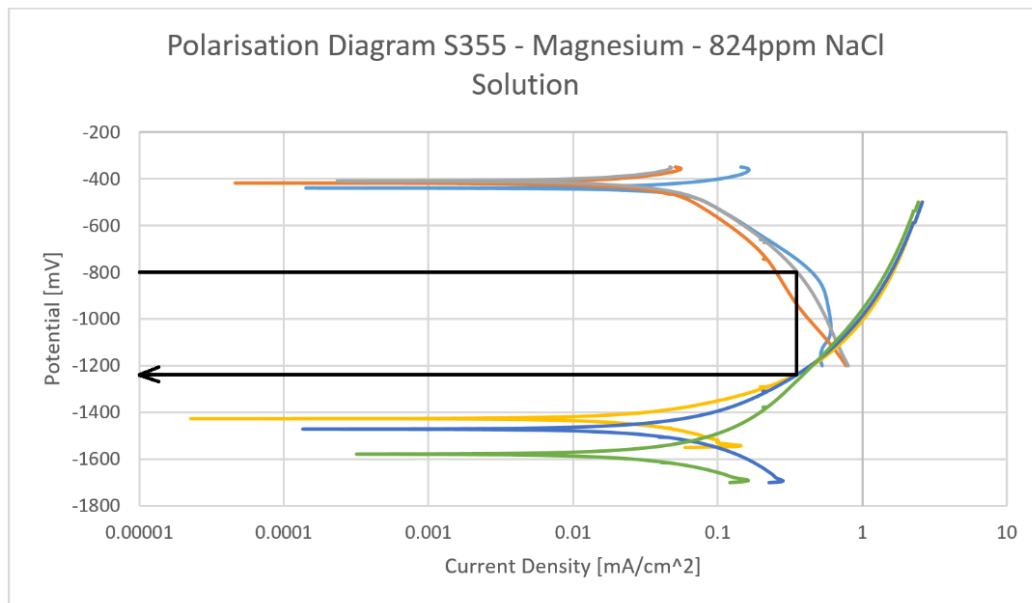


**Figure 5-8.** Measurement of the closed circuit anode potential using polarisation curves.

For long flush mounted anodes ( $L \geq 4 \cdot \text{width}$  and  $L \geq 4 \cdot \text{thickness}$ ) the anode resistance is calculated using the following formula, which is suggested in [5.1]:

$$R_a = \frac{\rho}{2 \cdot S} [\Omega] \quad (5-5)$$

where  $S$  is the arithmetic mean of anode length and width.

These calculations evaluate the anode current output based on the anode resistance to remote water. The current output of the anodes can be predicted more accurately by the simulation of the sacrificial anode cathodic protection system.

- Anode Current Capacity

The anode current capacity is the current that an anode of specific material and geometry can provide throughout its life span. The individual and the total anode current capacity can be calculated using **Equation 5-6** and **Equation 5-7** respectively.

Individual anode current capacity:

$$C_a = m_a \cdot \varepsilon \cdot u [A \cdot h] \quad (5-6)$$

where  $m_a$  [Kg], is the net mass per anode.

The total current capacity for a cathodic protection system with  $N$  number of anodes becomes:

$$C_{a,total} = N \cdot C_a [A \cdot h] \quad (5-7)$$

If anodes of different geometry and size and hence, anode current capacity and current output are utilised,  $N \cdot C_a$  and  $N \cdot I_a$  will have to be calculated for each individual geometry and size and then added for calculation of the total anode current capacity and total anode current output.

The following requirements should be met:

$$C_{a,tot} = N \cdot C_a \geq I_c \cdot t_f \cdot 8760 \quad (5-8)$$

$$I_{a,tot} = N \cdot I_a \geq I_c \quad (5-9)$$

In the case the above requirements are not met, for the anode net mass and dimensions initially selected, larger anode sizes should be selected and the calculations repeated until these requirements are met.

- Distribution of Anodes

The number of anodes that have been calculated shall be so distributed as to provide uniform current and potential distribution over the surfaces under protection, ensuring in this way that there will not be any under-protected or over-protected areas. The current demand of individual members and any coatings used shall be taken into account. Finally, the sacrificial anode cathodic protection system should be modelled using numerical methods, in order for the performance of the system to be predicted and proper modifications made to the system, before it is applied in the field.

- Effect of Slurries

In the case the pumped fluid is slurry, testing should be performed on the specific environment and also on the anode and cathode materials. Firstly, the conductivity of the solution should be measured and the anode material selected appropriately. Furthermore, the polarisation curves for the anode and cathode materials in this solution should be obtained. Both conductivity and polarisation curves (boundary conditions) will be used as input data for the solving of the simulation model. Finally, as the simulation software BEASY CP cannot predict the effect of erosion on the CP system behaviour, the anode material may be tested in slurry so as to measure the

effect of erosion corrosion on the mass loss of the material and consequently on the final life span of the anodes.

## **5.3 Guidelines for Prediction of Cathodic Protection Systems Performance Using Modelling Techniques**

### 5.3.1 Introduction to Cathodic Protection Modelling

The use of modelling techniques allows for the prediction of a cathodic protection system's behaviour, in various working conditions, without the need of in-field measurements. Moreover, at this stage the designer is able to apply modifications to the system in order to improve its efficiency in providing adequate current distribution over the entirety of the protected surfaces.

The modelling procedure consists of three main steps, as has been already described in **Chapter 2**. In this section the steps that should be taken in order to model the performance of sacrificial anode cathodic protection systems aimed for the corrosion protection of the internal surfaces of pipelines and WEIR Minerals GEHO PD pumps, using BEASY CP software, are presented.

### 5.3.2 Model Creation

#### *5.3.2.1 Model Geometry*

The procedure starts with the creation of the model's geometry. Geometries can be directly created in BEASY CP software using GiD interface. The geometrical characteristics of a model need to be defined in sufficient detail, although narrow geometries and sharp angles should be avoided. The effectiveness of cathodic protection systems is dramatically reduced in narrow geometries, as has been suggested by J. Baynham and T. Froome in [5.12] and can be avoided either by insulation or redesigning. Also, sharp angles may affect the accuracy of the results of the simulation process.

### 5.3.2.2 Normal Vectors to Surfaces

After the geometrical characteristics of the model are defined, the critical step of setting the orientation of the normal vectors to surfaces, is undertaken. The rule is, and so does in the case of cathodic protection systems protecting the internal surfaces of pipelines or GEHO PD pumps, that these vectors should point out of the electrolyte to be modelled. In this way the wetted surfaces of the model, on which the boundary conditions would apply and as a result the geometry of the electrolyte, are defined.

### 5.3.2.3 Anodic, Cathodic and Insulated Surfaces

The next step concerns the defining of the surfaces of the model to act as anodic, cathodic or insulated. In this way, the relevant boundary conditions will be applied on each of them, by the BEASY CP software. In the case of insulated surfaces, BEASY CP applies the default boundary condition, which is a normal current density of zero, as stated in [5.13].

### 5.3.2.4 Mesh Generation

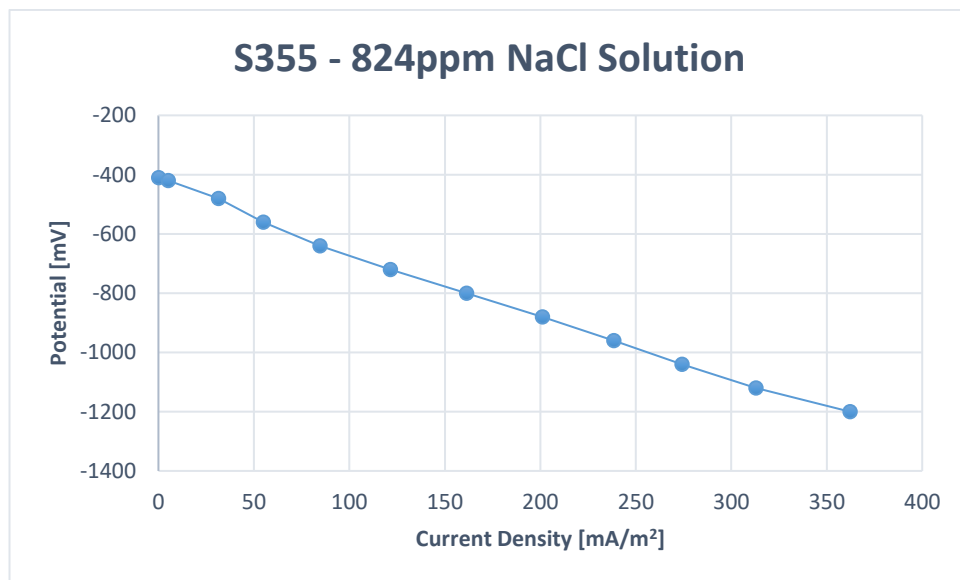
Meshing is the process of covering the surfaces that enclose the electrolyte with elements. These elements are usually of triangular or quadrilateral shape. In general, at regions of the model where the geometry changes abruptly, it is recommended to apply a finer mesh, in order to capture the variations of the solution, while at regions away from these areas elements may be graded to larger sizes. In this way, the number of elements is reduced leading to the decrease of the calculation process times.

In the case of pipeline's sacrificial anode cathodic protection system model meshing, the size of the elements applied on the pipeline or on the rod anode may be of the same size, as the behaviour of the system is not expected to change significantly across the surface. On the contrary, while meshing a GEHO PD pump model, elements of smaller sizes should be applied on areas of rapid change of the geometry, such as valves and valve seats.

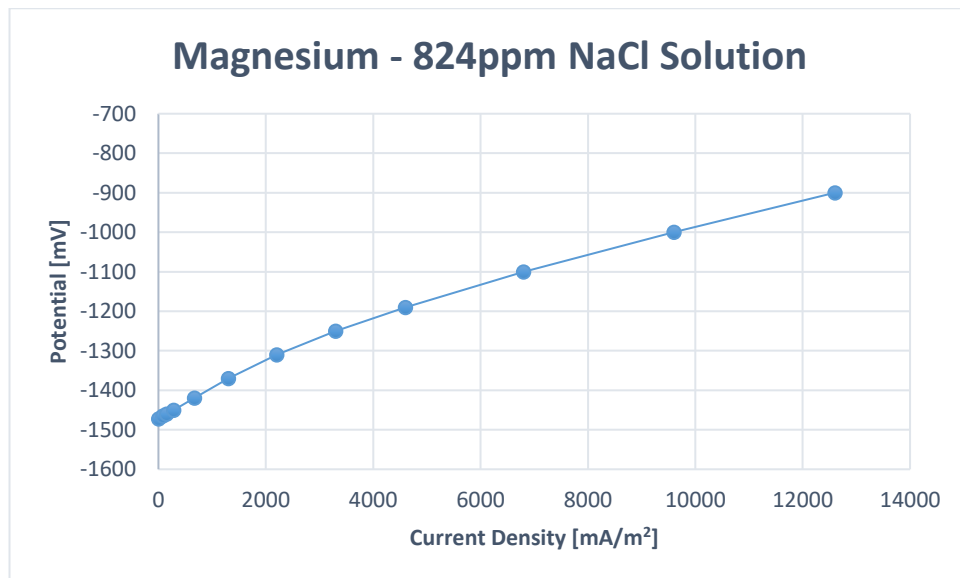
### 5.3.2.5 Polarisation Data

Prior to beginning the simulation process, the fundamental step of introducing the polarisation data of the materials, obtained from the polarisation scanning, into the system, should be taken. At this step, the boundary conditions to be applied on the elements of the anodic and cathodic surfaces are defined in a material file. The data are introduced in the form of tables of electrode potential and current density values. The polarisation curves introduced to BEASY CP for the modelling of the sacrificial anode cathodic protection systems of both the pipeline and the GEHO PD pump, are presented in **Figures 5-9** and **5-10**.

The polarisation curve of S355J2G3+N, working in turbulent 824ppm NaCl aqueous solution of 0.1712S/m conductivity, has been adjusted to the current density requirement of 161.4mA/m<sup>2</sup>, to polarise bare steel to a potential level of -800mV<sub>SSC</sub>, in oxygenated turbulent fresh water, as recommended in [5.14], assuming that the slope of the curve does not change significantly.



**Figures 5-9.** Polarisation data of S355J2G3+N in flowing 824ppm NaCl aqueous solution.



**Figures 5-10.** Polarisation data of Magnesium anode alloy in flowing 824ppm NaCl aqueous solution.

### 5.3.3 Solver Launching

After the model is created, it is ready to be introduced into the BEASY CP system in order to be solved. This can be done using the BEASY CP Wizard solver. The solver follows the process, described in **Chapter 2**, to solve the assembled boundary element equations, representing the electrolyte, coupling them with the equations derived from the polarisation data. When the process is finished, BEASY CP system creates a documents that contains the results of the modelling process, with the extension post.res. Furthermore, a summary report document is created, which contains modelling results regarding the number of iterations that were needed to achieve convergence and the total current flow in the system. Also, this report includes the surface area of the cathodes and anodes, the current output of each anode and the minimum and maximum values of the current density and potential at each anode and cathodes. These information are very useful in terms of assessing the performance of the sacrificial anode cathodic protection systems, especially in the case of GEHO PD pump modelling where anodes of various types are used. In this way, the current output and so the service life of each anode can be predicted.

### 5.3.4 Simulation Results

The results of the simulation can be post-processed using the BEASY CP software tools via GiD user interface, by shifting to post-process mode. The system allows for creation of contour plots of the protection potentials and the visualisation of current densities on the different surfaces. By assessing the predicted performance of the cathodic protection system modelled, the designer can make modifications to the type, size and the distribution of the anodes and repeat the procedure until satisfactory results are achieved. Finally, the need of sealing narrow geometries (if it has not been done so in the beginning of the modelling process) and of using also coating systems may become obvious.

## 5.4 Conclusions

In this Chapter guidelines for analytical design and simulation of sacrificial anode cathodic protection systems to be used for the protection of the internal surfaces of pipelines and WEIR Minerals PD pump components, has been presented. The analytical design offers an initial estimation of the system's behaviour but the prediction of its actual performance requires the simulation of the cathodic protection system, as is also discussed in detail in **Chapter 6**.

The accuracy of the analytical design and simulation are highly dependent on the polarisation curves, which are obtained experimentally by testing the materials involved, in real working conditions. Moreover, it has been seen that polarisation data obtained from long-term exposures offer more accurate results and so increases the efficiency of the design procedure in predicting the system's behaviour.

The modelling of cathodic protection systems enables the designer to make modification, without the need of in-field measurements, in order to improve the system's performance before it is applied. Regarding this fact, the cost of applying cathodic protection on an actual system may be reduced dramatically.

In the next Chapter the presented design method will be applied for the design and simulation of sacrificial anode cathodic protection systems for the corrosion protection of the internal surfaces of small diameter pipelines and WEIR Minerals GEHO TZPM

PD pumps, working in corrosive aqueous environments of 824ppm NaCl concentration.

## 5.5 References

- [5.1] Recommended Practice DNV-RP-B401, Cathodic Protection Design (2010).
- [5.2] NACE Standard RP0176-2003, Corrosion Control of Steel Fixed Offshore Structures Associated with Petroleum Production, ISBN 1-57590-170-6, NACE International, Houston TX (2003).
- [5.3] BS EN 12499:2003, Internal Cathodic Protection of Metallic Structures (2003).
- [5.4] Recommended Practice DNV-RP-F103, Cathodic Protection of Submarine Pipelines by Galvanic Anodes (2010).
- [5.5] International Standard ISO 15589-1, Petroleum and Natural Gas Industries – Cathodic Protection of Pipeline Transportation Systems, Part 1: On-land Pipelines (2003).
- [5.6] International Standard ISO 15589-2, Petroleum, Petrochemical and Natural Gas Industries - Cathodic Protection of Pipeline Transportation Systems, Part 2: Offshore Pipelines (2012).
- [5.7] ASTM International, Standard Reference Test Method for Making Potentiodynamic Anodic Polarization Measurements, Designation: G5 – 14 (2014).
- [5.8] Harvey P. Hack, Atlas of Polarization Diagrams for Naval Materials in Seawater, Carderock Division Naval Surface Warfare Center, CARDIVNSWC-TR-61—94/44, Bethesda, USA (1995).
- [5.9] J. L. Solis and J. Genesca, Effect of Calcareous Deposit Formation on Galvanic Anode Cathodic Protection of Steel in Seawater, NACE International, Corrosion 2009 Conference & Expo, Paper No. 09520 (2009).

- [5.10] R. Johnsen and H. W. Stangeland, Cathodic Protection in Cold Seawater – Current Density Requirements, NACE International, Corrosion 2009 Conference & Expo, Paper No. 09521 (2009).
- [5.11] M. Esmaily, J. E. Svensson, S. Fajardo, N. Birbilis, G. S. Frankel, S. Virtanen, R. Arrabal, S. Thomas and L.G. Johansson, Fundamentals and Advances in Magnesium Alloy Corrosion, Progress in Materials Science, Volume 89, pp. 92–193 (2017).
- [5.12] J. Baynham and T. Froome, Assessment of Effects of Cavities and Narrow Channels on CP Design in the Marine Environment, NACE-2017-9275, NACE International (2017).
- [5.13] BEASY Cathodic Protection Software, User Guide (2013).
- [5.14] NACE International, CP3 – Cathodic Protection Technologist Course Manual, version 1 (2014).

# CHAPTER 6

## Analytical Design and Simulation of SACP Systems for Pipelines and GEHO Positive Displacement Pumps

### 6.1 Introduction

In this chapter the design methods, presented in **Chapter 5**, are applied in order to design sacrificial anode cathodic protection systems for the corrosion protection of the internal surfaces of pipelines and WEIR Minerals GEHO TZPM PD pumps. The cathodic protection systems are calculated analytically, using data of critical parameters that were obtained experimentally. Furthermore, numerical methods are adopted in order to simulate the performance of the systems in various working conditions.

In the first case, a sacrificial anode cathodic protection system was designed, using a commercial long slender stand-off magnesium sacrificial anode, concentrically placed into the pipeline. The analytical design procedure, which comprises of the conceptual design and the detailed design, is presented. The behaviour of the system was then simulated using the commercial software BEASY CP, to predict the performance of the cathodic protection system. In the simulation, the experimentally obtained polarisation data of the materials involved, were used as input into the software for accurate prediction of the behaviour of the cathodic protection system.

In the case of the WEIR Minerals GEHO TZPM PD pump, the function of which has been described in [6.1], a sacrificial anode cathodic protection system for the protection of the internal surfaces of its components, was designed analytically and then simulated using BEASY CP software. The system comprised of flush mounted and bracelet Magnesium alloy anodes, placed into the pump in such a way as to

minimise the effect of anode's interference with the pumped liquid flow, on the pump's performance. What is more, extra simulations have been run in order to predict the effect of current drain, due to the connection of the pump to pipelines at the inlet and outlet, on the cathodic protection system's behaviour. In this way, it was possible to determine the need of application of electrical isolation systems on the pump.

Finally, the effectiveness of both cathodic protection systems in sufficiently protecting the internal surfaces of the structures, is evaluated by the successful polarisation of the entirety of the protected surfaces to potentials equal or more electronegative than  $-800\text{mV}_{\text{SSC}}$ , which is used as the protection criterion.

## 6.2 Design of Pipeline Cathodic Protection System

### 6.2.1 Analytical Design of SACP System for Pipeline Test Rig

#### 6.2.1.1 Conceptual Design

A sacrificial anode cathodic protection system will be designed for the protection of the internal surface of a low-alloy steel grade S355 pipeline of 0.1071m internal diameter and 1.5m length. No coating system will be applied into the internal surface of the pipeline. The electrolyte is an 824ppm NaCl tap water solution of  $5.84\Omega\text{m}$  resistivity and the flowing conditions in the pipeline will be turbulent. A commercial long slender stand-off magnesium sacrificial anode of 0.0334m diameter and 0.0034m core diameter, offered by Mag Specialties Inc., will be used to provide the protective current to the pipeline. Finally, the anode will be placed concentrically into the pipeline held by polymer holders (centralizers).

#### 6.2.1.2 Detailed Design

- Surface Area Calculations

In **Table 6-1** the result of the calculations of the pipeline internal surface area is shown.

**Table 6-1.** Cathode surface area calculations.

Cathode Surface Area Calculations	
Internal Diameter $d$ [m]	0.1071
Length $L$ [m]	1.5
Surface Area $A_c$ [m <sup>2</sup> ]	0.5044

The formula used for the calculation of the internal surface area of the pipeline is presented below:

$$A_c = \pi \cdot d \cdot L = \pi \cdot 0.1071 \cdot 1.5 = 0.5044[m^2] \quad (6-1)$$

- Current Demand Calculations

In **Table 6-2** the result of the calculations of the current demand for the protection of the pipeline internal surface, is shown. The value of the current density has been taken from NACE International CP3 manual [6.2], for bare steel in contact with fresh water with dissolved oxygen, in turbulent flowing conditions.

**Table 6-2.** Current demand calculations.

Current Demand Calculations	
Current Density $i_{c,dem}$ [A/m <sup>2</sup> ]	0.1614
Coating Breakdown Factor $f_c$	1
Current Demand $I_{c,dem}$ [A]	0.0814

**Equation 5-1** was used for the calculation of the current demand, as is shown below:

$$I_{c,dem} = A_c \cdot i_{c,dem} \cdot f_c = 0.5044 \cdot 0.1614 \cdot 1 = 0.0814[A]$$

- Anode Resistance Calculations

The calculation of the anode resistance for the specific set-up is not a straight forward procedure as the formula suggested in [6.3], for the calculation of the resistance of long slender stand-off anodes, is valid for 0.15m minimum distances between the anode and the structure. By the use of the equation suggested in [6.4], that is widely used in cathodic protection practice for the calculation of the resistance of a cylindrically shaped anode, when  $4L/r \geq 16$ , an approaching, but still conservative, value of the anode resistance, is obtained. The results are presented in **Table 6-3**.

**Table 6-3.** Cylindrically shaped anode resistance calculations.

Anode Resistance Calculations	
Electrolyte Resistivity $\rho$ [ $\Omega\text{m}$ ]	5.84
Distance (Anode-Cathode) $l$ [m]	0.0369
Anode Diameter $d_a$ [m]	0.0334
Anode Surface Area $A_a$ [ $\text{m}^2$ ]	0.1573
Anode Resistance $R_a$ [ $\Omega$ ]	2.643

The calculations of the cylindrically shaped anode resistance are shown below:

$$R_a = \rho \cdot \frac{K}{L} \left[ \ln \left( \frac{4L}{r} \right) \right] - 1 = 584.11 \cdot \frac{0.159}{150} \left[ \ln \left( \frac{4 \cdot 150}{1.67} \right) \right] - 1 = 2.643 [\Omega] \quad (6-2)$$

Where  $r$  [cm], is the anodes radius and  $K=0.159$  if  $L$  and  $r$  units are in cm. In this equation, the value of the electrolyte resistivity was expressed in  $\Omega \cdot \text{cm}$ .

- Anode Current Output Calculations

The anode current output is calculated using **Equation 5-3**. The actual current output of the anode is expected to be less, as the polarization of the anode and cathode is expected to be higher, decreasing the available driving voltage. The results of the relevant calculations are presented in **Table 6-4**.

**Table 6-4.** Anode current output calculations.

Anode Current Output Calculations	
Protective Potential $E_c$ [V]	-0.8
Anode Closed Circuit Potential $E_a$ [V]	-1.459
Number of Anodes $N$	1
Anode Resistance $R_a$ [ $\Omega$ ]	2.643
Anode Current Output $I_a$ [A]	0.249

The calculations of the anode current output are shown below:

$$I_c = N \cdot I_a = I_a = \frac{E_c - E_a}{R_a} = \frac{-0.8 - (-1.459)}{2.643} = 0.249 [A]$$

- System Life Calculations

In **Table 6-5** the results of the system's life calculations are presented. The diameter of the anode when consumed to its utilisation limit, has been calculated according to [6.3], the value of which was used for the calculation of the final anode resistance and current output. Finally, the system's life is calculated using **Equation 5-2**.

**Table 6-5.** System service life calculations.

System Life Calculations	
Anode Core Diameter $d_{a,core}$ [m]	0.0034
Anode Material Density $D$ [kg/m <sup>3</sup> ]	1,738
Net Anode Mass $m_a$ [kg]	2.259
Electrochemical Capacity $\epsilon$ [Ah/Kg]	1,230
Final Anode Diameter $d_{a,u}$ [m]	0.0064
Final Anode Resistance $R_{a,u}$ [ $\Omega$ ]	3.66
Final Current Output [A]	0.179
System Life $t$ [hrs]	11,685
System Life $t$ [months]	16.2

The calculation of the net anode mass is shown below:

$$m_a = D \cdot V_{an} = D \frac{\pi(d_a^2 - d_{a,core}^2)}{4} L [Kg] \Rightarrow \quad (6-3)$$

$$m_a = 1,738 \frac{\pi(0.0334^2 - 0.0034^2)}{4} 1.5 = 2.259 [Kg]$$

where  $V_a$  [m<sup>3</sup>], is the net anode material volume and  $d_{a,core}$  [m], is the diameter of the anode's steel core.

Using the method suggested in [6.3], the anode diameter, when the anode is consumed to its utilisation factor, was calculated to be  $d_{a,u} = 0.0064\text{m}$  or 6.4mm, assuming that the consumption of the anode was radially and axially uniform, due to the fact that its ends were insulated. In the calculations, the value of 0.9 for the utilisation factor of long slender stand-off anodes, was used.

The final anode diameter ( $d_{a,u}$ ) value was used for the calculations of the final anode resistance and final current output, by using **Equations 6-2** and **5-3**, respectively. The results of the calculations are presented below:

$$R_{a,u} = \rho \cdot \frac{K}{L} \left[ \ln \left( \frac{4L}{r} \right) \right] - 1 = 3.66 [\Omega]$$

$$I_{a,u} = \frac{E_c - E_a}{R_a} = 0.179 [A]$$

The final anode current output was found to be larger than the design current demand and for this reason, it is assumed that the anode will continue to provide adequate protection to the internal surface of the pipeline, until its utilisation limit is reached.

Finally, the system's service life is determined by using **Equation 5-2**, as shown below.

$$t = \frac{u \cdot \varepsilon \cdot m_a}{(I_a + I_{a,u})/2} = \frac{0.9 \cdot 1230 \cdot 2.259}{(0.249 + 0.179)/2} = 11,685 \text{ [hrs] or } 16.2 \text{ [months]}$$

The next step is to simulate the sacrificial anode cathodic protection system, using a commercial cathodic protection modelling software, to evaluate the accuracy of the calculated system's performance. Moreover, cathodic protection modelling will make it possible to predict the current distribution on the surface of the pipeline and so evaluate the level of protection provided by the system. The procedure and the results of the CP modelling are presented and discussed in the next section.

## 6.2.2 Simulation of Pipeline Cathodic Protection System

### 6.2.2.1 Model Creation

- Creation of Model Geometry

The modelling procedure of the pipeline sacrificial anode cathodic protection system, included the creation of two models representing the working conditions of the system at the beginning of its application and after the anode is consumed to its utilisation limit. The scope is to predict the initial performance of the system and the capability of the specific set-up in providing adequate corrosion protection to the internal surface of the pipeline, when the anode reaches the end of its service life. In this way, the actual life span of the system can be predicted.

The first step of the modelling was completed using GID drawing software, to create the geometry of the model [6.5]. This software works as an interface between the model geometry and the BEASY solver software [6.6-6.7]. In **Figures 6-1** and **6-2** the geometry of the cathodic protection system models, are illustrated. The models include the cathodic, anodic and the insulated surfaces.

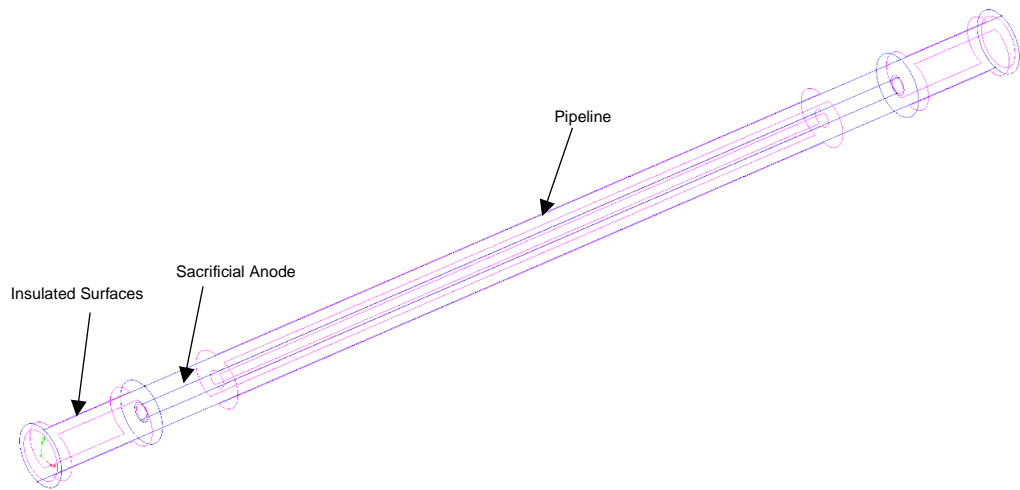


**Figure 6-1.** Initial geometry of pipeline sacrificial anode cathodic protection system.

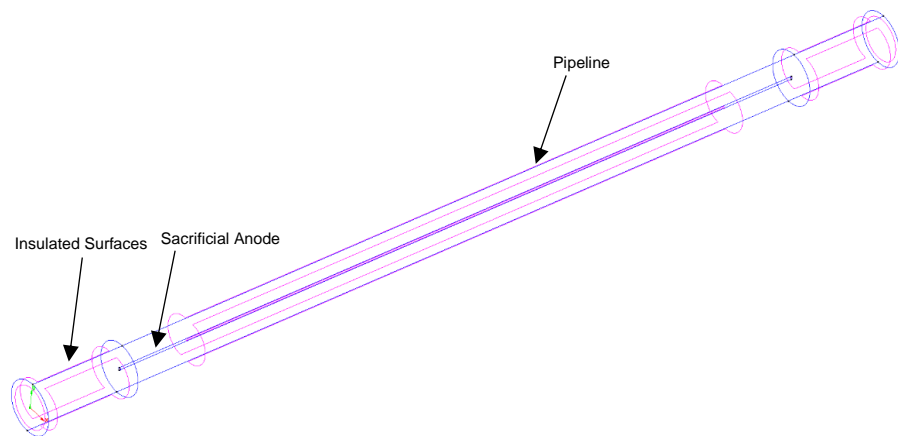


**Figure 6-2.** Final geometry of pipeline sacrificial anode cathodic protection system.

After the creation of the geometry, the groups of the surfaces to act as anodes, cathodes and insulated were defined in the BEASY CP system. The units of the models were set as m, mA and mV, in order to be compatible with the input data of the polarization curves (boundary conditions) and the conductivity of the electrolyte was set to 0.1712S/m.

- Mesh Creation

The next step of the modelling procedure, after setting the orientation of the normal vectors to surfaces, is the application of meshing on the surfaces of the models. The pipeline, the sacrificial anode and the insulated surfaces have been discretised in 288

triangular and 7,600 quadrilateral elements, giving a total of 7,888 elements for the initial geometry model and 232 triangular and 6,600 quadrilateral elements, giving a total of 6,832 elements, in the case of the final geometry model, as is shown in **Figures 6-3** and **6-4**. Although a full convergence study was not carried out, with discussion with experts and comparison to the literature, it is considered that the meshes are fully converged.

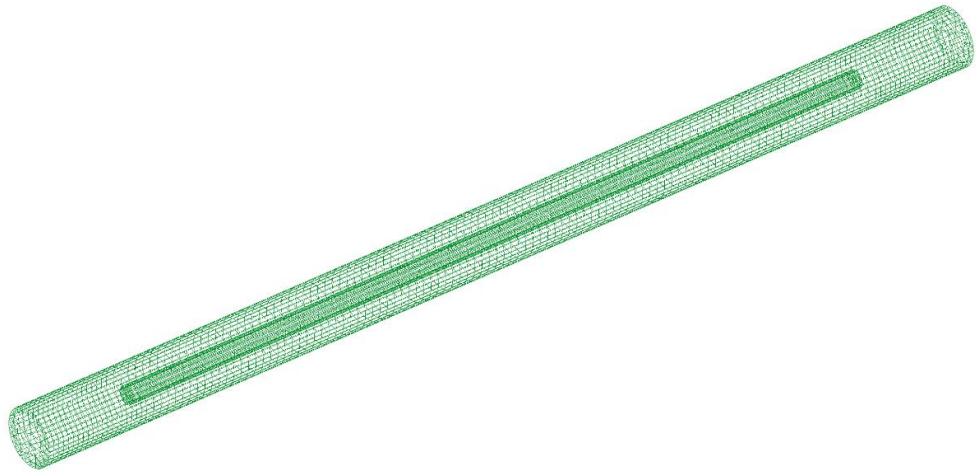


**Figure 6-3.** Meshing of the initial geometry model's surfaces.

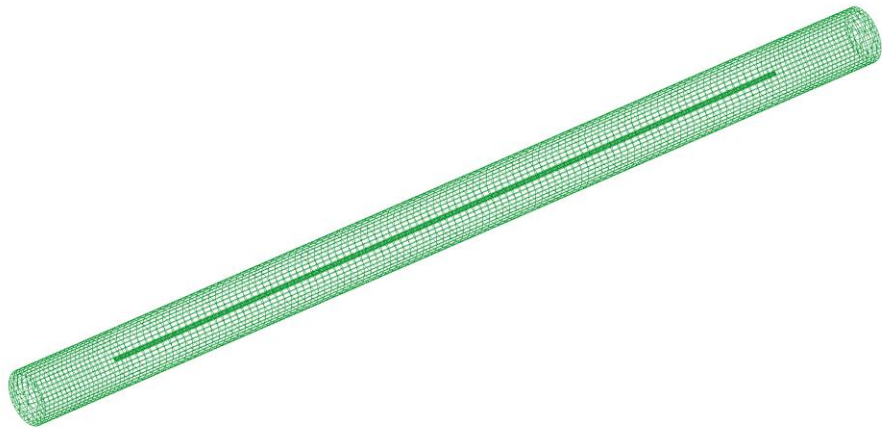


**Figure 6-4.** Meshing of the final geometry model's surfaces.

- Boundary Conditions

Before launching the BEASY solver the boundary conditions should be defined into the BEASY software. The polarization curves for the low alloy steel grade S355 and

Magnesium anode material, which were obtained in the same environmental conditions for both materials, were used as boundary conditions in the BEASY solver.

#### 6.2.2.2 Simulation Results

At this stage the models are ready to be introduced into the BEASY CP system to be solved, using the BEASY CP Wizard solver. A common laptop pc was used for the solving of the models and the process time was 5÷10min per model. After the process was completed, the results of the simulation were used to create contour plots of the potential distribution over the anodic and cathodic surfaces. For this purpose, BEASY CP software tools were employed via GiD user interface, by shifting to post-process mode. The cathodic protection system performance prediction results, obtained by the BEASY solver for both scenarios, are presented in **Figures 6-5** and **6-6**.

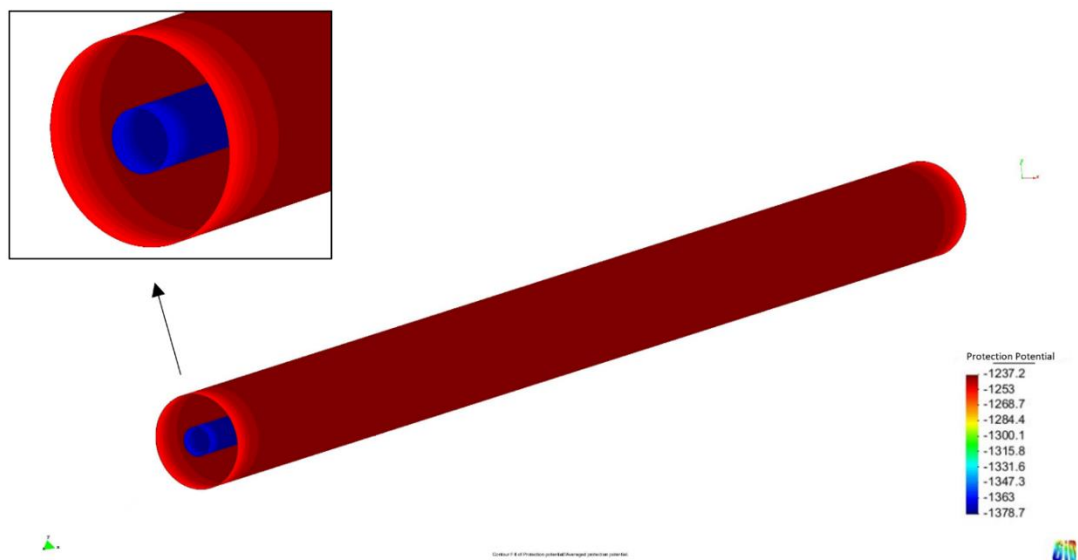


**Figure 6-5.** Initial potential distribution on the pipeline surface.

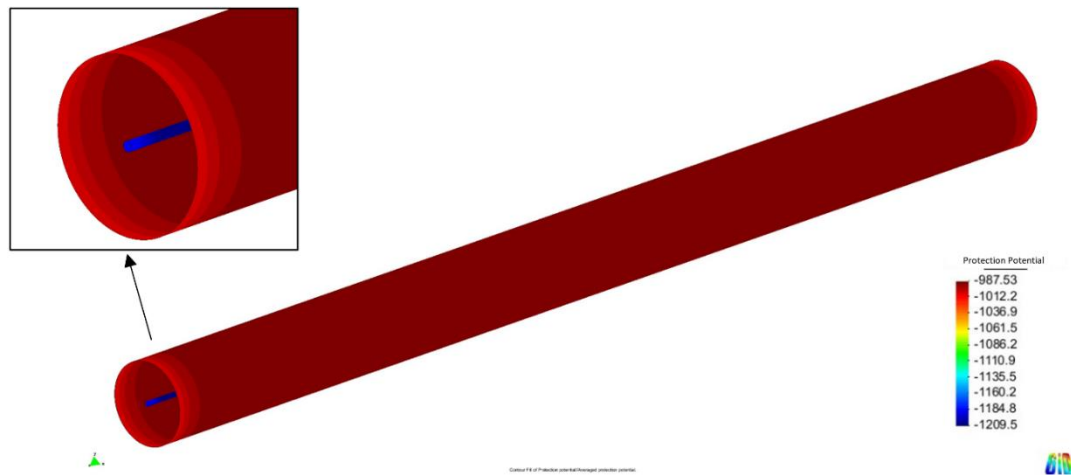


**Figure 6-6.** Potential distribution on the pipeline surface after the anode is consumed to its utilization limit.

According to the results, in the first case, the lowest achieved protection potential on the internal surface of the pipeline is  $-1237.2\text{mV}_{\text{SSC}}$ . This potential is more electronegative than the design protective potential, as this has been suggested in literature [6.2-6.4, 6.8-6.9], showing that the pipeline is sufficiently protected from corrosion. The anode current output is  $194.27\text{mA}$  that is lower compared to the calculated value, due to the higher polarisation of both anode and cathode that led to a reduction of the driving voltage. Also, the anode resistance is shown to be  $0.73\Omega$ , proving that the calculated value is conservative. As is shown in **Figure 6-6**, the system continues to provide adequate current for the protection of the internal surface of the pipeline, up to the anode consumption to its utilisation limit. In this way it is shown that the system will work satisfactorily until the anode is consumed to the diameter of  $d_{a,u} = 0.0064\text{m}$  or  $6.4\text{mm}$ . At this stage, the anode current output has been found to be  $154.29\text{mA}$ , which is still higher than the current demand. The higher polarisation observed on both anode and cathode ends is attributed to the fact that at these parts the anode current output increases, due to widening of the cross - section of the current - flow path, as has been suggested by J. Baynham and T. Froome [6.10]. Furthermore, by recalculating the system's life, using the average of the anode current output, it is found that the anode will need to be replaced after  $14,498$  hours or  $20.1$  months. Finally, based on the modelling results, the analytical design method is proved to provide conservative predictions of the anode resistance and the system's service life.

## 6.3 Analytical Design and simulation of GEHO Positive Displacement Pump Cathodic Protection System

### 6.3.1 Analytical Design of GEHO PD Pump Cathodic Protection System

#### 6.3.1.1 Conceptual Design

A sacrificial anode cathodic protection system will be designed for the protection of the internal surfaces of a GEHO TZPM PD pump. No coating system will be applied on the internal surfaces of the pump. The electrolyte is an 824ppm NaCl tap water solution of 5.84Ωm resistivity and the flowing conditions in the pipeline are assumed to be turbulent. Magnesium sacrificial anodes of Density  $D=1738\text{Kg/m}^3$ , Electrochemical Capacity  $\epsilon=1230\text{ Ah/Kg}$  and  $E= -1.5V_{\text{SSC}}$  nominal potential, will be used to provide the protective current to the protected surfaces. Flush mounted and bracelet anodes are to be used, as the insertion of anodes, directly into the flow, is expected to negatively affect the performance of the pump.

#### 6.3.1.2 Detailed Design

- Surface Area Calculations

After the creation of the 3d model of the pump and the relevant simplifications, the surface area to be protected was measured to be 1.334m<sup>2</sup>.

- Current Demand Calculations

In **Table 6-6** the result of the calculations of the current demand for the protection of the pump internal surface are shown. The value of the current density has been taken from NACE International CP3 manual [6.2] for bare steel in contact with fresh water with dissolved oxygen, in turbulent flowing conditions, as has been done in the case of the pipeline sacrificial cathodic protection system.

**Table 6-6.** Current demand calculations.

Current Demand Calculations	
Current Density $i_{c,dem}$ [A/m <sup>2</sup> ]	0.1614
Coating Breakdown Factor $f_c$	1
Current Demand $I_{c,dem}$ [A]	0.2153

**Equation 5-1** was used for the calculation of the current demand, as is shown below:

$$I_{c,dem} = A_c \cdot i_{c,dem} \cdot f_c = 1.334 \cdot 0.1614 \cdot 1 = 0.2153[A]$$

- Anode Mass Calculations

The anode mass required to protect the pump over a specific period of time can be calculated using **Equation 5-2**, as suggested in [6.3, 6.11]. In order for the calculations to be conservative the utilisation factor for all of the anodes is set to be 0.8. The calculated anode mass is the least required to protect the pump over this period of time.

$$M_a = \frac{I_{c,dem} \cdot t_{f,[yrs]} \cdot 8760}{u \cdot \epsilon} = \frac{I_{c,dem} \cdot t_{f,[months]} \cdot 720}{u \cdot \epsilon} = \frac{I_{c,dem} \cdot t_{f,[hrs]}}{u \cdot \epsilon} [Kg] \Rightarrow$$

$$M_a = \frac{0.2153 \cdot 2 \cdot 8760}{0.8 \cdot 1230} = 3.84 [Kg]$$

The final anode mass required may vary due to the geometrical characteristics of the anodes and subsequently due to their individual current output. The geometrical characteristics of the anodes to be used are presented in **Table 6-7**.

**Table 6-7.** Geometrical characteristics of sacrificial anodes.

Code Name	Anode Type	Number	Dimensions [m]	Active Surface Area [m <sup>2</sup> ]	Volume [m <sup>3</sup> ]	Mass [Kg]
SA1 (Anodes 2&8)	Disc	2	D=0.1, L=0.04	0.02	0.000314	0.545732
SA2 (Anodes 3&9)	Disc	2	D=0.14, L=0.0266	0.02414	0.000409	0.710842
SA3 (Anode 1)	Bracelet	1	ID=0.1, L=0.0394, t=0.025	0.01259	0.000387	0.672606
SA4 (Anode 7)	Bracelet	1	ID=0.1, L=0.0426, t=0.025	0.01339	0.000418	0.726484
SA5 (Anodes 4&10)	Bracelet	2	ID=0.1, L=0.0296, t=0.025	0.009295	0.00029	0.50402
SA6 (Anodes 5&6)	Long Flush Mounted	2	OD=0.454, W=0.066, a= 133.28°, c=45°, t=0.02	0.04297	0.0005	0.869
				SA <sub>tot</sub> =0.21879	V <sub>tot</sub> =0.003831	m <sub>tot</sub> =6.658278

- Anode Resistance Calculations

The calculations of the anode resistance for a specific set-up is not a straight forward procedure due to the complexity of anode geometries and the fact that the formulas included in the industrial standards refer to the anode resistance to remote water. For this reason, it is more convenient to calculate the resistance and the current output of each anode using simulation methods. In order to have an initial estimation of the performance of the SACP system, the resistance of the anodes can be calculated

using **Equation 5-4** for the disc and bracelet anodes and **Equation 5-5** for the long flush mounted anodes, as suggested in [6.3, 6.12].

- Anode Current Output Calculations

The anode current output is calculated using **Equation 5-3**. The actual current output of the anode is expected to be less as the polarization of the cathode is expected to be higher, decreasing the available driving voltage.

- Anode Current Capacity Calculations

The individual anode current capacity is calculated using **Equation 5-6** and the total current capacity of the SACP system is calculated using **Equation 5-7**.

The results of the calculations of the Anode Resistance, Anode Current Output and Anode Current Capacity for the individual anodes are presented in **Tables 6-8 to 6-13**.

**Table 6-8.** Type SA1 anode Resistance, Current Output and Current Capacity calculations.

Type SA1 Anode Calculations	
Electrolyte Resistivity $\rho$ [ $\Omega\text{m}$ ]	5.84
Number of Anodes <b>N</b>	2
Anode Surface Area <b>Aa</b> [ $\text{m}^2$ ]	0.02
Anode Net Mass <b>ma</b> [Kg]	0.545732
Utilisation Factor <b>u</b>	0.8
Anode Resistance <b>Ra</b> [ $\Omega$ ]	13.01
Anodes Current Output <b>Ia</b> [A]	0.101
Anodes Current Capacity <b>Ca</b> [A·h]	1074.0

**Table 6-9.** Type SA2 anode Resistance, Current Output and Current Capacity calculations.

Type SA2 Anode Calculations	
Electrolyte Resistivity $\rho$ [ $\Omega\text{m}$ ]	5.84
Number of Anodes <b>N</b>	2
Anode Surface Area <b>Aa</b> [ $\text{m}^2$ ]	0.02414
Anode Net Mass <b>ma</b> [Kg]	0.710842
Utilisation Factor <b>u</b>	0.8
Anode Resistance <b>Ra</b> [ $\Omega$ ]	11.84
Anodes Current Output <b>Ia</b> [A]	0.111
Anodes Current Capacity <b>Ca</b> [A·h]	1398.9

**Table 6-10.** Type SA3 anode Resistance, Current Output and Current Capacity calculations.

<b>Type SA3 Anode Calculations</b>	
Electrolyte Resistivity $\rho$ [ $\Omega\text{m}$ ]	5.84
Number of Anodes <b>N</b>	1
Anode Surface Area <b>Aa</b> [ $\text{m}^2$ ]	0.01259
Anode Net Mass <b>ma</b> [Kg]	0.672606
Utilisation Factor <b>u</b>	0.8
Anode Resistance <b>Ra</b> [ $\Omega$ ]	16.39
Anodes Current Output <b>Ia</b> [A]	0.040
Anodes Current Capacity <b>Ca</b> [A·h]	661.8

**Table 6-11.** Type SA4 anode Resistance, Current Output and Current Capacity calculations.

<b>Type SA4 Anode Calculations</b>	
Electrolyte Resistivity $\rho$ [ $\Omega\text{m}$ ]	5.84
Number of Anodes <b>N</b>	1
Anode Surface Area <b>Aa</b> [ $\text{m}^2$ ]	0.01339
Anode Net Mass <b>ma</b> [Kg]	0.726484
Utilisation Factor <b>u</b>	0.8
Anode Resistance <b>Ra</b> [ $\Omega$ ]	15.90
Anodes Current Output <b>Ia</b> [A]	0.041
Anodes Current Capacity <b>Ca</b> [A·h]	714.9

**Table 6-12.** Type SA5 anode Resistance, Current Output and Current Capacity calculations.

<b>Type SA5 Anode Calculations</b>	
Electrolyte Resistivity $\rho$ [ $\Omega\text{m}$ ]	5.84
Number of Anodes <b>N</b>	2
Anode Surface Area <b>Aa</b> [ $\text{m}^2$ ]	0.009295
Anode Net Mass <b>ma</b> [Kg]	0.50402
Utilisation Factor <b>u</b>	0.8
Anode Resistance <b>Ra</b> [ $\Omega$ ]	19.08
Anodes Current Output <b>Ia</b> [A]	0.069
Anodes Current Capacity <b>Ca</b> [A·h]	991.9

**Table 6-13.** Type SA6 anode Resistance, Current Output and Current Capacity calculations.

<b>Type SA6 Anode Calculations</b>	
Electrolyte Resistivity $\rho$ [ $\Omega\text{m}$ ]	5.84
Number of Anodes <b>N</b>	2
Anode Surface Area <b>Aa</b> [ $\text{m}^2$ ]	0.04297
Anode Net Mass <b>ma</b> [Kg]	0.869
Utilisation Factor <b>u</b>	0.85
Anode Resistance <b>Ra</b> [ $\Omega$ ]	9.83
Anodes Current Output <b>Ia</b> [A]	0.134
Anodes Current Capacity <b>Ca</b> [A·h]	1817.1

Calculating the total anode current outputs and the total anode current capacity, it is possible to evaluate that the requirements of **Equations 5-8** and **5-9** are met. The results are presented in **Table 6-14**.

**Table 6-14.** Results of total anode current output, total anode current capacity and requirements.

Total Anodes Current Output $I_{a,tot}$ [A]	0.497
Total Anodes Current Capacity $C_{a,tot}$ [A·h]	6658.6
$I_{c,dem} \cdot t_f$	3772.1
$C_{a,tot} > I_{c,dem} \cdot t_f$	YES
$I_{a,tot} > I_c$	YES

The next step is to simulate the sacrificial anode cathodic protection system, using the commercial CP modelling software BEASY CP, to evaluate the accuracy of the calculated system's performance. Moreover, CP modelling will make it possible to predict the current distribution on the surface of the pump and so to evaluate the level of protection provided by the system.

### 6.3.2 Simulation of GEHO PD Pump Cathodic Protection System

#### 6.3.2.1 Model Creation

- Creation of Model Geometry

The first step of the modelling process was to create the geometry of the GEHO TZPM PD pump model, using GID drawing software. By including the geometrical characteristics of the anodes, as these were determined in the previous section, the model preparation was complete. In **Figure 6-7** the geometry of the cathodic protection system model, is illustrated. The model includes the cathodic, anodic and the insulated surfaces, as suggested in BEASY CP user guide [6.5].

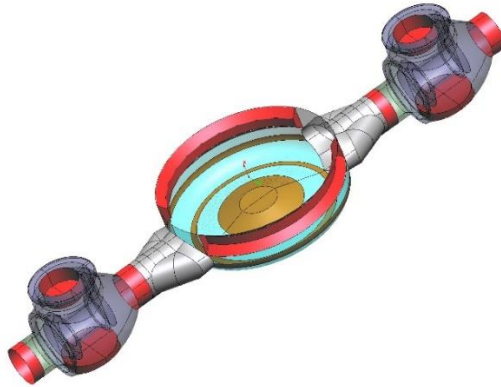


**Figure 6-7.** Geometry of the pump model and cathodic protection system.

In **Figure 6-8** the geometry of the sacrificial anode cathodic protection system is presented, having excluded the cathodic surfaces.

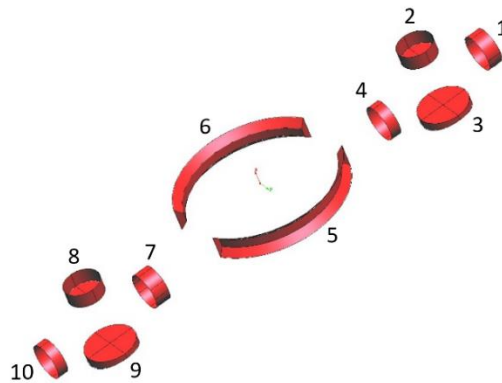


**Figure 6-8.** Geometry of the sacrificial anode cathodic protection system.

- Model Simplifications

As has already been mentioned, narrow geometries must be avoided by either insulation or redesigning because in such parts the resistance is too high and so very difficult to obtain adequate current distribution. Also, sharp angles should be avoided as they may affect the accuracy of the simulation results. The simplifications that have been made to the model are presented below.

The first simplification that has been made to the model is the sealing of the narrow part between the diaphragm and the diaphragm housing cover insert, as is shown in **Figure 6-9**.

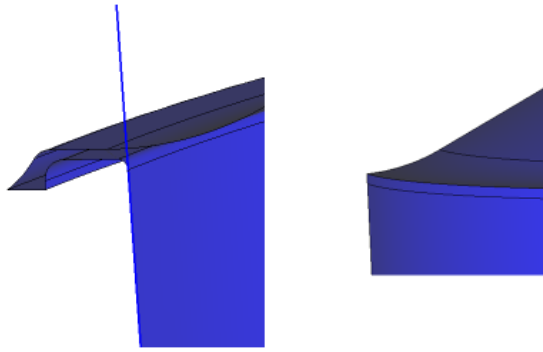


**Figure 6-9.** Model simplification of the narrow part between the diaphragm and the diaphragm housing cover insert.

The next simplification is the elimination of the sharp angles on the tubular part of the diaphragm housing, as is shown in **Figures 6-10** and **6-11**.

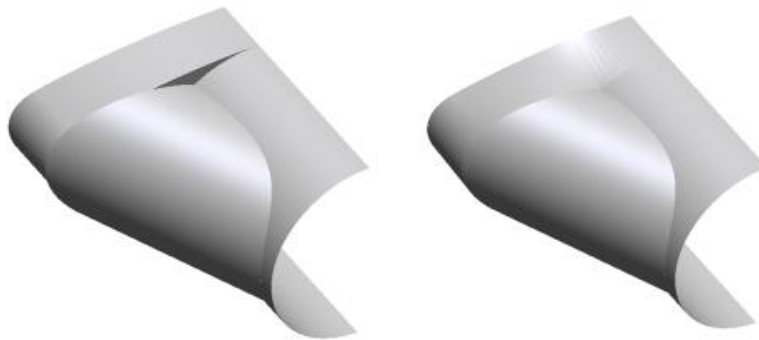


**Figure 6-10.** Model simplification of the sharp angles on the tubular part of the diaphragm housing (external view).

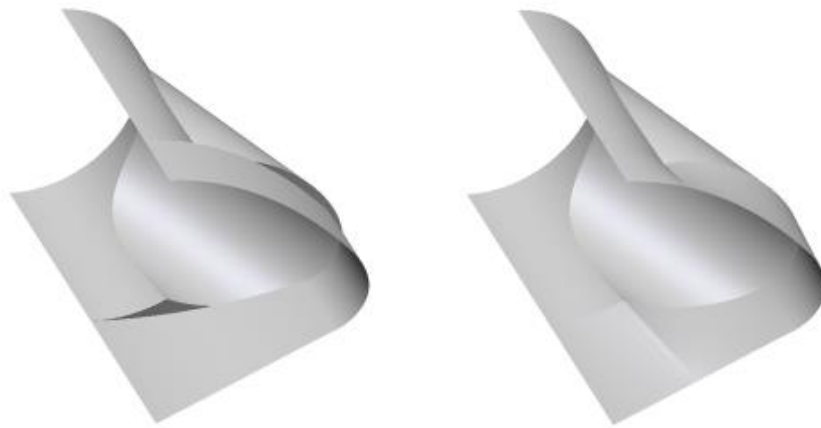


**Figure 6-11.** Model simplification of the sharp angles on the tubular part of the diaphragm housing (internal view).

The last model simplification that has been made, is the sealing of the narrow part between the valve housing and the valve seat, as is show in **Figure 6-12**.

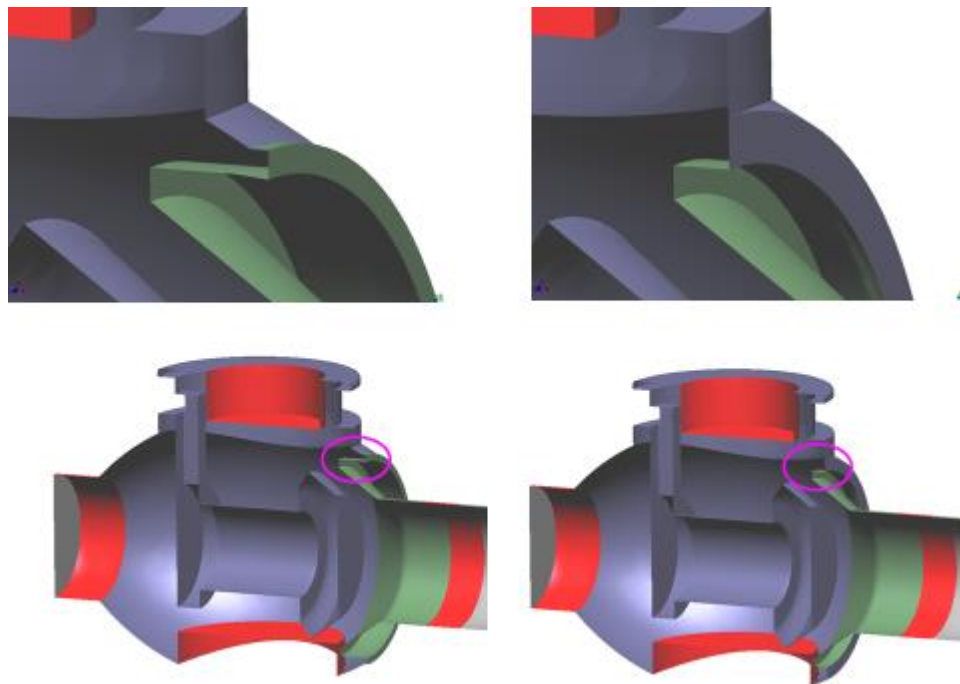


**Figure 6-12.** Model simplification of narrow part between the valve housing and the valve seat.

- Mesh Creation

After setting the orientation of the normal vectors to surfaces, meshing was applied on the surfaces of the models. The cathodic, anodic and the insulated surfaces have been discretised in 4,366 triangular and 10,752 quadrilateral elements, giving a total of 15,118 elements, as is shown in **Figure 6-13**. Although a full convergence study was not carried out, with discussion with experts and comparison to the literature, it is considered that the meshes are fully converged.

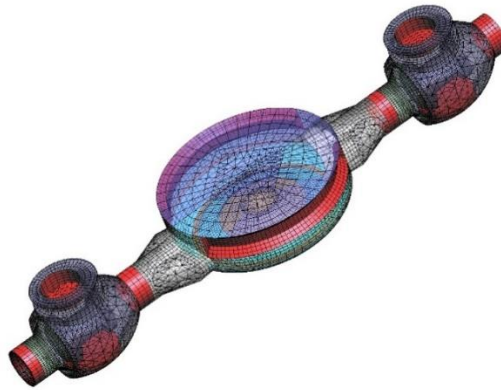


**Figure 6-13.** Meshing of the pump model's surfaces

- Boundary Conditions

The same polarisation curves for the low alloy steel grade S355 and Magnesium anode material, as used in the case of the pipeline cathodic protection system, were also used in the modelling process of the GEHO TZPM PD pump, as boundary conditions in the BEASY solver.

### 6.3.2.2 Simulation Results

The sacrificial anode cathodic protection system has been modelled in order to predict its performance in actual working conditions. The specific set up of the anodes is expected to have minimum effect on the pump's performance, as it is comprised of flush mounted and bracelet anodes, aimed for minimising the interference with the

pumped liquid flow. What is more, extra simulations have been run to predict the effect of current drain on the cathodic protection system's performance. In this way the need of electrical insulation of the pump can be evaluated. A common laptop pc was used for the solving of the models and the process time was 20÷30min per model.

In **Figures 6-14** and **6-15** the results of the simulation of the cathodic protection system are presented. The less electronegative potential on the pump surface is -908.84mV showing that the protection level is sufficient.

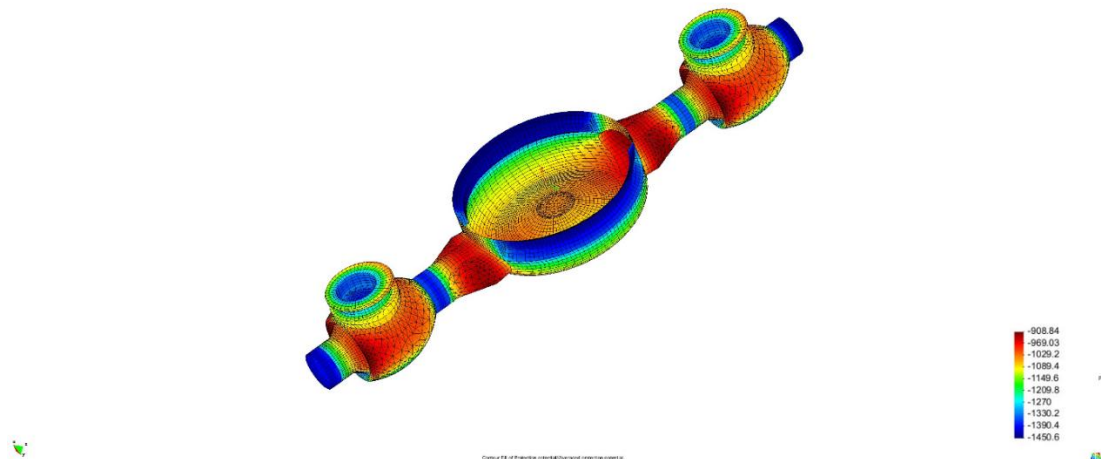


**Figure 6-14.** Simulation results of the sacrificial anode cathodic protection system.

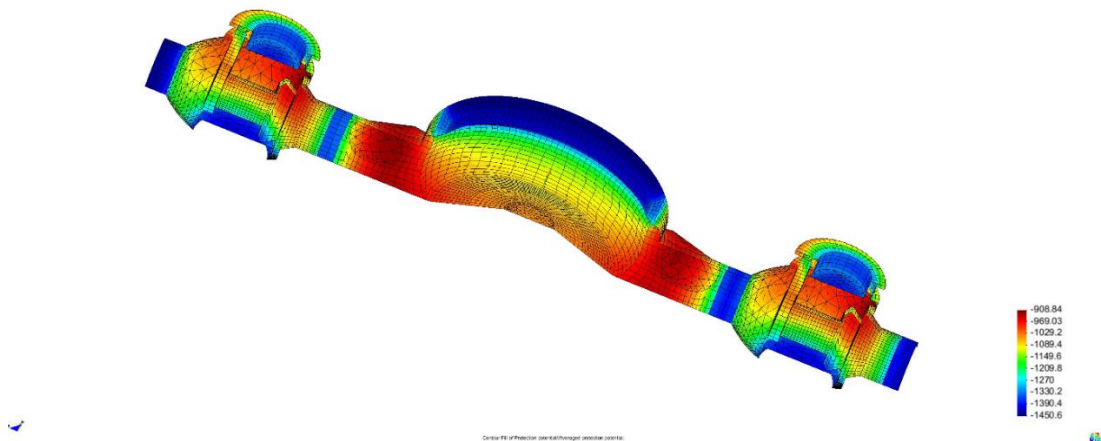


**Figure 6-15.** Simulation results of the sacrificial anode cathodic protection system, cross sectional view.

The cross sectional view enables the estimation of the cathodic protection system's capability of protecting the internal parts of the valve housings. As can be seen in **Figure 6-15**, the valves and valve seats are shown to be sufficiently protected from corrosion by the specific cathodic protection system set-up.

### 6.3.2.3 Effect of Current Drain on System's Performance

The effect of current drain on the performance of the cathodic protection system has been investigated by placing pipe lengths of 0.1m internal diameter, electrically connected to the pump, at the inlet and outlet, as is the case in real working conditions. Models of the systems have been created and simulated for lengths of pipeline of 0.5m increment. Thus, the maximum length of pipeline, which affects the performance of the cathodic protection system can be estimated. Pipelines of higher length are expected to have no further effect on the system's behaviour.

In **Figures 6-16** and **6-17** the effect of the current drain of 0.5m pipes, placed at the inlet and outlet of the pump is presented. According to the results, the current drain caused by the pipe lengths has little effect on the performance of the system.

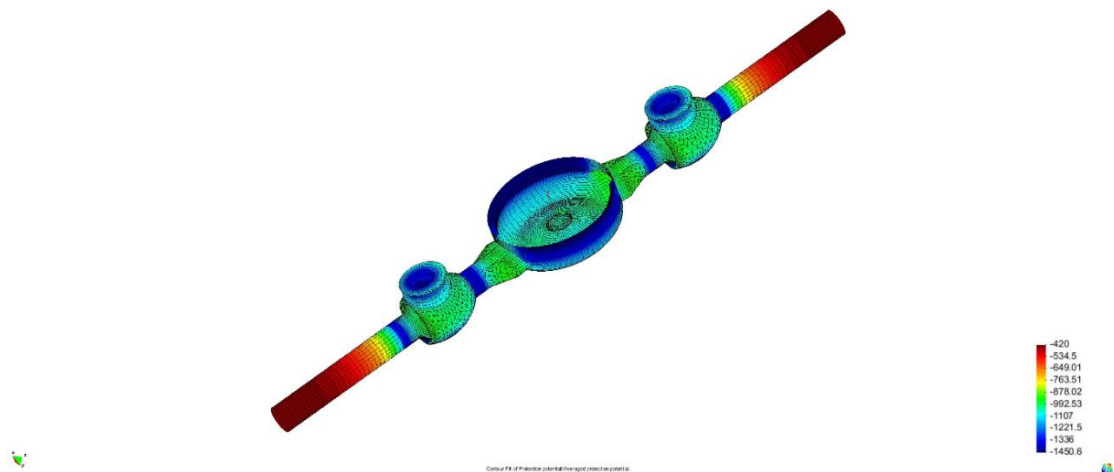


**Figure 6-16.** Current drain effect of 0.5m length pipelines on the performance of the sacrificial anode cathodic protection system.

As can be seen in **Figure 6-17**, the current drain, caused by the connection of 0.5m pipe lengths to the pump, decreased the least protective (most electropositive) potential, observed on the pump components surfaces, by only 2.02mV.

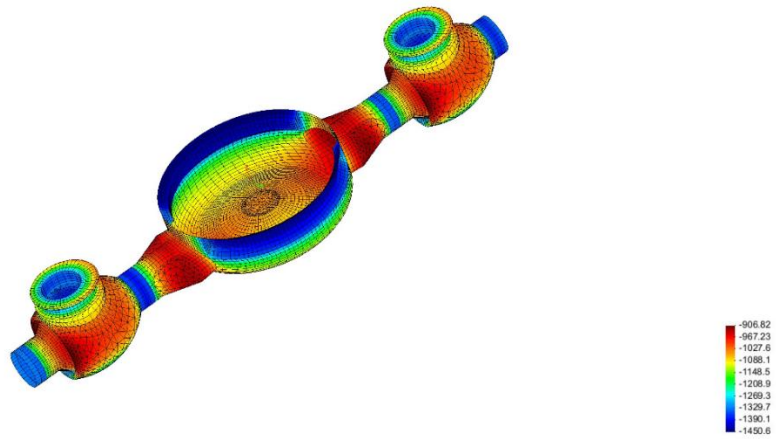


**Figure 6-17.** Current drain effect of 0.5m length pipelines on the simulation results of the potential distribution over the pump components surfaces.

In **Figures 6-18** and **6-19** the effect of the current drain of 1.0m pipes, placed at the inlet and outlet of the pump, is presented. According to the results, the current drain caused by the extended pipe lengths has no further effect on the performance of the sacrificial anode cathodic protection system.

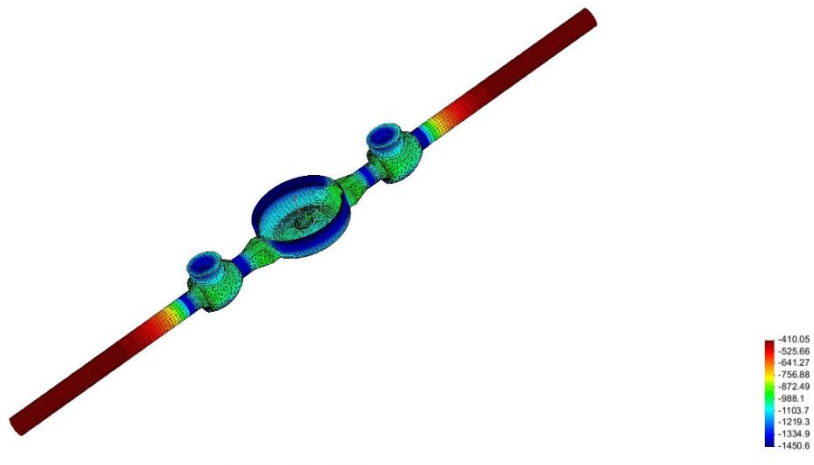


**Figure 6-18.** Current drain effect of 1.0m length pipelines on the performance of the sacrificial anode cathodic protection system.

As shown in **Figure 6-19**, the extension of the pipelines from 0.5 to 1.0m, did not affect the protection level of the pump components any further and the most electropositive value of the potential observed, remained unaltered.

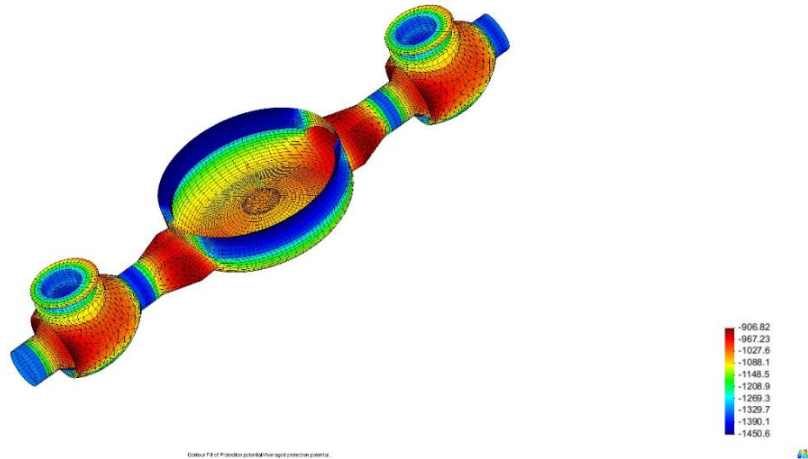


**Figure 6-19.** Current drain effect of 1.0m length pipelines on the simulation results of the potential distribution over the pump components surfaces.

After placing the anodes to the pump, the exposed cathodic surface area decreases and so does the current demand. The new values are shown in **Table 6-15**.

**Table 6-15.** New values of cathodic surface area and current demand.

Current Demand Calculations	
Surface Area <b>A<sub>c,new</sub></b> [m <sup>2</sup> ]	0.911177
Current Density <b>i<sub>c</sub></b> [A/m <sup>2</sup> ]	0.1614
Coating Breakdown Factor <b>f<sub>c</sub></b>	1
Current Demand <b>I<sub>c,dem,new</sub></b> [A]	0.1962

The current output and life span for each individual anode have been calculated based on the simulation results. Calculations were made for the cases of all three scenarios simulated: electrically insulated pump, 0.5m pipelines electrically connected to the pump and 1.0m pipelines electrically connected to the pump. In this way, the effect of current drain, on the performance of each anode can be evaluated. The results of the calculations are presented in **Table 6-16**.

**Table 6-16.** Anode current outputs and anode service lives.

Group name	Current [mA]	Current 0.5m [mA]	Current 1.0m [mA]	Mass [Kg]	E. Capacity [mAh/Kg]	u Factor	Anode Life [yrs]	Anode Life [yrs] 0.5m	Anode Life [yrs] 1.0m
Anode1	9.807176	19.23556	19.23639	0.672606	1230000	0.8	7.70	3.93	3.93
Anode2	33.79958	33.96478	33.96482	0.545732	1230000	0.8	1.81	1.80	1.80
Anode3	33.95843	34.34029	34.34035	0.710842	1230000	0.8	2.35	2.33	2.33
Anode4	16.02774	16.03428	16.03429	0.50402	1230000	0.8	3.53	3.53	3.53
Anode5	41.27662	41.27654	41.27658	0.869	1230000	0.85	2.51	2.51	2.51
Anode6	41.27648	41.27639	41.27644	0.869	1230000	0.85	2.51	2.51	2.51
Anode7	17.94743	17.95795	17.95796	0.726484	1230000	0.8	4.55	4.54	4.54
Anode8	33.84815	33.99628	33.99631	0.545732	1230000	0.8	1.81	1.80	1.80
Anode9	34.03797	34.31156	34.31161	0.710842	1230000	0.8	2.35	2.33	2.33
Anode10	8.532705	17.50033	17.50111	0.50402	1230000	0.8	6.64	3.24	3.23
	<b>Σ=270.512281</b>	<b>Σ=289.89396</b>	<b>Σ=289.89586</b>	<b>Σ=6.658278</b>					

The life of each anode has been calculated using **Equation 6-4**.

$$t_f = \frac{m_a \cdot u \cdot \varepsilon}{8760 \cdot I_a} \text{ [yrs]} \quad (6-4)$$

By calculating the new total anode current outputs it is possible to determine whether the requirement of **Equation 5-9** is met or not. The results are presented in **Table 6-17**.

**Table 6-17.** Requirement for anodes current output.

Total Anodes Current Output $I_{a,tot}$ [A]	0.2899
$I_{a,tot} > I_c$	YES

According to the simulation results it is obvious that even if the pump is not electrically isolated from connected pipelines, as is suggested in literature [6.3-6.4, 6.12-6.13], the system will provide sufficient protection current, polarising the entirety of the protected surfaces to potentials equal to  $-800\text{mV}_{SSC}$  or more electronegative. Also, the life span of the anodes will not be significantly affected except for the bracelet anodes 1 and 10.

## 6.4 Conclusions

The design process of sacrificial anode cathodic protection systems has been presented. The analytical procedure comprising of the conceptual and detailed design has been based on standard methods used in industry, making also use of experimental data for determining critical parameters. The commercial simulation software BEASY CP has been adopted in order to predict the performance of the cathodic protection systems, in various working conditions.

According to the results, sacrificial anode cathodic protection systems can be successfully applied to protect the internal surfaces of pipelines and GEHO PD pumps. The design procedure showed that in both cases, the anodes used are capable of providing sufficient current distribution, resulting in the polarisation of the entirety of the protected surfaces to potential levels of  $-800\text{mV}_{SSC}$  or more electronegative.

The analytical method, using experimental data of the actual working conditions of the materials involved, can be successfully used to provide a conservative estimation of the cathodic protection system's performance. In terms of anode current output, the analytical method does not predict the actual polarisation of the anodes and cathode, because the potential values are set to be constant, based on the minimum desired protection potential (protection criterion), resulting in a higher anode current

output. In this way, the anode consumption rate predicted is higher than the value provided by the simulation process and so the cathodic protection system's service life is conservative. This may have significant effect on the cost of using such systems, as the anodes would be replaced more frequently than desired.

In the case of pipeline cathodic protection, by using rod shape anodes along the whole length of the pipe, almost uniform current distribution can be achieved, but in the case of pumps this is practically impossible. The anode mass calculated analytically, is the minimum required for adequate corrosion protection of a structure throughout a specific period of time, but when the current distribution is not uniform over the entire protected surfaces, higher anode mass may be needed to achieve sufficient protection over this period. Because the available space for anodes, in both cases, is very limited, the aim is to use as much anode material as possible in order to increase system's service life and at the same time increase the protection level, by providing higher anode free surface, affecting the performance of the protected equipment as less as possible.

Finally, the use of simulation tools enabled for the prediction of the effect of current drain in GEHO PD pumps. According to the simulation results, the pump may not be electrically isolated from the pipelines connected at the inlet and outlet, as the protection level provided is not affected significantly, but the service lives of specific anodes will decrease and so they should be replaced more often.

## 6.5 References

- [6.1] Ralph van Rijswijk, Arno Talmon and Cees van Rhee, Fluid Structure Interaction (FSI) in Piston Diaphragm Pumps, The Canadian Journal of Chemical Engineering, Volume 94, pp. 1116 - 1126 (2016).
- [6.2] NACE International, CP3 – Cathodic Protection Technologist Course Manual, version 1 (2014).
- [6.3] Recommended Practice DNV-RP-B401, Cathodic Protection Design (2010).

- [6.4] NACE Standard RP0176-2003, Corrosion Control of Steel Fixed Offshore Structures Associated with Petroleum Production, ISBN 1-57590-170-6, NACE International, Houston TX (2003).
- [6.5] BEASY Cathodic Protection Software, User Guide (2013).
- [6.6] Mohammed Al-Otaibi, The Application of BEASY Software to Simulate Cathodic Protection of Pipelines and Storage Tanks, The University of British Columbia, Vancouver (2010).
- [6.7] Nicolas Gantiva, Design of Cathodic Protection Using BEM for Components of the Pilot Ocean Energy System, College of Engineering and Computer Science, Florida Atlantic University, Boca Raton, Florida (2010).
- [6.8] NORSOK Standard, Common Requirements - Cathodic Protection, M-CR-503 (1994).
- [6.9] I. Gurrappa, Cathodic Protection of Cooling Water Systems and Selection of Appropriate Materials, Journal of Materials Processing Technology, Volume 166, pp. 256–267 (2005).
- [6.10] J. Baynham and T. Froome, Assessment of Effects of Cavities and Narrow Channels on CP Design in the Marine Environment, NACE-2017-9275, NACE International (2017).
- [6.11] Recommended Practice DNV-RP-F103, Cathodic Protection of Submarine Pipelines by Galvanic Anodes (2010).
- [6.12] International Standard ISO 15589-2, Petroleum, Petrochemical and Natural Gas Industries - Cathodic Protection of Pipeline Transportation Systems, Part 2: Offshore Pipelines (2012).
- [6.13] International Standard ISO 15589-1, Petroleum and Natural Gas Industries – Cathodic Protection of Pipeline Transportation Systems, Part 1: On-land Pipelines (2003).

# CHAPTER 7

## Concluding Remarks and Recommendations for Future Work

### 7.1 Introduction

The current Chapter presents the conclusions reached, based on the results of the investigation, contributing to the understanding of the mechanisms that lead to unexpected failures of low alloy steel WEIR Minerals GEHO PD pump components, working in hostile environments. Moreover, concluding remarks are made concerning the methodologies that should be used in order to design sacrificial anode cathodic protection systems for the corrosion protection of such equipment and the techniques applied for the prediction of their behaviour under various conditions.

In the last part of the Chapter, recommendations for further investigation are being made. These recommendations are aimed for the extension of the insight into those parameters that affect the performance of the materials investigated and the optimisation of the application of cathodic protection systems using sacrificial anodes. Finally, experimental methods for the investigation of the effect of cathodic protection on the corrosion-fatigue life of real size GEHO pumping equipment, are also suggested.

### 7.2 Concluding Remarks

The investigation showed that SACP and SCCP can be successfully used to effectively protect the low alloy steel grade tested, from liquid erosion-corrosion. The overall concluding remarks and outcomes from the experiments and analyses are summarised as follows:

1. The salinity level of the aqueous solution plays a significant role in the erosion-corrosion performance of the low alloy steel grade. Increasing Sodium Chloride concentrations increase the erosion-corrosion rate dramatically.

2. Zinc alloy sacrificial anodes and a Zinc rich sacrificial coating eliminated the effect of liquid erosion-corrosion, while Magnesium alloy sacrificial anodes proved to be of higher effectiveness in the lower salinity level, in terms of driving the electrode potential of the material to more electronegative values.
3. Potentiodynamic testing performed, revealed the effect of flow velocity, salinity level and sacrificial anode material on the behaviour of a SACP system. Increasing flow velocity caused depolarisation and increased the current needed to polarise the cathode to sufficient protective potential values. Higher salinity levels increase the conductivity of the electrolyte, cause depolarisation and dramatically increase the current demand for adequate protection. Finally, more active anodes allow for increased cathodic protection current flow, resulting in higher protection levels.
4. The use of the 1-D mathematical model allowed for the prediction of the response of SACP systems to working conditions variation. According to the results, increasing distance between anode and cathode, increases the resistance of the system, reducing the current flow and so the polarisation level. Increasing Sodium Chloride concentration resulted in increased polarisation of the cathode, as it allowed for higher current flow. Furthermore, the potential of the cathode becomes more electropositive and so less protective by increasing flow velocity. Increases in current flow in the system result in higher consumption rates of the anodes. Finally, more active anodes drive the electrode potential of the cathode to more electronegative levels.

Application of SACP proved to be a successful method for eliminating the effect of erosion-corrosion of the fatigue life of the material, driving the results back to in-air levels and restoring the fatigue limit. The concluding remarks and outcomes, from the experiments conducted, are summarised as follows:

1. Increases in salinity level dramatically reduce the fatigue life of the low alloy steel. As the stress level decreases, higher Sodium Chloride content caused the fatigue life to reduce even further.
2. Corrosion pitting on the fracture surface of the specimens, was revealed by topography. The corrosion pits acted as stress concentration sites, resulting in crack initiation.
3. Zinc alloy and Magnesium alloy anode cathodic protection, used in 824ppm and 35,000ppm NaCl solutions respectively, successfully protected the steel

specimens from corrosion prolonging its fatigue life to in-air levels and restoring the fatigue limit.

4. The deposition of (more likely) calcareous films dramatically reduced the current demand for sufficient protection, prolonging in this way the service life of the sacrificial anodes.

Cathodic protection systems using sacrificial anodes can be effectively used for the corrosion protection of the internal surfaces of small diameter pipelines and WEIR Minerals GEHO PD pump components. Conclusions reached based on the results of the investigation are as follows:

1. Accurate polarisation curves are an essential part of the analytical design and simulation process of cathodic protection systems. The results obtained from potentiostatic tests are more accurate compared to potentiodynamic testing of short-term exposures, since the effect of the formation of depositions on the protected surfaces is time dependant.
2. Application of modelling tools for the prediction of SACP systems performance enables for modifications to be applied while still at the design stage, without the need for in-field measurements. In this way, the cost of applying SACP reduces significantly as post installation modifications and so production delays, can be avoided.
3. The analytical design method can be used to obtain a conservative estimation of a SACP system's service life but it cannot sufficiently predict the system's performance, as the actual anode current output is overestimated and current distribution on the protected surfaces is not predicted. The fact that the geometrical characteristics of the protected structures (apart from the total protected surface area) are not taken into account and the actual polarisation of each individual anode and structure is not known, the process may lead to unnecessary oversizing of the system, to achieve a specific service life and probably to insufficiently protected (under-protected) areas.
4. Modelling of SACP systems provides an accurate performance prediction, as the actual geometrical characteristics of the system and the polarisation behaviour of the materials involved are taken into account, allowing for the prediction of the current output of each individual anode and the potential distribution over the surfaces under protection. In this way, it is possible to predict the service life of each anode and avoid the unnecessary replacing of

the whole anode array at the same time, reducing dramatically the maintenance cost.

5. According to the results of the simulation of SACP systems designed for the corrosion protection of pipelines and GEHO TZPM PD pumps, the entirety of the protected surfaces was sufficiently polarised to potential levels more electronegative than  $-800\text{mV}_{\text{SSC}}$ , indicating that the equipment was adequately protected.
6. The simulation process allowed for the investigation of the effect of current drain, due to the connection of pipelines to the GEHO TZPM PD pump, on the performance of the SACP system. The results showed that the protection level provided to the internal surfaces of the pump is not significantly affected but specific anodes are predicted to be required to be replaced more often as their service life decreases, due to the increase in their current output.

### **7.3 Recommendations for Future Work**

In this section suggestions for further investigation in relation to the outcomes of this Thesis are presented. The recommended topics could be used for the structuring of new research programmes that will extend the understanding of those mechanisms as lead to corrosion-fatigue failures in WEIR Minerals GEHO pumping equipment and enhance the effectiveness of applying corrosion protection techniques.

1. GEHO pumping systems are also used for the transportation of corrosive fluids in elevated temperatures. The effect of temperature on the corrosion-fatigue performance and on the behaviour of SACP systems, designed for the elimination of the effect of corrosion on the fatigue life, should be assessed.
2. Another critical parameter that should be investigated is the presence of solid particles into the pumped fluids. Slurries pumped through GEHO equipment may significantly affect corrosion-fatigue life by causing solid particle erosion phenomena.
3. Solid particle erosion may influence also the performance of SACP systems, in terms of destroying protective layers, increasing in this way the current demand for adequate protection. Furthermore, possible reduction of the service lives of sacrificial anodes, due to the erosion of anode material, should be assessed.

4. For accurate predictions of SACP systems behaviour, working in various environmental conditions faced by GEHO equipment, potentiostatic testing of the materials involved is required. This would allow for accurate prediction of the current demand for sufficient protection and the obtaining of accurate polarisation curves to be used as boundary conditions in the modelling process.
5. Before the in-field application of SACP systems aimed for the protection of small diameter pipelines and WEIR Minerals GEHO PD pumps, as these have been presented in this thesis, experimental investigation in real size test rigs is recommended, for the validation of the results of the design process. The environmental conditions of the testing should resemble those faced in the field. Moreover, the current output of each anode should be monitored in order to estimate the actual anode service life and consequently the frequency of replacement needed. Finally, it is recommended that the potential level on the protected surfaces should also be monitored and especially in those areas where it is expected to be lowest (less electronegative). In this way, the protection level provided by a specific SACP system can be assessed and modifications can be made to the system before it is applied in the field.